Experiments on Cross-Shore Sediment Transport Under Positive and Negative Solitary Waves

by

Andrew R. Lawrence

and

Nobuhisa Kobayashi

RESEARCH REPORT NO. CACR-03-03

September, 2003

Center for Applied Coastal Research
Ocean Engineering Laboratory
University of Delaware
Newark, DE 19716

TABLE OF CONTENTS

LIST OF FIGURES

LIST OF TABLES

ABSTRACT

Laboratory experiments were performed to examine the cross-shore sediment transport processes under breaking solitary waves on a fine sand beach. The initial beach slope of 1:12 was exposed to a positive solitary wave eight times. The beach was rebuilt and exposed to a negative solitary wave eight times. The wave motion and sediment transport were found to be affected little by the beach profile change from the initial profile. The positive solitary wave plunged violently near the shoreline and suspended a considerable volume of sand. The plunging wave with no seaward flow impeding its runup caused large runup on the foreshore. The strong downrush following the large runup resulted in erosion on the foreshore and deposition seaward of wave run-down. On the other hand, the negative solitary wave collapsed against the seaward flow induced by the free surface slope of the negative wave and caused less sediment suspension. The wave runup against the seaward flow was much smaller. The weak downrush following the small runup resulted in deposition on the foreshore and erosion near the wave collapsing point. These limited laboratory experiments indicate the importance of the initial wave profile for swash sediment dynamics and the capacity of a single wave in causing noticeable beach profile changes.

Chapter 1

INTRODUCTION

Sediment transport processes on beaches under tsunamis have been studied very little in comparison to a large number of studies performed for sediment transport processes under wind waves and currents as reviewed concisely by Kobayashi and Johnson [2001]. The sheets of marine-derived sediments deposited along the west coast of North America have been used to identify historic tsunamis [e.g., Clague et al., 1999; Witter et al., 2001], but tsunamis also caused beach erosion [Synolakis et al., 1995]. Presently, it is not possible to quantitatively relate the sediment deposition or beach erosion to the characteristics of tsunamis. Moreover, no data is available to develop a sediment transport model for tsunamis, partly because it is practically impossible to install the necessary instrument immediately before the arrival of a tsunami.

Wave runup and flooding caused by tsunamis have been studied using incident solitary waves or N-shaped waves [e.g., Tadepalli and Synolakis, 1994]. The semi-analytical solution of Carrier et al. [2003] for non-breaking tsunami runup and run-down on plane beaches has indicated that the maximum fluid velocity occurs at the shoreline during the downrush phase for predominantly positive initial waves and

during the uprush phase for predominantly negative initial waves, which may be caused by an offshore submarine landslide. On the basis of the computed velocities, they have predicted the seaward and landward movements of sediments under positive and negative initial waves, respectively. It is not clear whether their prediction holds for breaking waves because bore-generated turbulence has been shown to be important for sediment suspension and transport in the swash zone on a beach [Puleo et al., 2000].

In this study, laboratory experiments were conducted to examine the cross-shore sediment transport and beach profile changes under positive and negative solitary waves that broke on a fine sand beach. Chapter 2 describes the laboratory experiments. Chapters 3 and 4 present the positive and negative solitary wave test results, respectively, to show the importance of the initial wave profile in determining the breaker type, sediment suspension, uprush, downrush and net sediment transport. Chapter 5 summarizes the findings of this study. The paper summarizing this study has been submitted to Journal of Geophysical Research [Kobayashi and Lawrence, 2003].

Chapter 2

EXPERIMENTS

2.1 EXPERIMENTAL SETUP

The positive and negative solitary wave experiments were performed in a wave tank that was 30 m long, 2.4 m wide and 1.5 m high, as shown in Figure 2.1. The still water depth for the experiments was 80.0 cm. A piston-type wave paddle was used to generate the solitary waves. To reduce the amount of sand necessary for the experiments, a divider wall was constructed along the centerline of the tank. In order to support the upper berm area of the beach, a rear wall was also constructed. At the far end of the wave tank a rock slope was placed to absorb waves that propagated outside the experimental area. The same setup was used in previous irregular wave experiments by Giovannozzi and Kobayashi [2002] and Kobayashi and Tega [2002].

Before the positive and negative solitary wave tests a 1:12 fine sand beach was built in the 115 cm wide flume. The sand beach was exposed to the positive solitary wave eight times. These eight tests are called tests P1 to P8. After the completion of test P8, the beach was reconstructed to the initial slope of 1:12 and exposed to the negative solitary wave eight times. These eight tests are called tests

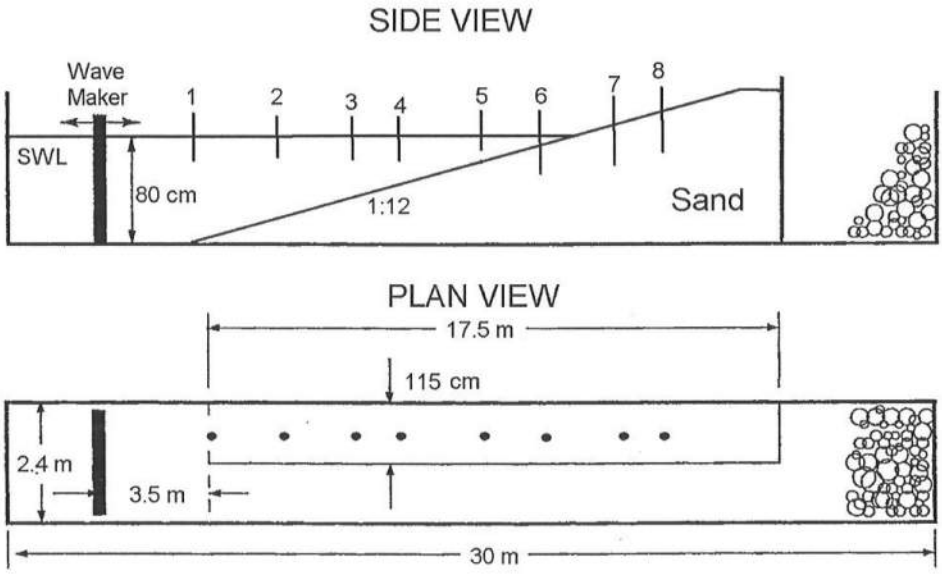

Figure 2.1: Experimental Setup

N1 to N8 in the following sections.

Free surface elevations were measured using eight wave gauges placed along the centerline of 115 cm wide flume, except for the location of the velocity and concentration measurements where the gauge was located 22.5 cm from the centerline. A micro acoustic-Doppler velocimeter (ADV) with a 3D down-looking probe and a 2D ADV with a side-looking probe were installed to measure fluid velocities at two locations simultaneously. In order to measure the suspended sediment concentration, a fiber optic sediment monitor (FOBS-7) was utilized. The velocities and concentrations were measured 6.0 cm above the local bottom before each test. The alongshore locations of the sampling volumes of the velocities and concentrations are depicted in Figure 2.2. The measurements are relative to the centerline of the 115 cm wide flume. The free surface, velocity and sediment concentration data were collected at a sampling rate of 20 Hz.

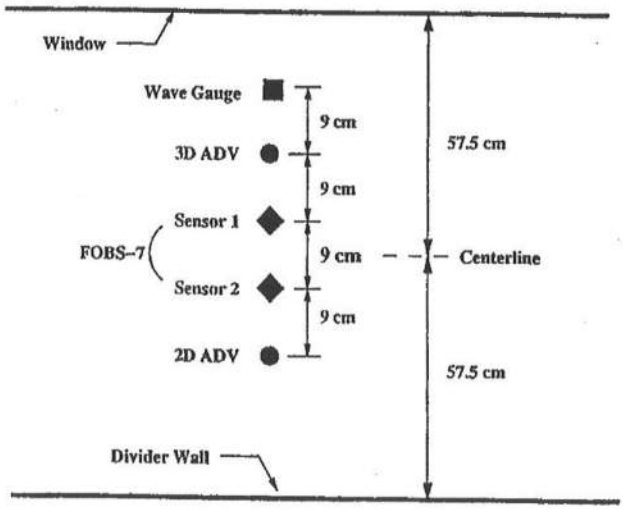

Figure 2.2: Alongshore Gauge Positions

2.2 GENERATION OF SOLITARY WAVES

The wave paddle trajectory used to generate a positive solitary wave was computed using the method described by Goring [1978]. In order to generate a solitary wave, the paddle was moved backward slowly from its original position and then forward rapidly, and finally returned to its initial position. The paddle displacement from its starting position is shown in Figure 2.3. To produce a negative solitary wave, the paddle motion was reversed, as depicted in Figure 2.3. The measured solitary wave profiles are discussed later in Chapters 3 and 4 with the positive and negative solitary wave results.

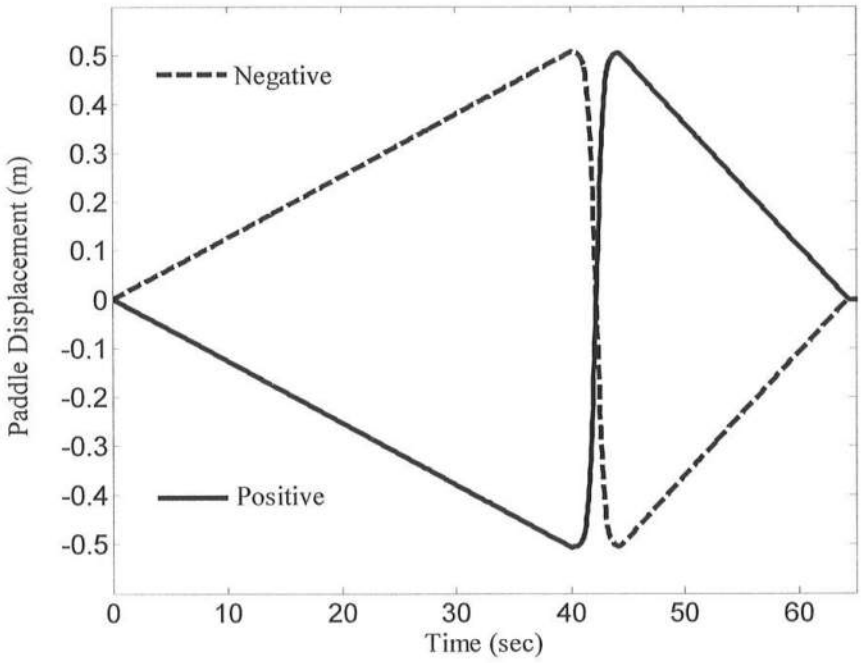

Figure 2.3: Solitary Wave Paddle Displacement

2.3 SAND CHARCTERISTICS

Approximately 9 tons of fine quarry sand was used to construct the 1:12 initial beach slope. Measurements were made of the sand characteristics such as its density, specific gravity, porosity, grain size distribution and fall velocity. Sand density is defined as the ratio between sand mass and sand volume. A known mass of sand was placed in a graduated cylinder with a known volume of water. The volume of water displaced by the sand is equal to the volume of the sand. The sand density is the known mass divided by the measured displaced water volume. The specific gravity is defined $s = \rho_s/\rho_w$, where ρ_s = sand density and ρ_w = density of pure water. The specific gravity was found to be 2.6. Using the measured dry sand mass with the known specific gravity and the measured total sample volume, the porosity, n_p, was determined to be 0.4. The average moisture content of the sand was 0.42%, and thus negligible.

The grain size distribution was measured using a sieve test procedure consisting of nine different sieve sizes. A sample of sand with a mass of 293.9 g was agitated for approximately 20 minutes. The test results are shown graphically in Figure 2.4 and are summarized in Table 2.1. The sand can be categorized as fairly uniform based on the steepness of the curve in the range of 10-90 percents. The median diameter, d_{50}, was calculated using the linear interpolation of the two data points corresponding to the sieve sizes of 0.150 mm and 0.212 mm. The sediment fall velocity was determined experimentally using a few grains from each size group of the sieve analysis. The grains were dropped in a clear glass cylinder filled with

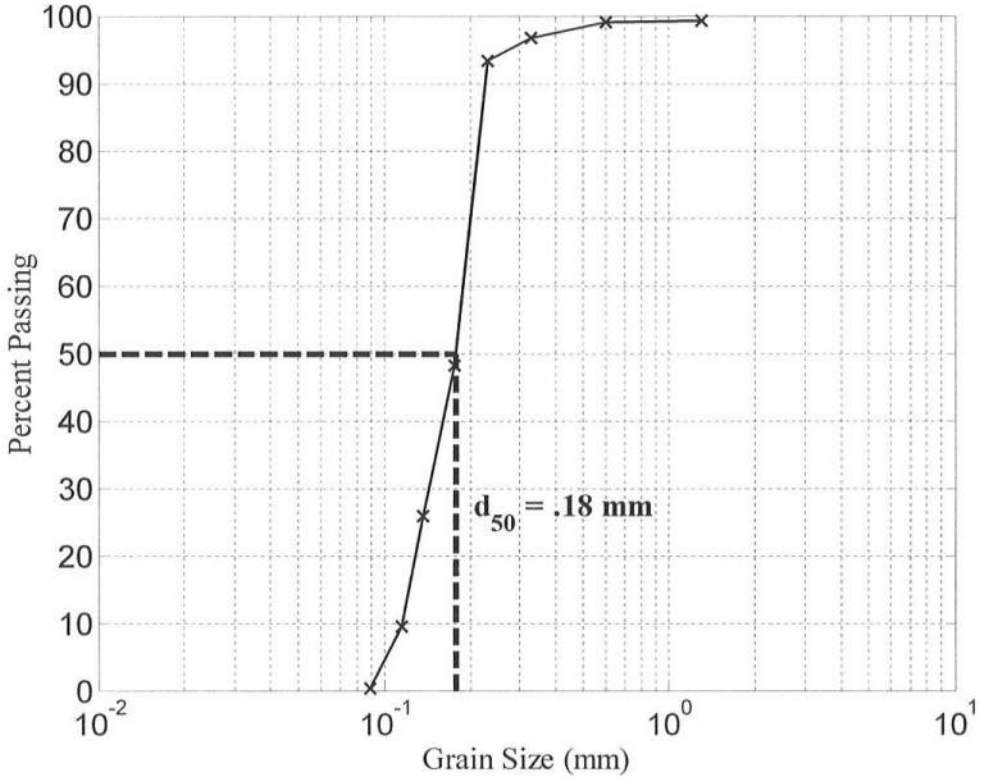

Figure 2.4: Sand Grain Size Distribution

Table 2.1: Summary of Sieve Test

Sieve Size (mm)	Geometric Mean Diameter (mm)	Mass (g)	Percent of M_{total}	Percent Passing
2.0	–	0	0	100.0
0.850	1.300	2.3	0.77	99.2
0.425	0.601	0.8	0.27	99.0
0.250	0.326	6.5	2.20	96.8
0.212	0.230	10.1	3.44	93.3
0.150	0.178	132.6	45.12	48.2
0.125	0.137	65.7	22.34	25.9
0.106	0.115	48.3	16.42	9.4
0.075	0.089	26.8	9.13	0.3
Pan	–	0.9	0.30	0.0
TOTALS		293.9	100	–

water and their motion was visually timed over a distance of one meter. Ten fall durations were recorded and the mean fall velocity was calculated for each size group, as shown in Table 2.2. The sizes of 2.0 mm and 0.85 mm were omitted because there was practically no mass in these groups in the whole sample. When the measured fall velocity was averaged with a weighting factor proportional to each group's percent of the total mass, the mean fall velocity was calculated as $w_f = 2.01$ cm/s. The value $w_f = 2.0$ cm/s will be used hereafter. The sediment characteristics are very similar to those found by Giovannozzi and Kobayashi [2002] and Kobayashi and Tega [2002].

2.4 MEASUREMENT OF BEACH PROFILES

During the positive and negative solitary wave tests detailed measurements of the beach profile were taken. In deep water, measurements were made using a

Table 2.2: Fall Velocity Measurements

Sieve Size (mm)	Percent of M_{total}	Measured w_f (cm/s)
0.425	0.27	7.92
0.25	2.22	3.94
0.212	3.46	2.55
0.15	45.47	2.01
0.125	22.51	1.46
0.106	16.55	1.12
0.075	9.20	0.781
PAN	0.30	0.663
Average w_f		2.01 (cm/s)

Panametrics 22DLHP ultrasonic depth gauge for the positive wave tests and a Panametrics 25DLHP for the negative wave tests. In the swash zone a manual pointer with a vernier scale was employed. The initial profile and profile after each test were measured along three cross-shore transects. The center transect was taken along the centerline of the beach area, while the other two were taken 23.5 cm to the left and right of the center transect. Each transect was measured at points spaced 5.0 cm apart. There was an overlap of 5 points at the transition from the ultrasonic depth gauge readings and the manual pointer readings. As illustrated in Figure 2.5, the measured profiles were essentially uniform alongshore. An average profile for each test was acquired by averaging the three transects and then employing a three-point smoothing routine to the averaged transect. Figure 2.6 shows a typical smoothed profile of the three transects displayed in Figure 2.5. The error or uncertainty of the measure profile elevation was approximately 1.0 mm.

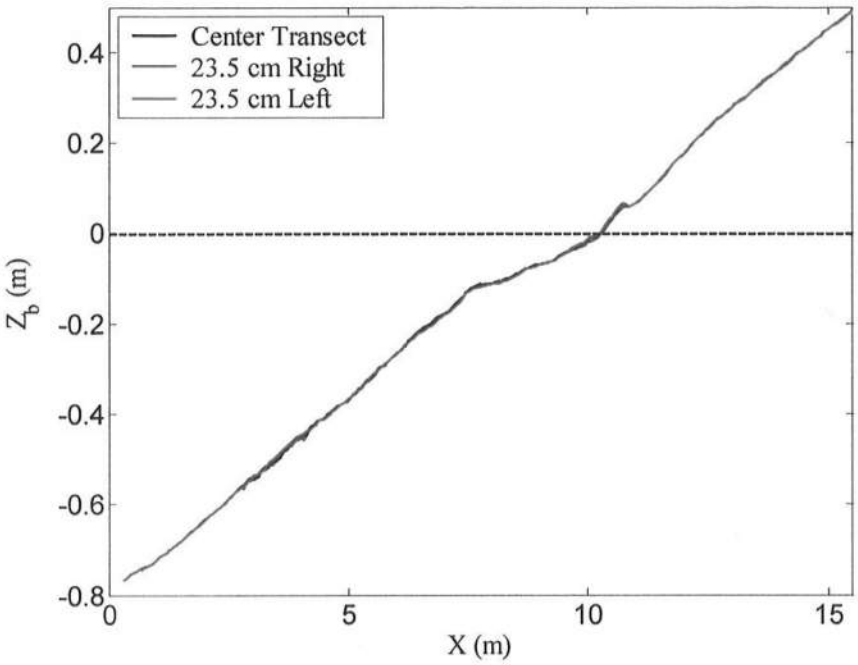

Figure 2.5: Unsmoothed Profile at Three Transects for Test P4

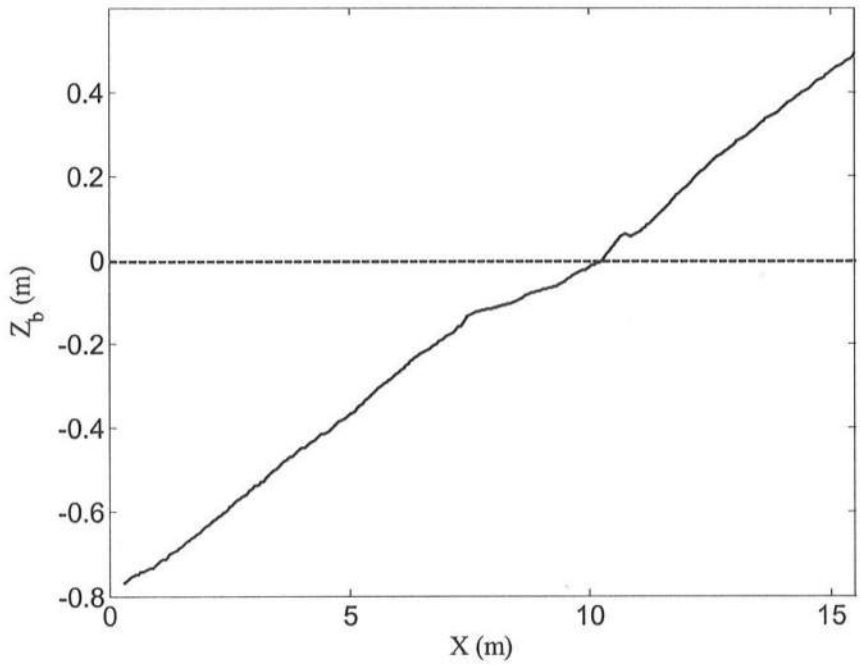

Figure 2.6: Smoothed Profile of Test P4

Table 2.3: Wave Gauge Locations

Wave Gauge	Onshore Distance (m)	
	Positive Solitary Wave Tests	Negative Solitary Wave Tests
1	0	0
2	3	2.5
3	5.5	5
4	7	6
5	8.5	7
6	9.55	8
7	10.55	9
8	12	10

2.5 WAVE GAUGES

The cross-shore locations of eight wave gauges (G1-G8) are shown in Figure 2.7 for the positive solitary wave experiment and in Figure 2.8 for the negative wave experiment over their initial profiles. The horizontal coordinate, x, is taken as positive shoreward with x = 0.0 m at the toe of the initial beach profile. Table 2.3 gives the cross-shore location, x, of the eight wave gauges for tests P1-P8 and tests N1-N8. Wave gauge 1 was placed at the toe of the 1:12 slope to measure the incident solitary wave and ensure the repeatability of the generated waves for the eight tests. Wave gauges 2-5 measured the solitary wave shoaling and breaking. Wave gauges 6-8 were buried in the sand to measure the solitary wave runup and rundown in the swash zone. The eight wave gauges were calibrated before each positive wave test by raising the water level in the tank 30.0 cm above the still water level (SWL), then gradually draining the tank until the water level reached 9.0 cm below SWL. The

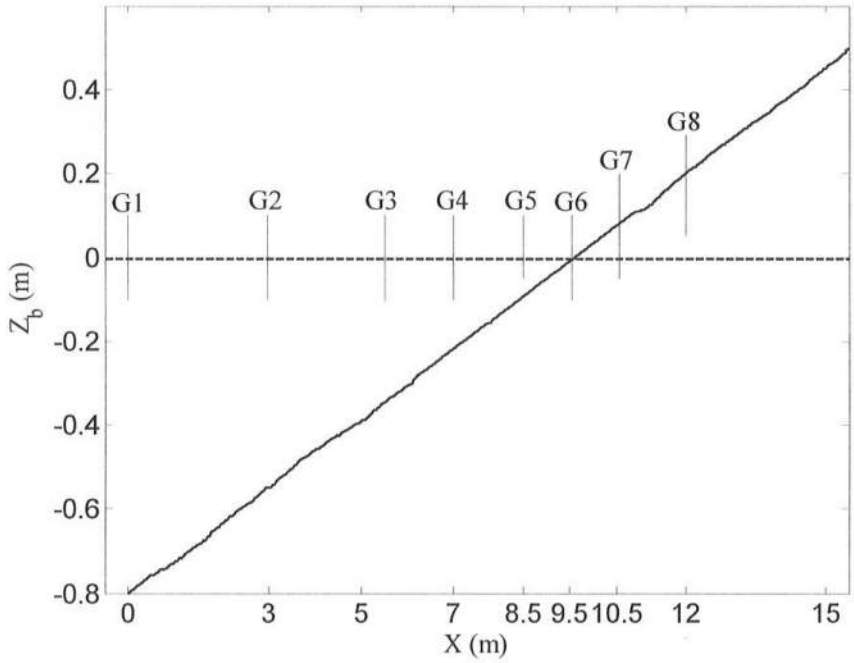

Figure 2.7: Wave Gauge Locations for Tests P1-P8

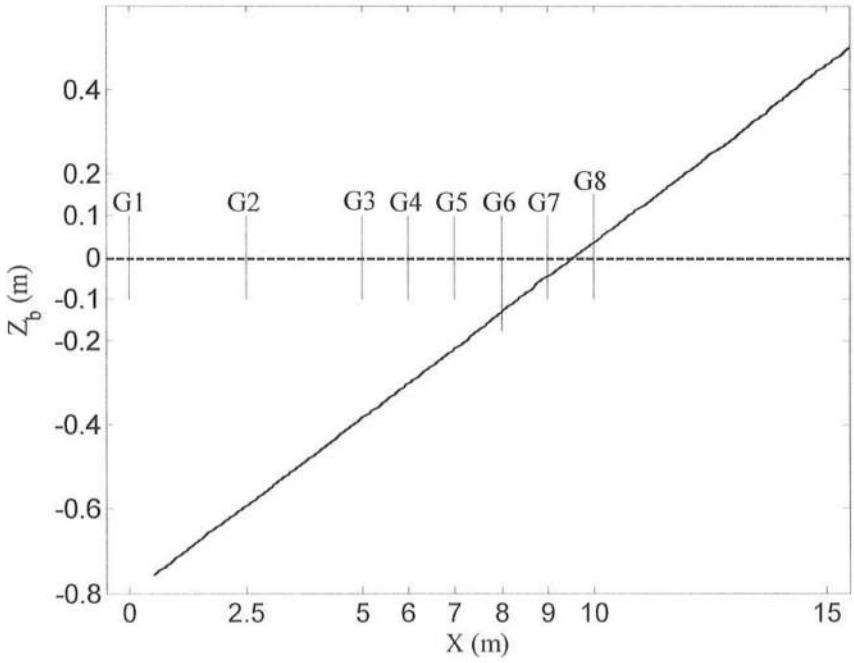

Figure 2.8: Wave Gauge Locations for Tests N1-N8

voltage readings of each wave gauge were recorded for every 1.0 cm change in the water level, totaling 40 points. The wave gauge calibration for the negative wave tests was performed in the same manner except that the water level above and below SWL was 15.0 cm and 5.0 cm, respectively, giving 21 points. This calibration procedure ensured that the sand above SWL was wet before each test.

The calibration data for wave gauges 1-5, which were not buried in the sand, generally followed a linear line, as illustrated for gauge 3, test P8, in Figure 2.9. The best fit slope to all the data points was obtained for each of these wave gauges. This slope is shown in Figure 2.9 as the solid line. The horizontal dashed line corresponds to the elevation of the SWL before each test to measure the free surface elevation

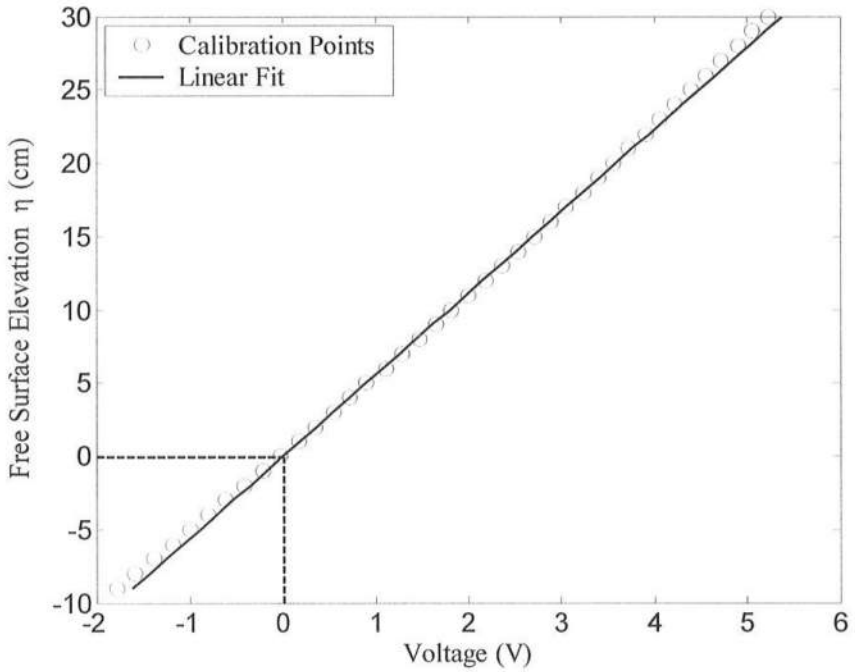

Figure 2.9: Representative Wave Gauge Calibration Curve for Gauges 1-5

above SWL. The calibration curves for gauges 1-5 were repeatable for the positive and negative wave tests.

For the buried gauges 6-8, the bed surface was ultimately exposed to air as the water level was lowered during calibration. The voltage reading remained practically constant after the bed surface was exposed to air. Figures 2.10 and 2.11 illustrate this occurrence for gauges 6 and 8, respectively. In both plots the voltage readings followed the linear line very well while the water level is above the bed surface. The readings departed from the straight line once the bed surface was exposed, perhaps due to the time lag of the water table in the sand compared to the water level in the tank. The departure from the straight line may have also been caused by the different

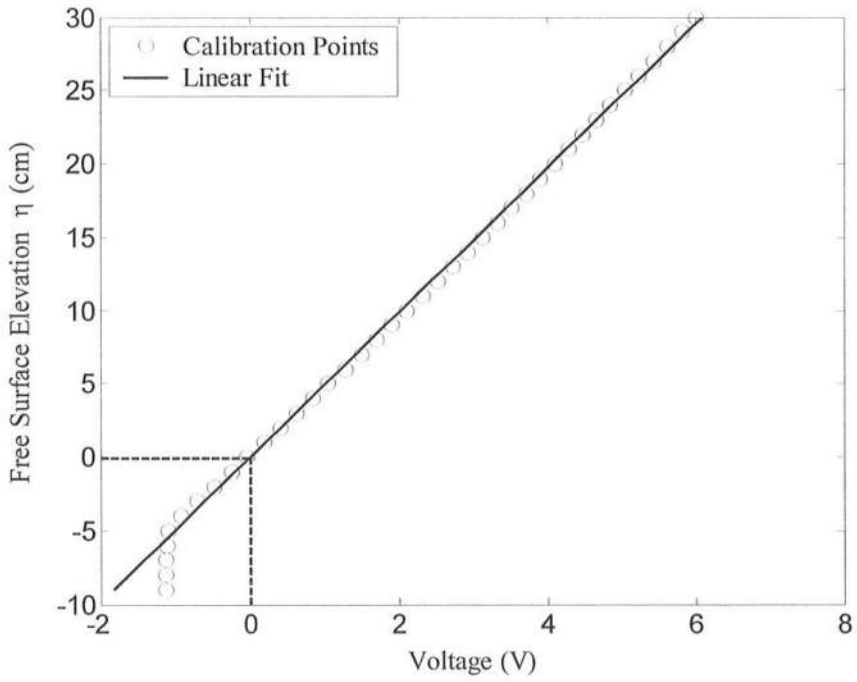

Figure 2.10: Representative Wave Gauge Calibration Curve for Gauge 6

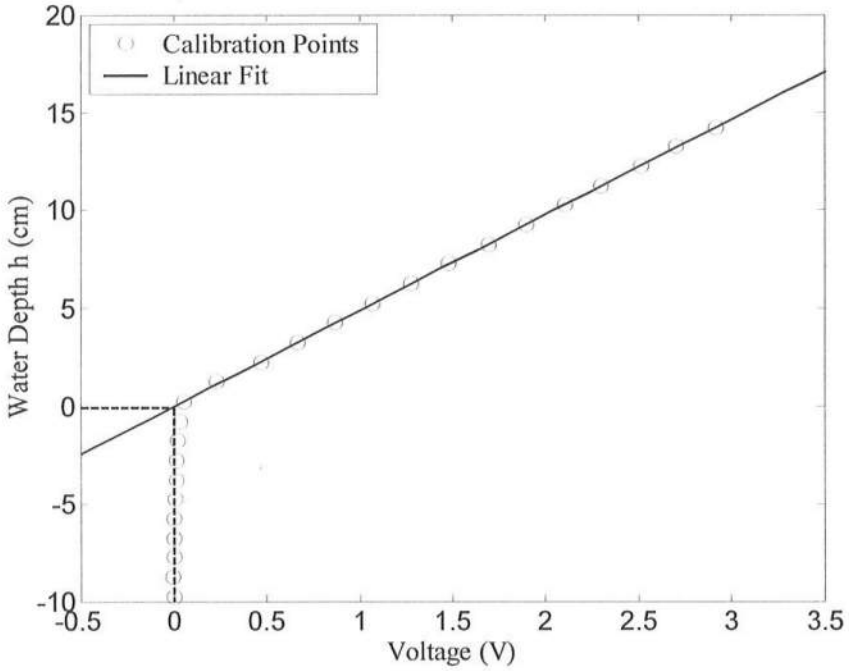

Figure 2.11: Representative Wave Gauge Calibration Curve for Gauge 8

capacitance of the material. For gauge 6 shown in Figure 2.10, the free surface elevation η relative to SWL was measured by the recorded voltage which was limited by the voltage corresponding to that of the saturated bed surface. For gauge 8 shown in Figure 2.11, the water depth h above the bed surface before each test was measured by the recorded voltage which was limited by the voltage corresponding to the exposed bed surface.

2.6 ACOUSTIC-DOPPLER VELOCIMETERS

A micro acoustic-Doppler velocimeter (ADV) with a 3D down-looking probe and another ADV with a 2D side-looking probe measured the cross-shore, alongshore

and vertical velocities where the 2D ADV did not measure the vertical velocity. The fluid velocities were measured 5.0 cm from the probe tip and 6.0 cm above the local bottom before each test. The sampling volume for each ADV was approximately 0.1 cm^3. Figure 2.2 displays the alongshore location of the sampling volume for each ADV. The fluid velocities were measured at the cross-shore location of wave gauge 3 for tests P1-P8 and wave gauge 4 for tests N1-N8. This location for tests P1-P8 was selected to measure the velocities reliably without the effect of bubbles produced by plunging breakers. For tests N1-N8, this cross-shore location was chosen to measure the fluid velocities near the breaking point of the solitary wave.

The ADVs were secured to adjustable mounts that could be raised or lowered to any desired elevation above the local bottom. Due to the changing profile, the ADVs had to be repositioned before each test. The elevation of the sampling volume of the 2D ADV was carefully measured with a tape measure within ±1 mm, starting with the probe touching the local bottom. The sampling volume elevation of the 3D ADV was determined using the ADV software supplied by the manufacturer and was accurate within ±0.5 mm. The ADV manufacturer also supplied formulas to convert ADV voltage output into the corresponding velocity and therefore calibration was not required.

2.7 FIBER OPTIC SEDIMENT MONITOR

A Fiber Optic Sediment Monitor (FOBS-7) with two sensors was used to measure the sand concentration at 6.0 cm above the local bottom at the two

alongshore locations shown in Figure 2.2. The FOBS-7 is a laboratory version of the optic sensors used for concentration measurements on natural beaches [Downing *et al.*, 1981]. The monitor measures sediment concentration by detecting infrared radiation (IR) backscattered from particles in the water. The measurement area is limited to the volume where the transmit and receive beams cross. The sampling volume, which is illustrated in Figure 2.12, is approximately 10 mm^3 and situated approximately 1.0 cm from the tip of the sensor.

The elevation, Z_m, of the sampling volume was determined using an adjustable mount similar to the ADVs. The sensor was lowered to the local bottom, to establish the sensor edge elevation Z_e = 0.0 cm above the local bottom. The sensor was then raised slowly and the corresponding voltage in the absence of waves was read. When the sampling volume emerged from the bed a sudden decrease in voltage was observed. This point of sudden voltage drop was regarded as Z_m = 0.0 cm on the

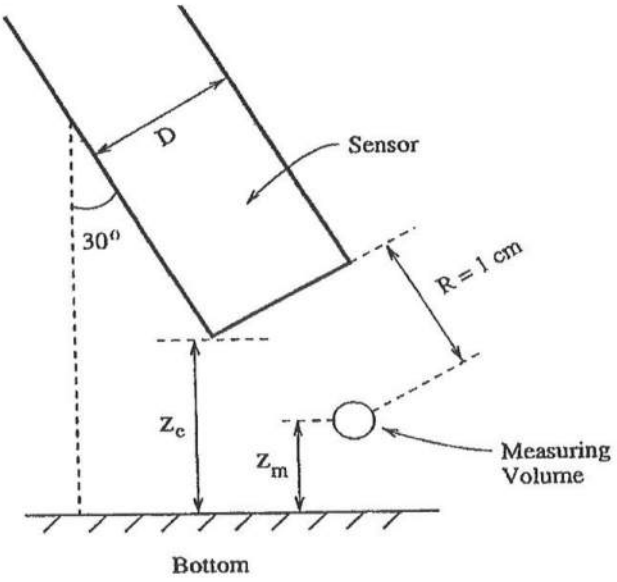

Figure 2.12: Illustration of FOBS-7 Sensor

local bottom. The sensors were then raised 6.0 cm from the bottom point to the desired elevation. As shown in Figure 2.12, the sensors were mounted at an angle 30° from vertical. From simple geometric relationships, the sampling volume elevation, Z_m, was determined to be $Z_m = (Z_e - R\cos\theta + D/2\sin\theta)$, where $R = 1.0$ cm is the distance from the sensor tip to the sampling volume, $D = 1.0$ cm is the diameter of the sensor tip and $\theta = 30°$, all of which are shown in Figure 2.12. Therefore, the sampling volume elevation of $Z_m = 6.0$ cm corresponds to $Z_e = 6.62$ cm where $Z_m = 0.0$ cm relates to $Z_e = 0.62$ cm on the local bed.

The sensors were calibrated before the positive solitary wave tests and after the negative solitary wave tests in order to determine the relationship between sediment concentration and voltage. For each sensor this was done by measuring the time series of known sand concentrations from 0 g/L to 28 g/L in 4 g/L increments, at a rate of 20 Hz for 60 seconds in a well-mixed blender. A sample of a measured time series used for the calibration of sensor 1 for the positive solitary wave tests with concentration 20 g/L at an elevation $Z_m = 6.0$ cm above the bottom of the blender is plotted in Figure 2.13 where the solid line is the mean and the dotted lines are the mean plus and minus one standard deviation. The time series were recorded at elevations 5, 6 and 7 cm above the bottom of the blender to make certain there was no stratification in the blender. Figures 2.14 and 2.15 show the calibration curves of sensors 1 and 2 for the positive and negative wave tests, respectively. The time-averaged and vertically averaged voltages are represented by dots and the mean ± one standard deviation is represented by circles. The first three data points were fitted

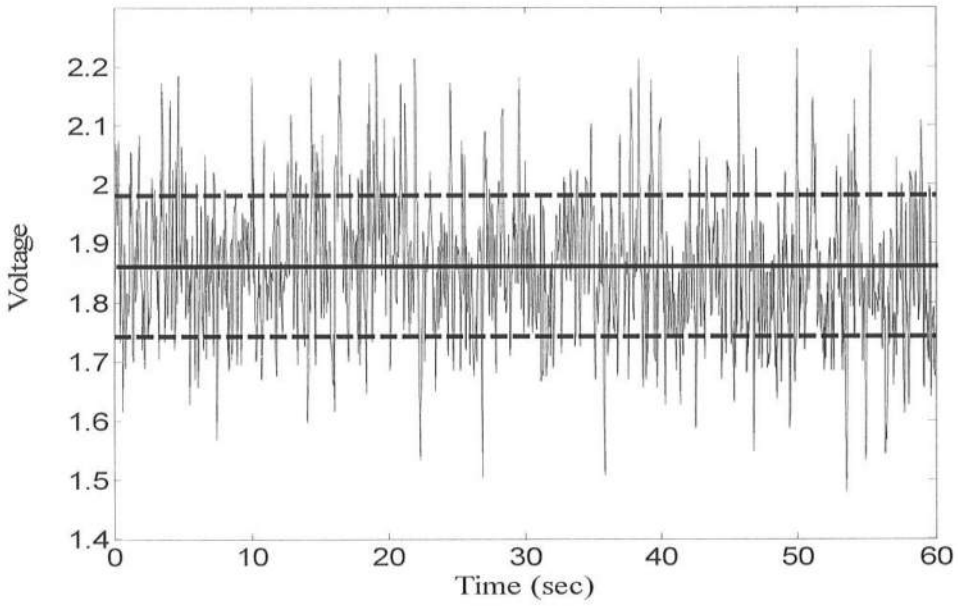

Figure 2.13: Sample FOBS-7 Time Series Used for Calibration

with a linear line, while the other five points were fitted with a second degree polynomial for the positive solitary wave calibration. For sensor 2 for the negative solitary wave calibration, the first four points were fitted with a linear line, while the next four points were fitted with a second degree polynomial.

2.8 EXPERIMENTAL PROCEDURE

The following is a summarization of the experimental procedures for tests P1-P8. The initial beach profile was measured and the eight wave gauges, two ADVs and two sediment concentration sensors were placed at specific locations on the beach. A positive wave was then generated and all data was collected at a rate of 20 Hz for 200 seconds which exceeded the duration of the wave action sufficiently. In

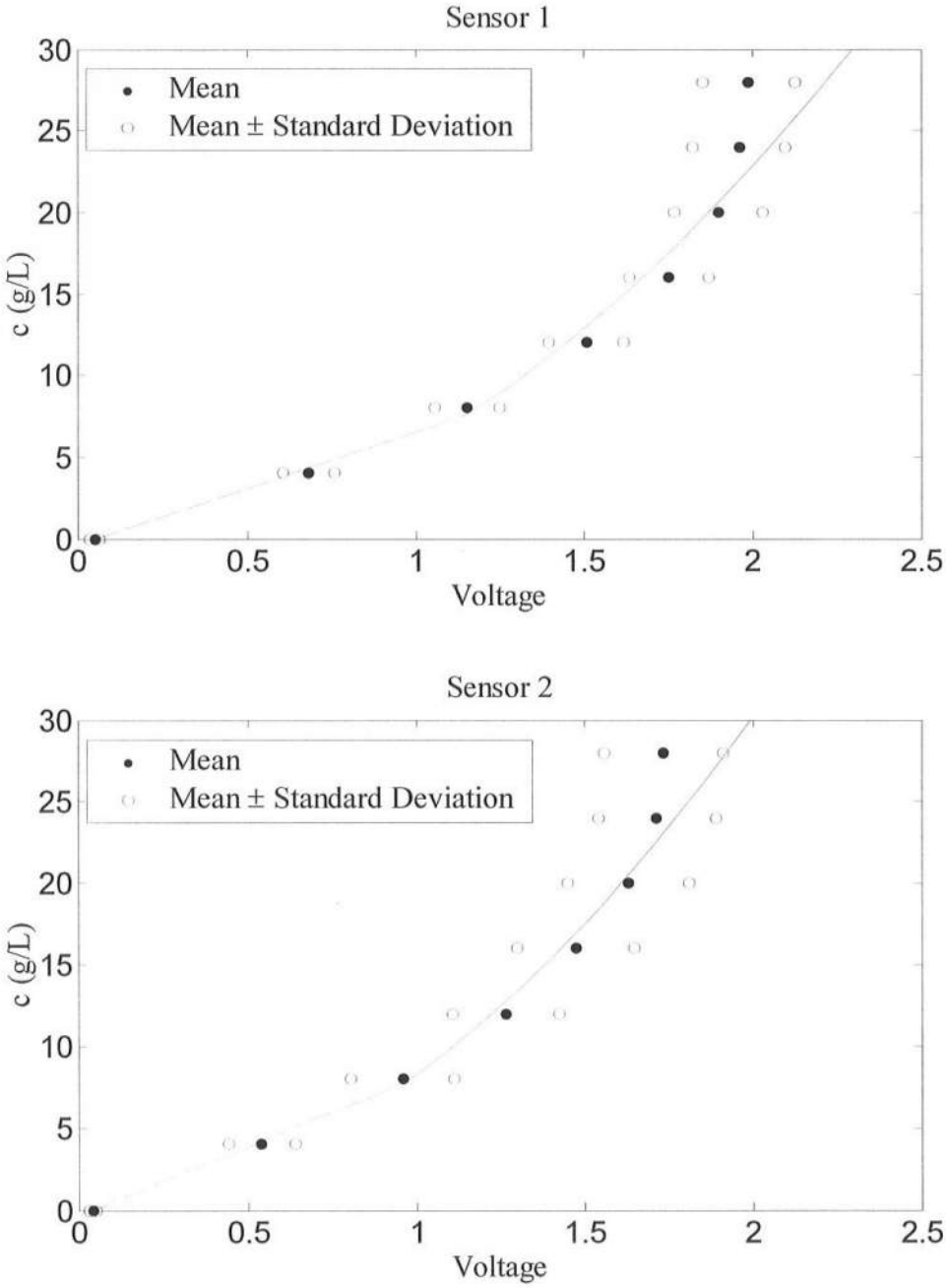

Figure 2.14: FOBS-7 Calibration Curves for Positive Solitary Wave Tests

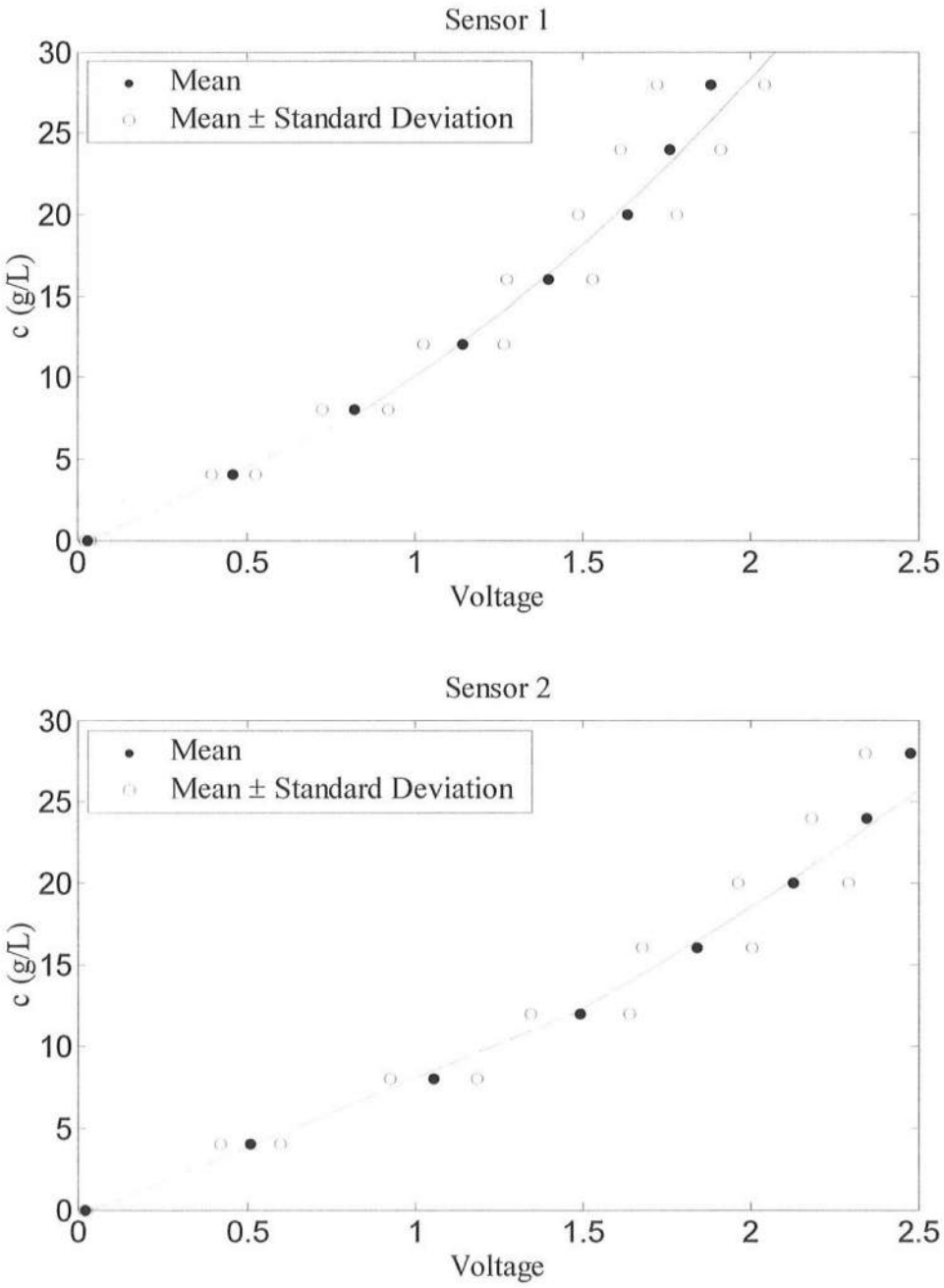

Figure 2.15: FOBS-7 Calibration Curves for Negative Solitary Wave Tests

order to allow the synchronous data collection for each test, the wavemaker, wave gauges, ADVs and FOBS-7 were attached to a 16 channel National Instruments data acquisition board. The beach profile was measured to quantify the vertical profile change on the order of 1.0 cm. The elevations of the velocimeter and concentration sensors were adjusted to measure the velocities and concentrations at an elevation of 6.0 cm above the deformed bottom. The subsequent solitary wave was generated on the deformed beach to assess the effects of the evolving beach profile on the solitary wave transformation and beach profile change. The beach was exposed to eight positive solitary waves at the end of test P8. After tests P1-P8, the beach was reconstructed to a 1:12 slope and the initial beach profile was measured before the eight negative solitary wave tests. The experimental procedure for tests N1-N8 is the same as for tests P1-P8 except for the incident solitary wave which was negative.

Chapter 3

POSITIVE SOLITARY WAVE TESTS

3.1 INCIDENT SOLITARY WAVE

The temporal variations of the free surface elevation η_1 above SWL measured by wave gauge 1 for tests P1-P8 where time $t=0$ at the start of the wave paddle movement, as shown by Figure 2.3, is given in Figure 3.1. The backward paddle movement caused the decrease $\eta_{\text{down}} = -0.25$ cm of the water level for the eight tests. The wave height H measured from the decreased water level to the wave crest elevation was in the range of 21.2 – 21.9 cm. Use is made of the average wave height $H = 21.6$ cm in the following. The arrival time $t_{\max}$ of the wave crest was $t_{\max} = 43.9$ s for all the tests. The values of η_{down}, H, and t_{max} for each test are summarized in Table 3.1. Table 3.1 shows the repeatability of the solitary wave generation within errors of 2%. The theoretical solitary wave profile [e.g., Goring, 1978] plotted in Figure 3.1 is given by

$$\eta_1(t) = H \operatorname{sech}^2\left[\left(\frac{3H}{4h}\right)^{1/2}\frac{C}{h}(t - t_{\max})\right] + \eta_{\text{down}} \tag{1}$$

with

$$C = \left[g\left(H + h\right)\right]^{1/2} \tag{2}$$

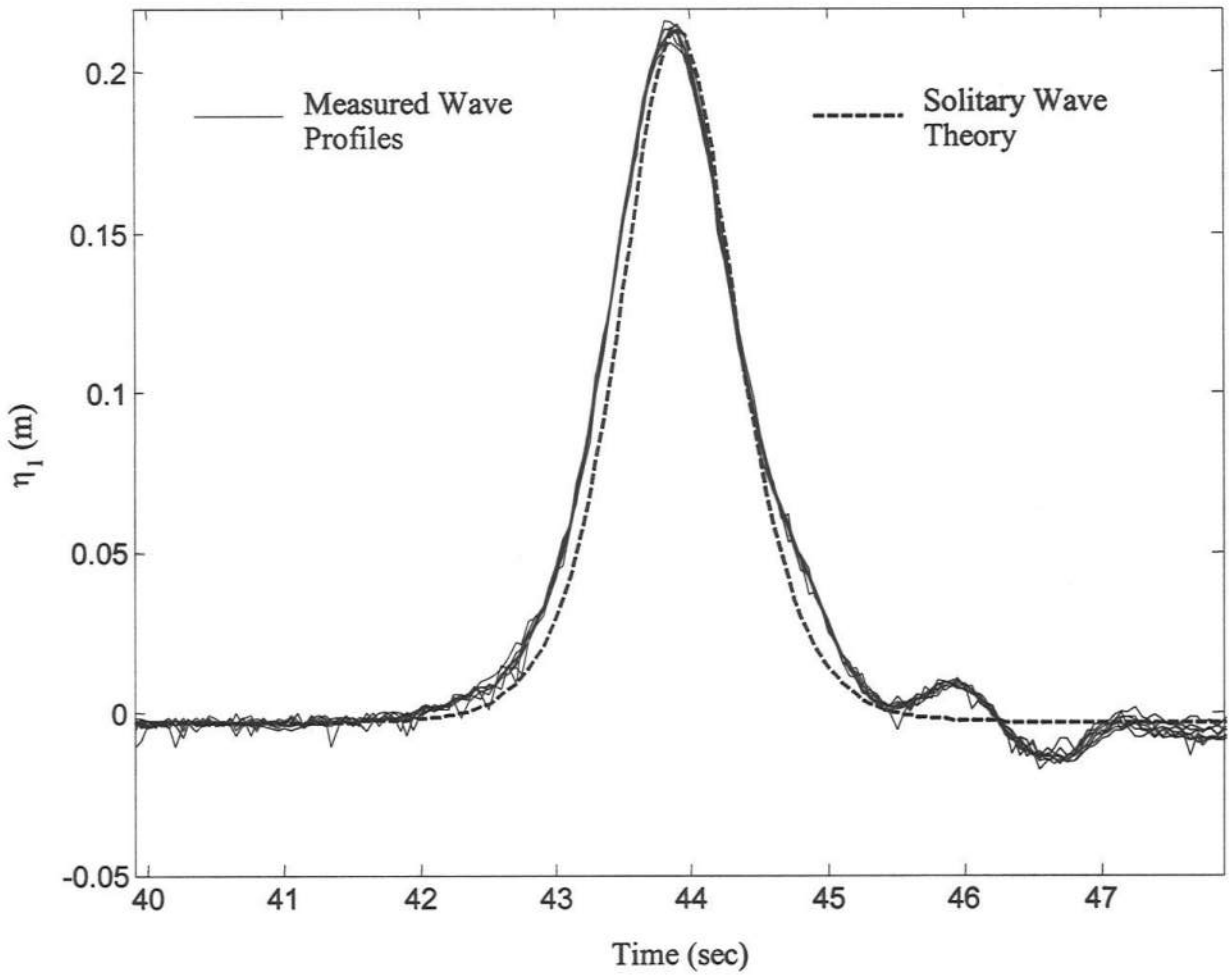

Figure 3.1: Measured and Theoretical Positive Solitary Wave Profiles at Wave Gauge 1

Table 3.1: Incident Positive Solitary Wave at Wave Gauge 1 for Tests P1-P8

Test	h (cm)	η_{down} (cm)	H (cm)	t_{max} (sec)	C (m/s)
P1	80.0	-0.25	21.7	43.9	3.16
P2	80.0	-0.25	21.6	43.9	3.16
P3	80.0	-0.25	21.6	43.9	3.16
P4	80.0	-0.25	21.2	43.9	3.15
P5	80.0	-0.25	21.5	43.9	3.16
P6	80.0	-0.25	21.6	43.9	3.16
P7	80.0	-0.25	21.6	43.9	3.16
P8	80.0	-0.25	21.9	43.9	3.16
Mean	80.0	-0.25	21.6	43.9	3.16

where g is the gravitation acceleration, the still water depth h is 80 cm at wave gauge 1 and the solitary wave celerity C is 316 cm/s. The generated solitary wave profiles are practically identical and slightly wider than the theoretical profile given by (1).

Several parameters were used to show that the incident solitary wave was practically the same for tests P1-P8; the ratio σ between horizontal and vertical length scales as defined by Kobayashi and Karjadi [1994], the solitary wave period T, the surf similarity parameter ξ, the solitary wave runup height R, and the Dean Number D. The range of σ = 16.3-16.9 for tests P1-P8 as listed in Table 3.2 implies that the horizontal length scale is much larger than the vertical length scale. The solitary wave period T was introduced by Kobayashi and Karjadi [1994] who examined the similarity and difference of solitary and regular waves breaking on a smooth uniform slope $\tan\theta$. The solitary wave period T is defined such that $(\eta_1 - \eta_{down}) > 0.05H$ for $(t_{max} - T/2) < t < (t_{max} + T/2)$. This definition of T with (1) yields $T = 2.5$ s as shown in Table 3.2. The surf similarity parameter ξ defined as $\xi = \tan\theta/(H/L_0)^{1/2}$

with $L_0 = gT^2/(2\pi)$ is 0.55 for $\tan\theta = 1/12$. The value of $\xi = 0.55$ suggested that the solitary wave would break as a plunging breaker. The solitary wave runup height R above SWL estimated using the empirical formula $R/H = 2.955\xi^{0.395}$ [Kobayashi and Karjadi, 1994] is 50.4 cm and much larger than the regular wave runup height R = 12 cm estimated using the empirical formula $R/H = \xi$. The predicted value of R = 50 cm was used before the tests to determine the height of the sand beach required for no wave overwash. In addition, the Dean number $D = H/(w_f T)$ with the sediment fall velocity $w_f = 2$ cm/s is 4.4 which suggested beach erosion for regular waves [Dalrymple, 1992]. It may be noted that this criterion based on the value of D suggested the difficulty in producing beach accretion using the positive solitary wave whose height is larger than approximately 10 cm. This prompted us to conduct the negative solitary wave tests in this study.

Table 3.2: Representative Wave Period and Estimated Wave Runup and Dean Number

Test	σ	T (sec)	ξ	R (cm)	D
P1	16.4	2.45	0.546	50.6	4.44
P2	16.5	2.46	0.550	50.4	4.40
P3	16.5	2.45	0.549	50.4	4.41
P4	16.9	2.48	0.562	49.9	4.26
P5	16.6	2.46	0.552	50.3	4.38
P6	16.5	2.46	0.550	50.4	4.40
P7	16.6	2.46	0.551	50.4	4.39
P8	16.3	2.44	0.543	50.8	4.49
Mean	16.6	2.46	0.550	50.4	4.40

3.2 MEASURED BEACH PROFILES

Figure 3.2 shows the measured beach profiles and the locations of the eight wave gauges (G1-G8) for tests P1-P8. The profile change from the initial profile was approximately proportional to the number of solitary waves indicated by the numeral next to the letter *P*, which is illustrated in Figure 3.3. The solitary wave at wave gauge 1, shown in Figure 3.1, plunged near wave gauge 5 and caused considerable sediment suspension and large runup. The jet from the plunging breaker impinged on the front face of the wave as photographed by Li and Raichlen [2003]. The strong downrush following the large runup resulted in erosion on the foreshore and deposition seaward of wave run-down. The wave runup height was approximately 0.5 m above SWL but the visible beach erosion in Figure 3.2 was limited to the elevation of about 0.3 m above SWL. The depth and area of erosion and deposition in Figure 3.2 are discussed later after the other measurements are presented.

3.3 CROSS-SHORE WAVE TRANSFORMATION

Figures 3.4-3.7 show the measured time series of the free surface elevation η_j above SWL at wave gauge $j = 1 - 6$ for tests P1-P8 where the instantaneous water depths h_7 and h_8 are plotted because the bed elevations at wave gauges 7 and 8 were above SWL during the tests, as shown in Figure 3.2. The water depth h in the region above SWL is relative to the local bed at the start of each test because the buried wave gauge was calibrated before each test. The negative value of h at the end of each test corresponded approximately to the erosion depth of the local bed. Each

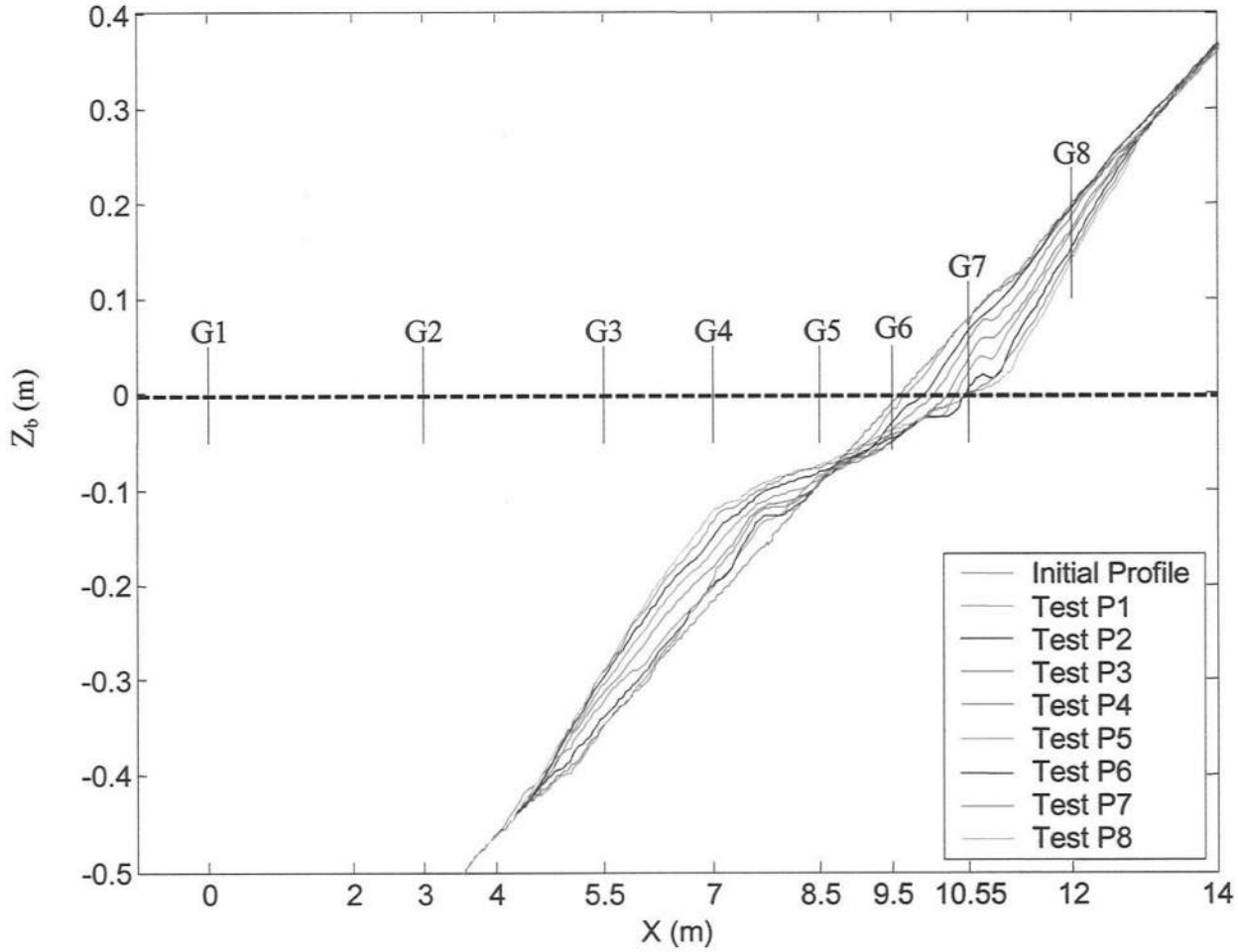

Figure 3.2: Measured Beach Profiles and Wave Gauge Locations for Tests P1-P8

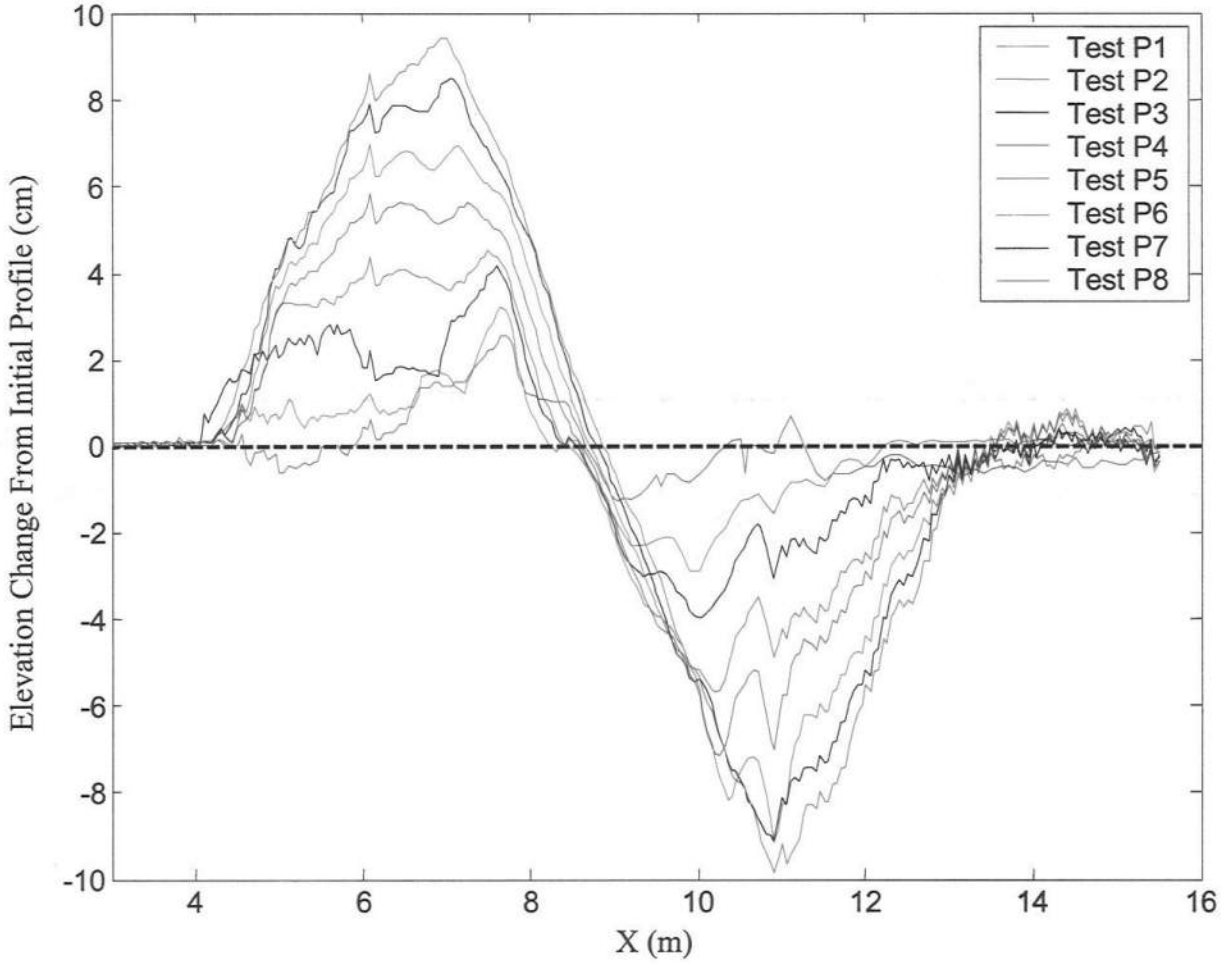

Figure 3.3: Elevation Change from Initial Profile for Tests P1-P8

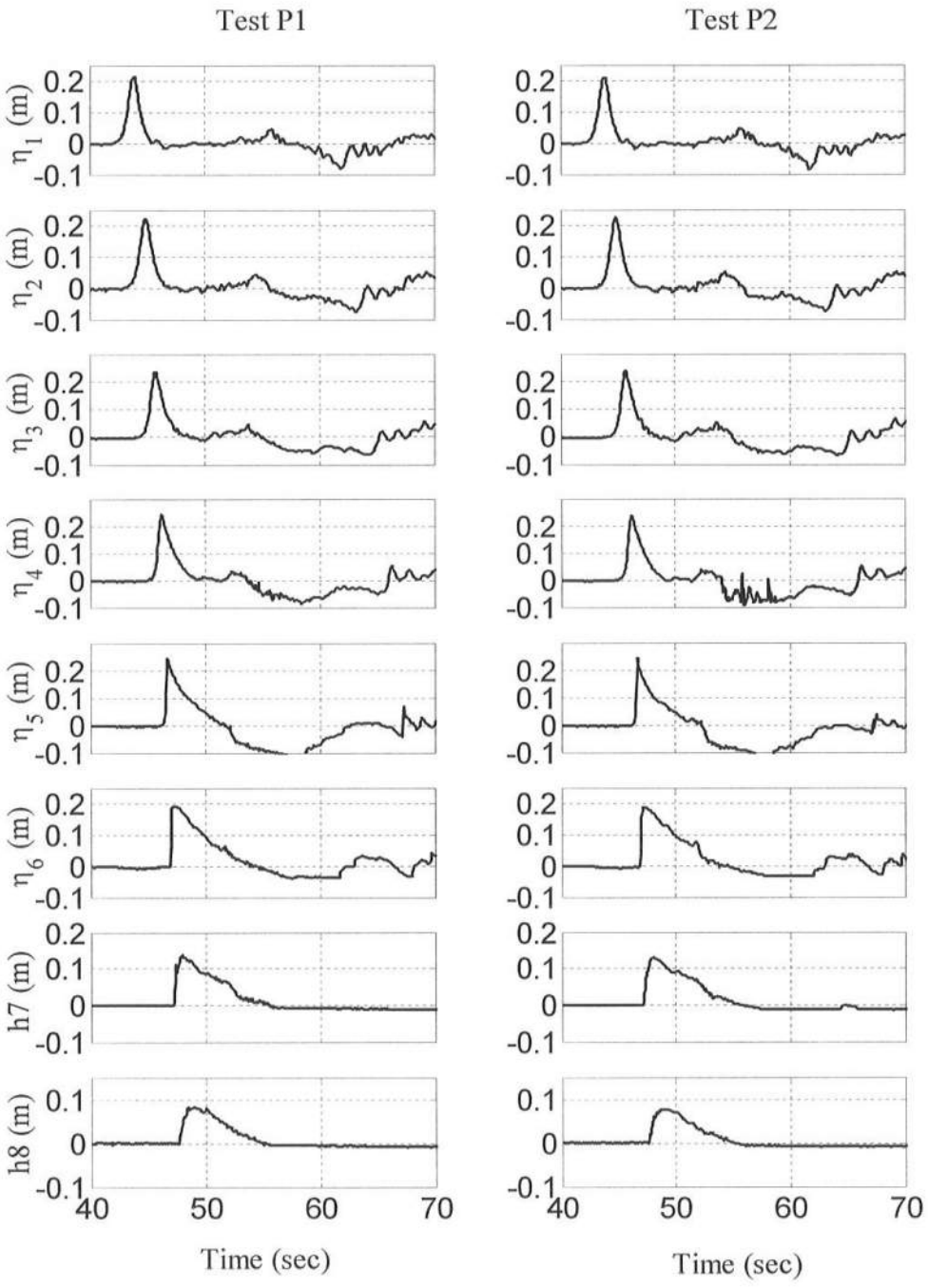

Figure 3.4: Measured Free Surface Elevations at Wave Gauges 1-6 and Water Depth at Wave Gauges 7 and 8 for Tests P1 and P2

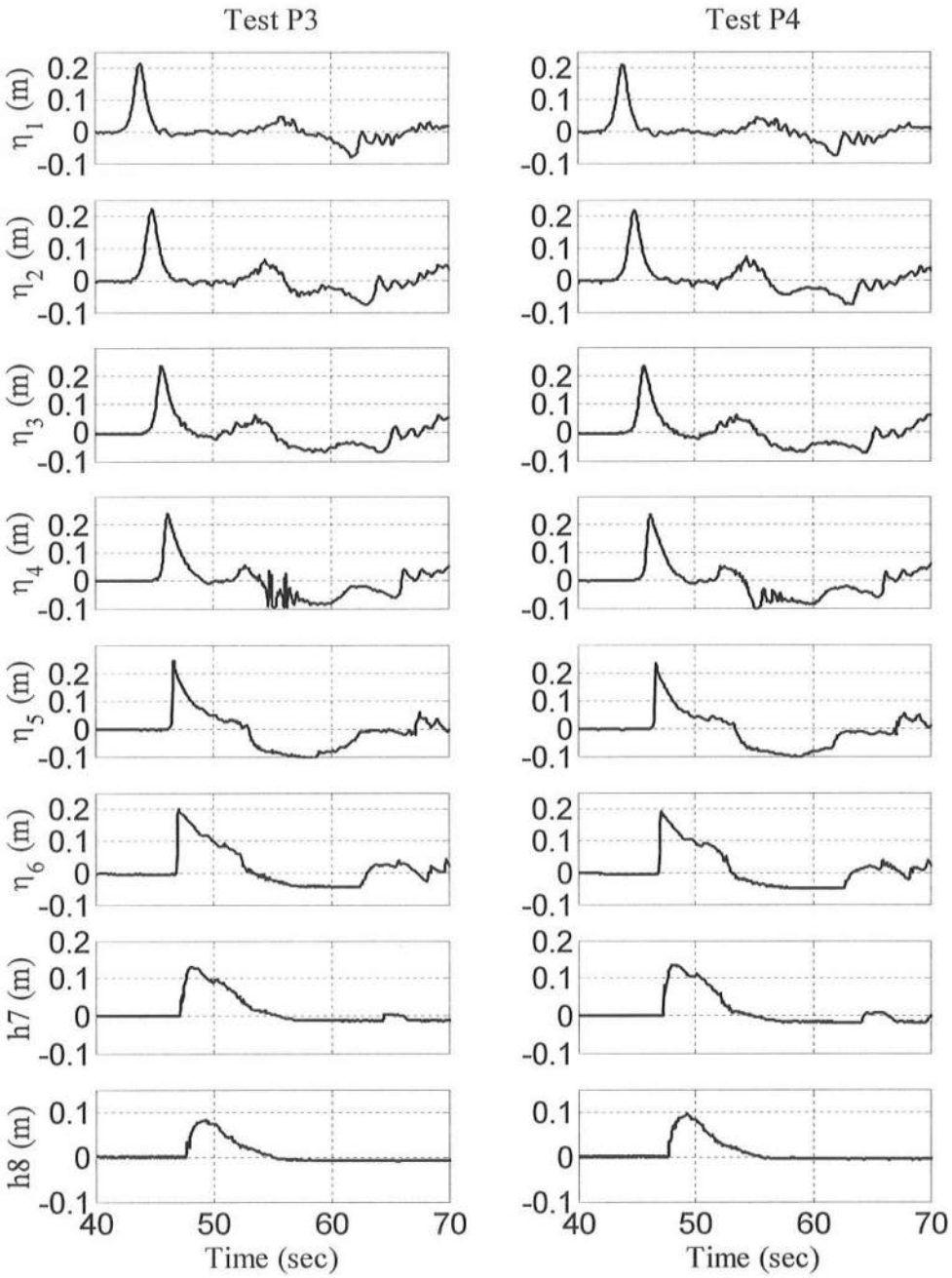

Figure 3.5: Measured Free Surface Elevations at Wave Gauges 1-6 and Water Depth at Wave Gauges 7 and 8 for Tests P3 and P4

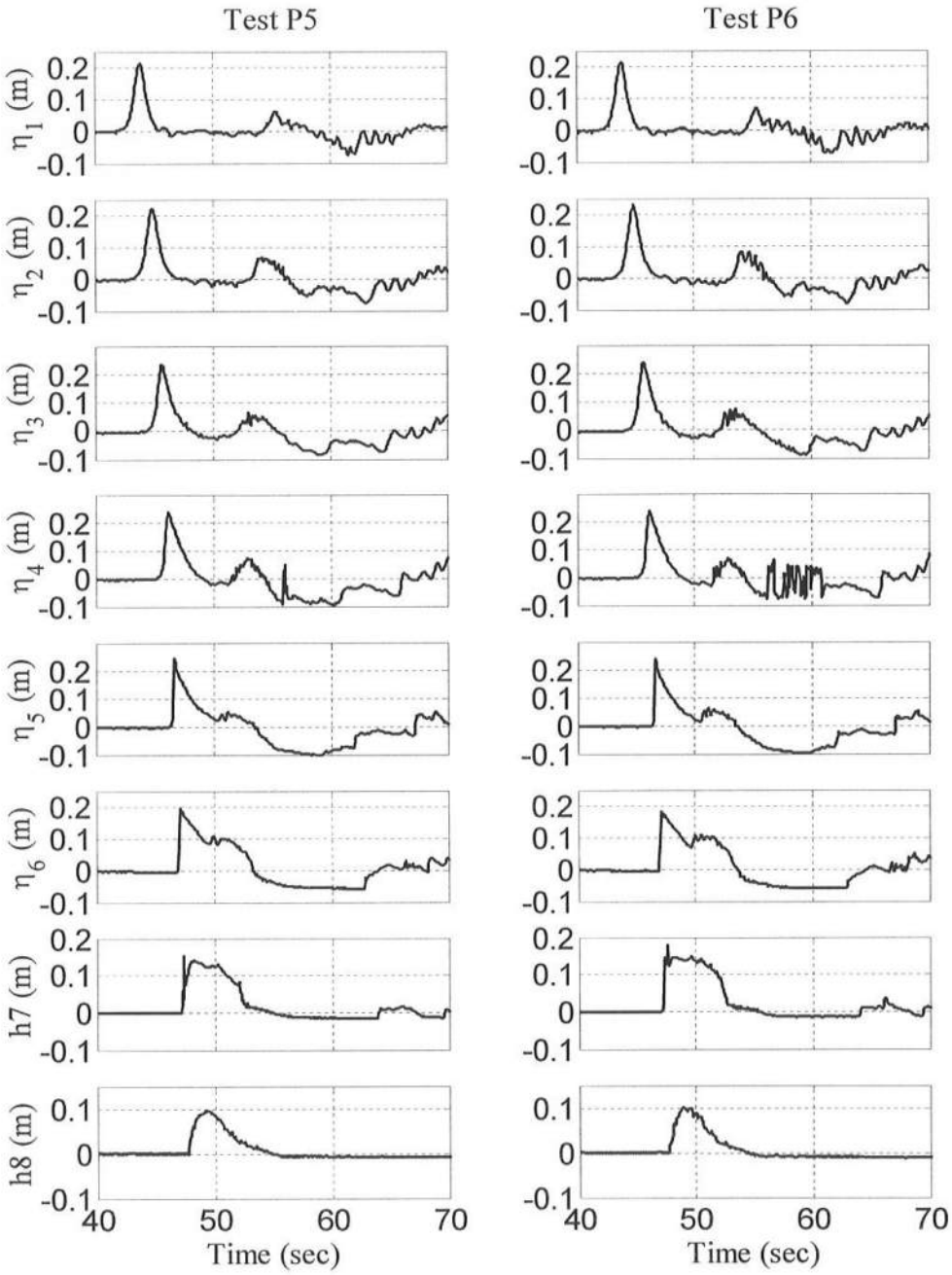

Figure 3.6: Measured Free Surface Elevations at Wave Gauges 1-6 and Water Depth at Wave Gauges 7 and 8 for Tests P5 and P6

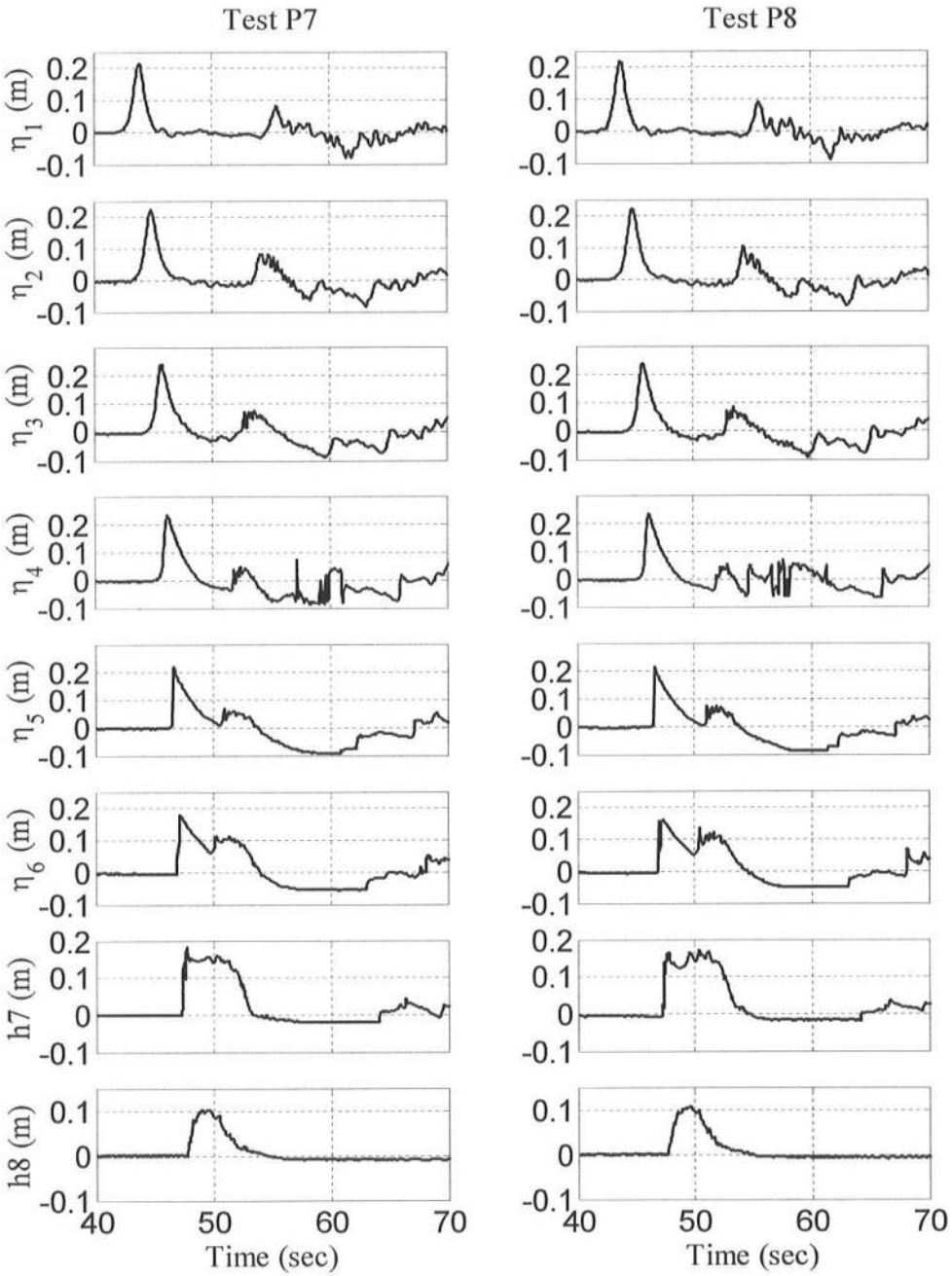

Figure 3.7: Measured Free Surface Elevations at Wave Gauges 1-6 and Water Depth at Wave Gauges 7 and 8 for Tests P7 and P8

figure depicts the steepening and breaking of the shoaling solitary wave front and the solitary wave runup and reflection from the foreshore. The decrease of the free surface elevation below SWL at wave gauges 3-6 for the duration $55 < t < 60$ s occurred during the strong downrush following the large runup. Table 3.3 lists the maximum free surface elevation η_{max} at wave gauges 1-6 and the maximum water depth h_{max} at wave gauges 7 and 8. A slight landward shift of the breaking point may be discernible on the basis of the maximum value of η_{max}. The water depth at gauges 7 and 8 increased due to erosion. There was little change at gauges 1-4.

Table 3.3: Maximum Free Surface Elevation, η_{max} (cm) at Wave Gauges 1-6 and Water Depth h_{max} (cm) at Wave Gauges 7 and 8 for Tests P1-P8

Gauge	x (m)	Test P1	Test P2	Test P3	Test P4	Test P5	Test P6	Test P7	Test P8
1	0	21.5	21.3	21.4	20.9	21.3	21.3	21.3	21.6
2	3	22.3	22.6	22.3	21.8	22.2	23.1	22.0	22.2
3	5.5	23.6	23.9	23.5	23.3	23.3	23.6	23.8	23.9
4	7	24.0	24.3	23.7	23.4	23.7	23.6	23.3	23.2
5	8.5	24.4	23.2	24.4	23.4	24.2	23.5	21.6	21.4
6	9.55	19.7	19.0	19.8	19.3	19.6	18.3	17.6	16.0
7	10.55	13.7	12.8	12.8	13.5	15.5	17.8	18.3	17.0
8	12	8.4	8.1	8.0	9.4	9.6	10.1	10.1	10.7

Figure 3.8 shows the arrival time t_{max} of the solitary wave crest at wave gauges 1-8 for tests P1-P8 where the onshore distance x from wave gauge 1 is used to indicate the location of each wave gauge depicted in Figure 3.2. The solid line in Figure 3.8 expresses the sum of x/C and t_{max} at wave gauge 1 where the celerity $C = 3.16$ m/s is calculated using (2) with $H = 21.6$ cm and $h = 80$ cm at wave gauge 1. The solitary wave propagated over the relatively short distance of 8.5 m between wave gauges 1-5 with little adjustment to the local depth before it slowed down during its uprush on the foreshore. The values of t_{max} at wave gauges 7 and 8 located at x = 10.55 and 12 m, respectively, are affected by the foreshore profile change. Table 3.4 summarizes the values of t_{max} for each test at wave gauges 1-8.

Table 3.4: Time t_{max} (sec) When $\eta = \eta_{max}$ at Wave Gauges 1-6 and $h = h_{max}$ at Wave Gauges 7 and 8 for Tests P1-P8

Gauge	x (m)	Test P1	Test P2	Test P3	Test P4	Test P5	Test P6	Test P7	Test P8
1	0	43.9	43.9	43.9	43.9	43.9	43.9	43.9	43.9
2	3	44.9	44.9	44.9	44.9	44.9	44.9	44.9	44.9
3	5.5	45.7	45.7	45.7	45.7	45.7	45.7	45.7	45.7
4	7	46.2	46.2	46.2	46.2	46.2	46.2	46.2	46.2
5	8.5	46.7	46.7	46.7	46.7	46.7	46.7	46.7	46.7
6	9.55	47.1	47.1	47.1	47.1	47.1	47.2	47.2	47.3
7	10.55	48.0	48.1	48.2	48.2	47.4	47.6	47.7	47.7
8	12	49.0	49.1	49.3	49.3	49.4	49.5	49.4	49.6

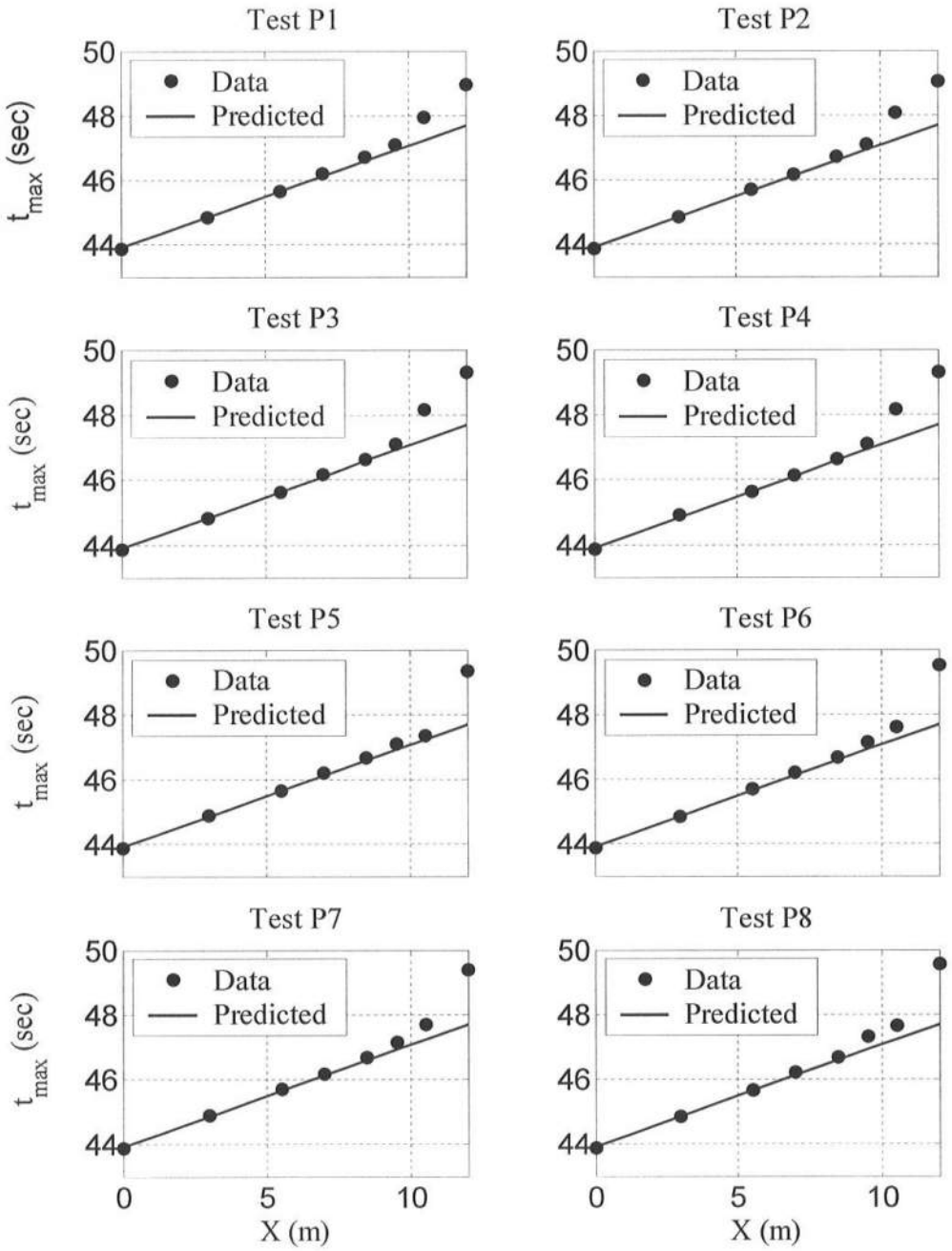

Figure 3.8: Arrival Time t_{max} of Positive Solitary Wave Crest at Wave Gauges 1-8 for Tests P1-P8

Figure 3.9 shows the cross-shore variation of the wave crest elevation $\eta_{\max}$ above SWL for tests P1-P8 where the solid line in these figures is the average profile of the measured profiles before and after each test. The positive solitary wave transformation on the average profile of each test was determined using Tables 3.5 and 3.6, with P0 corresponding to the initial beach profile. The maximum free surface elevation η_{max} for gauges 7 and 8 is given by $\eta_{max} = h_{max} + (Z_b)_{average}$ where $(Z_b)_{average}$ is the average value of the bottom elevations listed in Table 3.6 before and after each test. The wave crest elevation increased slightly from wave gauge 1 to wave gauge 5 and decreased due to wave plunging near the still water shoreline. The linear extrapolation of the values of $\eta_{\max}$ at x = 10.55 and 12 m crudely indicates the extent of wave runup on the foreshore.

Table 3.5: Maximum Free Surface Elevation η_{max} (cm) at Wave Gauges 1-8 for Tests P1-P8

Gauge	x (m)	Test P1	Test P2	Test P3	Test P4	Test P5	Test P6	Test P7	Test P8
1	0	21.5	21.3	21.4	20.9	21.3	21.3	21.3	21.6
2	3	22.3	22.6	22.3	21.8	22.2	23.1	22.0	22.2
3	5.5	23.6	23.9	23.5	23.3	23.3	23.6	23.8	23.9
4	7	24.0	24.3	23.7	23.4	23.7	23.6	23.3	23.2
5	8.5	24.4	23.2	24.4	23.4	24.2	23.5	21.6	21.4
6	9.55	19.7	19.0	19.8	19.3	19.6	18.3	17.6	16.0
7	10.55	21.7	20.1	18.9	18.3	18.7	19.3	18.6	17.0
8	12	28.1	27.5	27.0	27.4	26.7	26.2	25.1	25.1

Table 3.6: Measured Bottom Elevation Z_b (cm) Before and After Tests P1-P8

Gauge	x (m)	Test P0	Test P1	Test P2	Test P3	Test P4	Test P5	Test P6	Test P7	Test P8
1	0	-80.00	-80.00	-80.00	-80.00	-80.00	-80.00	-80.00	-80.00	-80.00
2	3	-54.75	-55.09	-54.61	-55.49	-53.67	-53.82	-53.51	-53.33	-53.57
3	5.5	-34.57	-34.59	-33.85	-33.33	-31.22	-30.38	-29.56	-28.96	-28.90
4	7	-21.69	-20.31	-20.06	-19.19	-18.31	-16.46	-14.97	-13.27	-12.27
5	8.5	-9.17	-8.50	-9.05	-9.10	-9.54	-8.93	-8.23	-7.71	-7.49
6	9.55	-0.45	-1.12	-2.56	-3.39	-4.53	-4.73	-4.43	-4.18	-3.61
7	10.55	7.90	7.99	6.63	5.55	4.08	2.43	0.59	-0.01	0.00
8	12	19.95	19.46	19.45	18.62	17.32	16.84	15.37	14.55	14.21

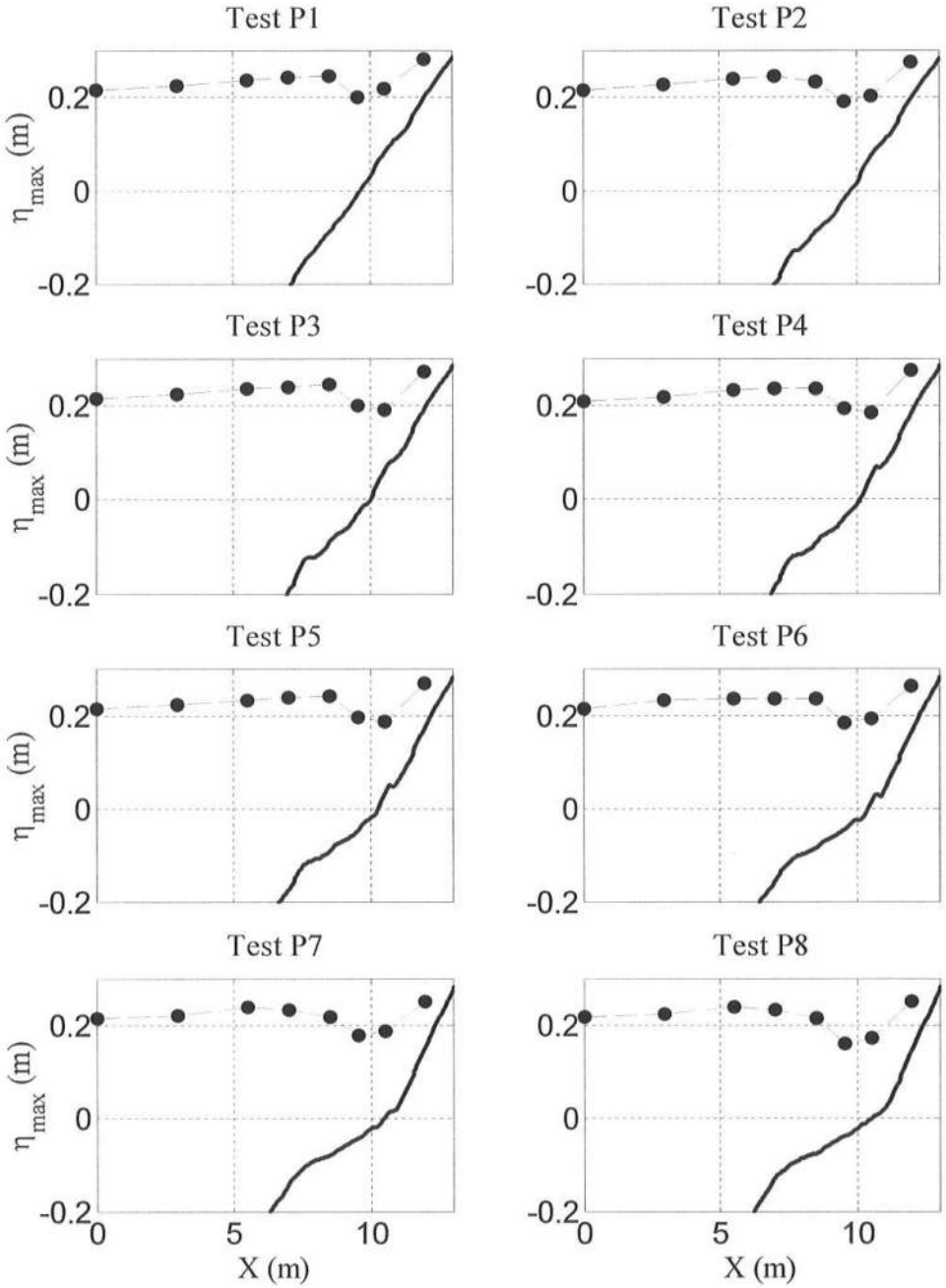

Figure 3.9: Cross-Shore Variation of Wave Crest Elevation above Measured Beach Profile for Tests P1-P8

3.4 VELOCITY AND CONCENTRATION DATA

The velocities and sand concentrations were measured at the elevation of 6 cm above the local bottom at the cross-shore location of wave gauge 3 in the region of deposition as shown in Figure 3.2. Figures 3.10-3.17 show the measured free surface elevation η_3, horizontal velocities u, alongshore velocities V, vertical velocity W, and suspended sediment concentrations c at wave gauge 3 for tests P1-P8. It is noted that the measured two time series of u, V and c are plotted in these figures. The reliable measurements of these quantities at the locations of wave gauges 4 and 5 were not possible due to the shallow depth during the wave downrush and the violent wave breaking near wave gauge 5. The measured alongshore and vertical velocities appeared noisy especially during the period of high sand concentrations as was observed by Giovannozzi and Kobayashi [2002] in their irregular wave experiments. However, there was no clear correlation between the high-frequency velocity fluctuations and high sand concentrations. On the other hand, the cross-shore velocities and sand concentrations measured at the two alongshore locations were essentially in phase apart from high frequency oscillations. The cross-shore velocity u and the sand concentration c presented in the following are the average of the measured time series at the two alongshore locations.

Figures 3.18-3.25 show the temporal variations of u and c together with the free surface elevation η_3 at wave gauge 3 for tests P1-P8. It is noted that the concentration of 26 g/ℓ corresponds to the volumetric concentration of 1%. The dotted line in the middle panel of Figures 3.18-3.25 is the cross-shore velocity u

predicted by solitary wave theory [e.g., Li and Raichlen, 2003]

$$u(t) = C_3\eta_3(t)/[\eta_3(t)+h_3] \quad ; \quad C_3 = [g(h_3+H_3)]^{1/2} \tag{3}$$

where h_3 and H_3 are the still water depth and solitary wave height at the location of wave gauge 3 during each test. The depth h_3 above the average bottom obtained from the measured profiles before and after each test decreased from 34.6 cm during test P1 to 28.9 cm during test P8. The wave height H_3 was in the range of 23.3 – 23.9 cm and varied very little. The solitary wave celerity at wave gauge 3 is about 239 cm/s, which is less than C at wave gauge 1 due to the smaller depth h_3 = 29 - 35 cm versus 80 cm. The incident solitary wave characteristics at wave gauge 3 are listed in Table 3.7. Equation (3), which is valid only for the solitary wave propagating landward, explains the correlation between $u(t)$ and $\eta_3(t)$ before the arrival of the reflected wave which caused the seaward velocity.

During the depression of η_3 for $55 < t < 65$ s in Figures 3.18-3.25 caused by the strong wave downrush, there was no clear correlation between η_3 and u perhaps because of the particular location of the velocity measurement which was 6 cm above the local bottom in Figure 3.2. The measured concentration c increased significantly during $60 < t < 65$ s due to the settling of sand particles suspended by plunging waves and advected seaward by the strong downrush. The measured time series of η_3, u and c are similar in each case except that the rise of c started somewhat earlier as the beach profile evolved. It is noted that sand particles were observed visually to move near the bed below the 6-cm elevation of the concentration measurement under the incident solitary wave with the onshore velocity of approximately 1 m/s.

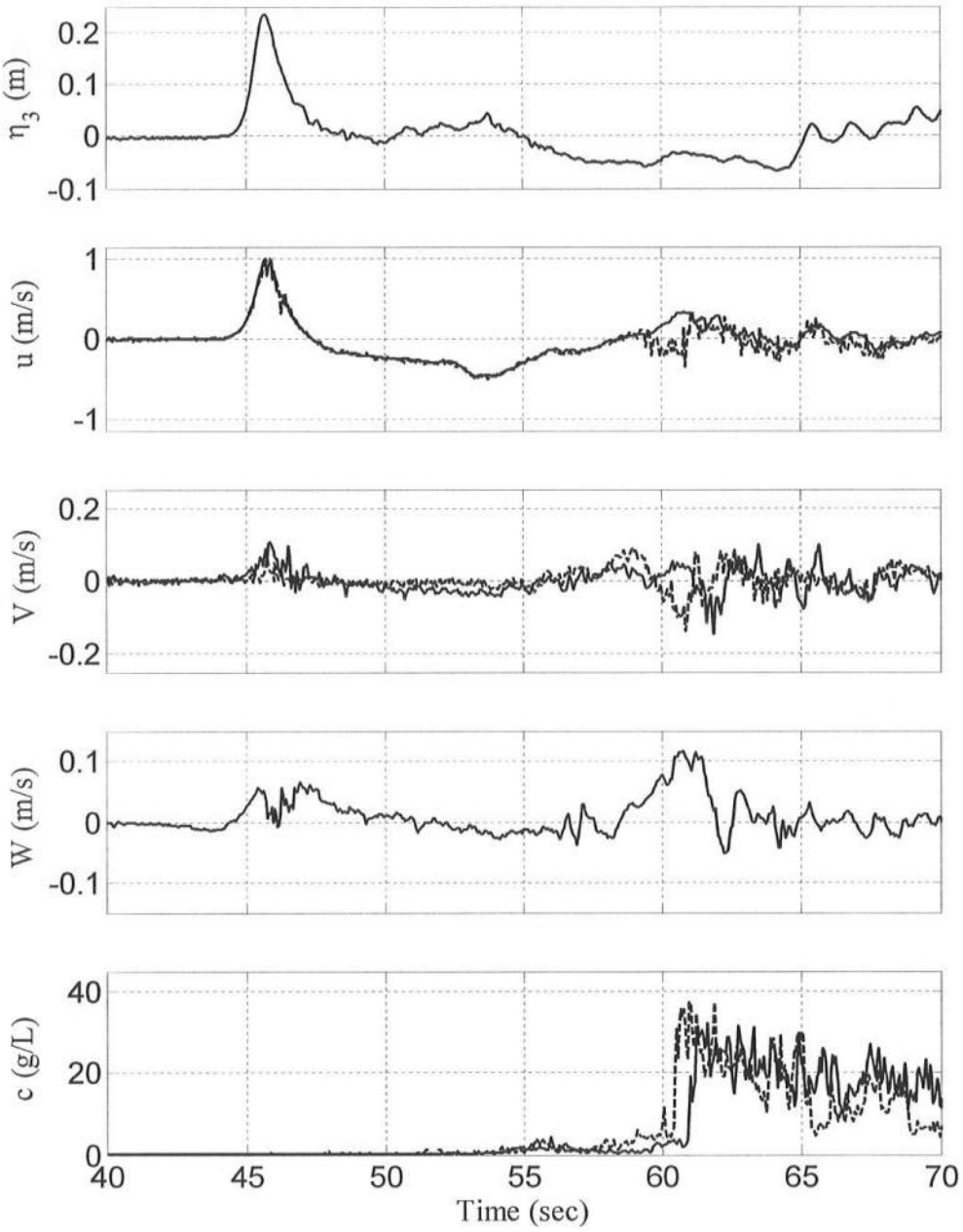

Figure 3.10: Measured Free Surface, Velocities and Sediment Concentrations for Test P1

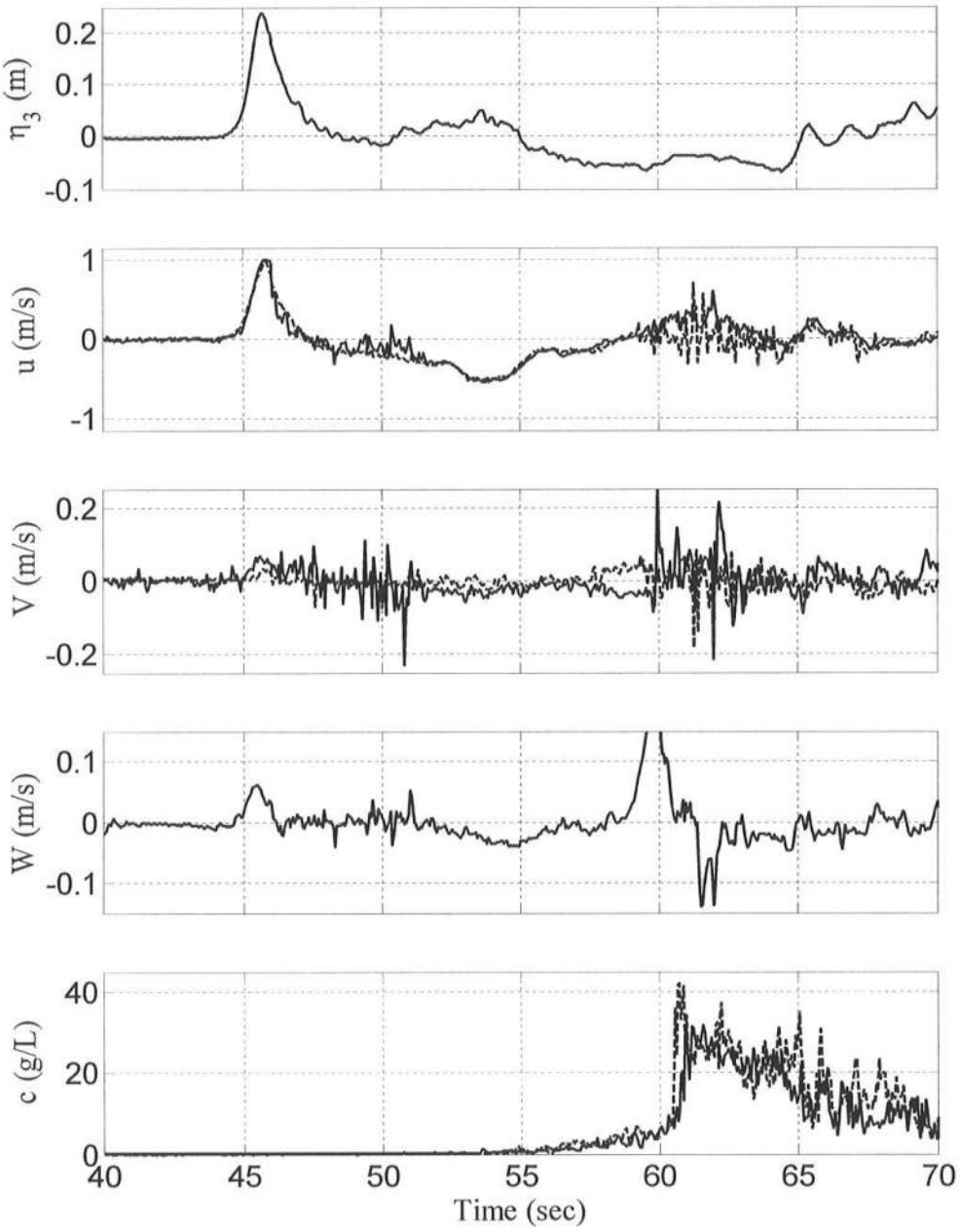

Figure 3.11: Measured Free Surface, Velocities and Sediment Concentrations for Test P2

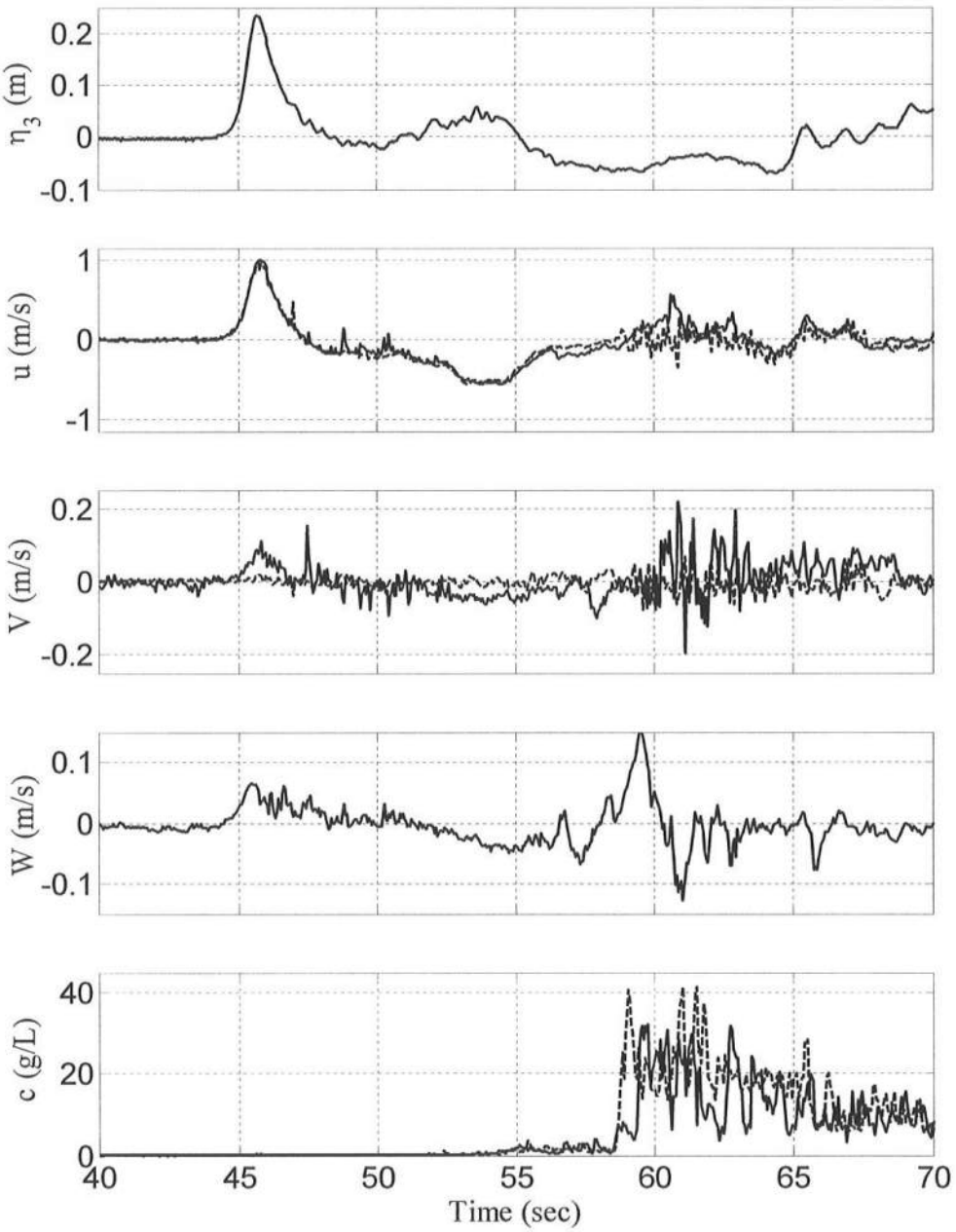

Figure 3.12: Measured Free Surface, Velocities and Sediment Concentrations for Test P3

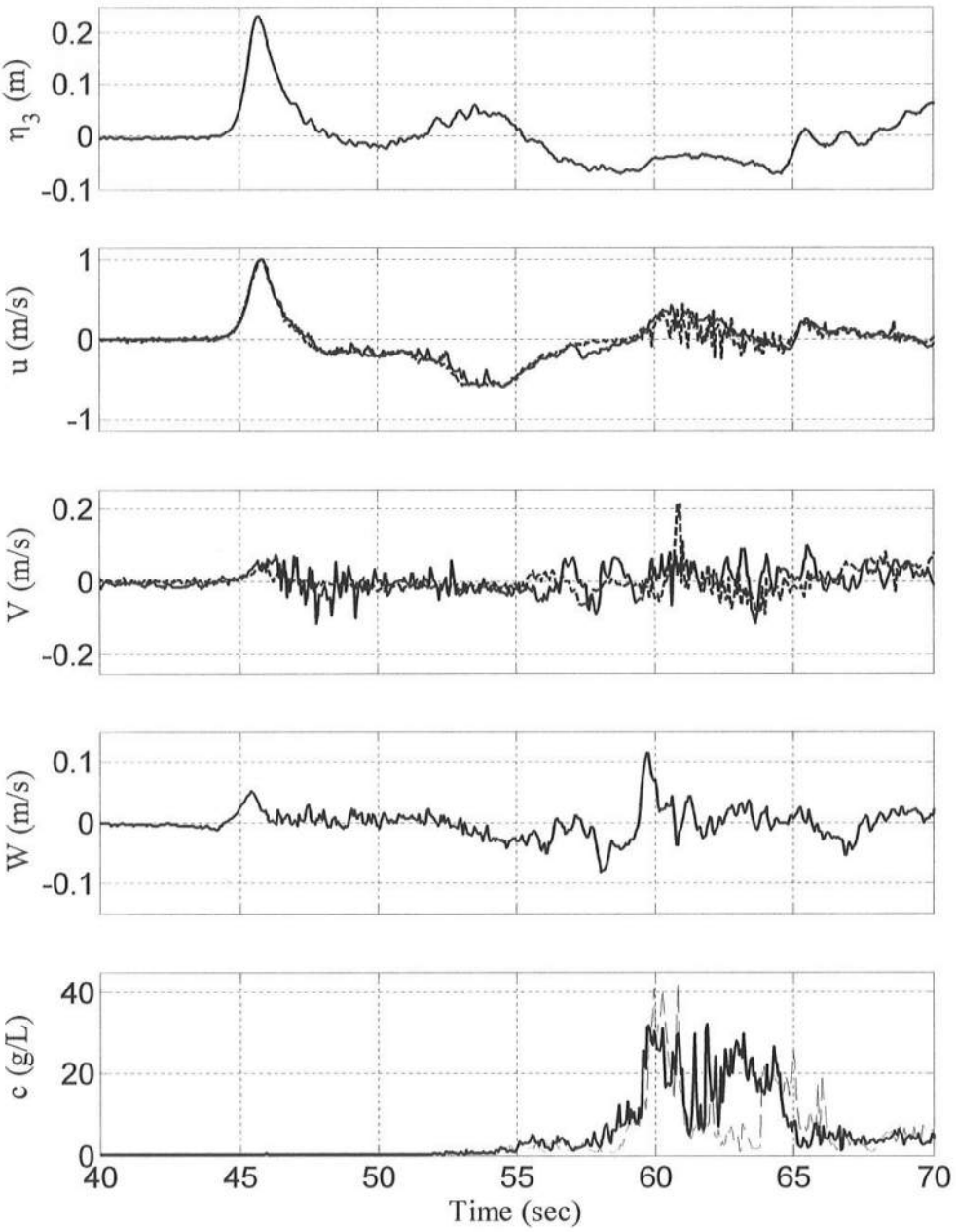

Figure 3.13: Measured Free Surface, Velocities and Sediment Concentrations for Test P4

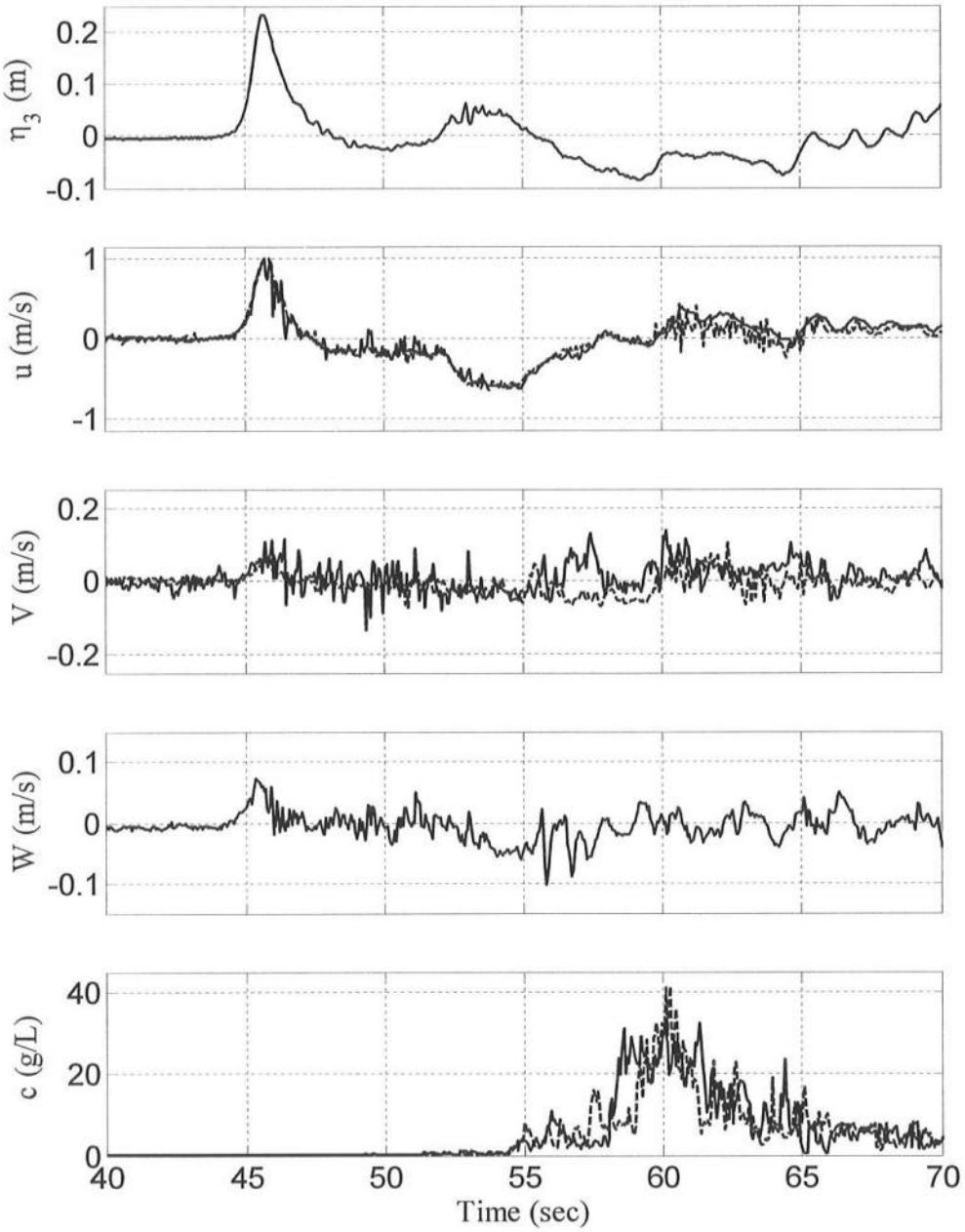

Figure 3.14: Measured Free Surface, Velocities and Sediment Concentrations for Test P5

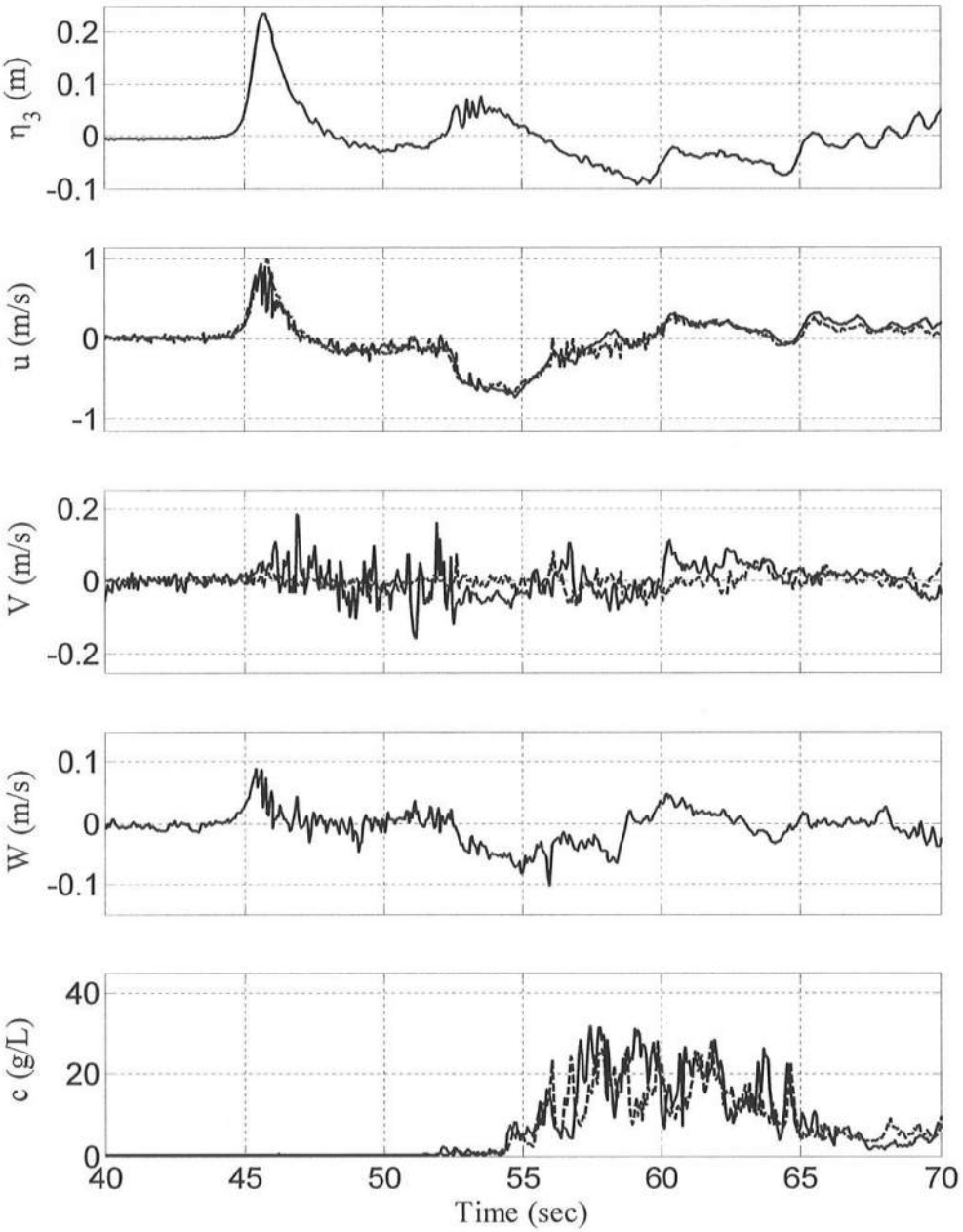

Figure 3.15: Measured Free Surface, Velocities and Sediment Concentrations for Test P6

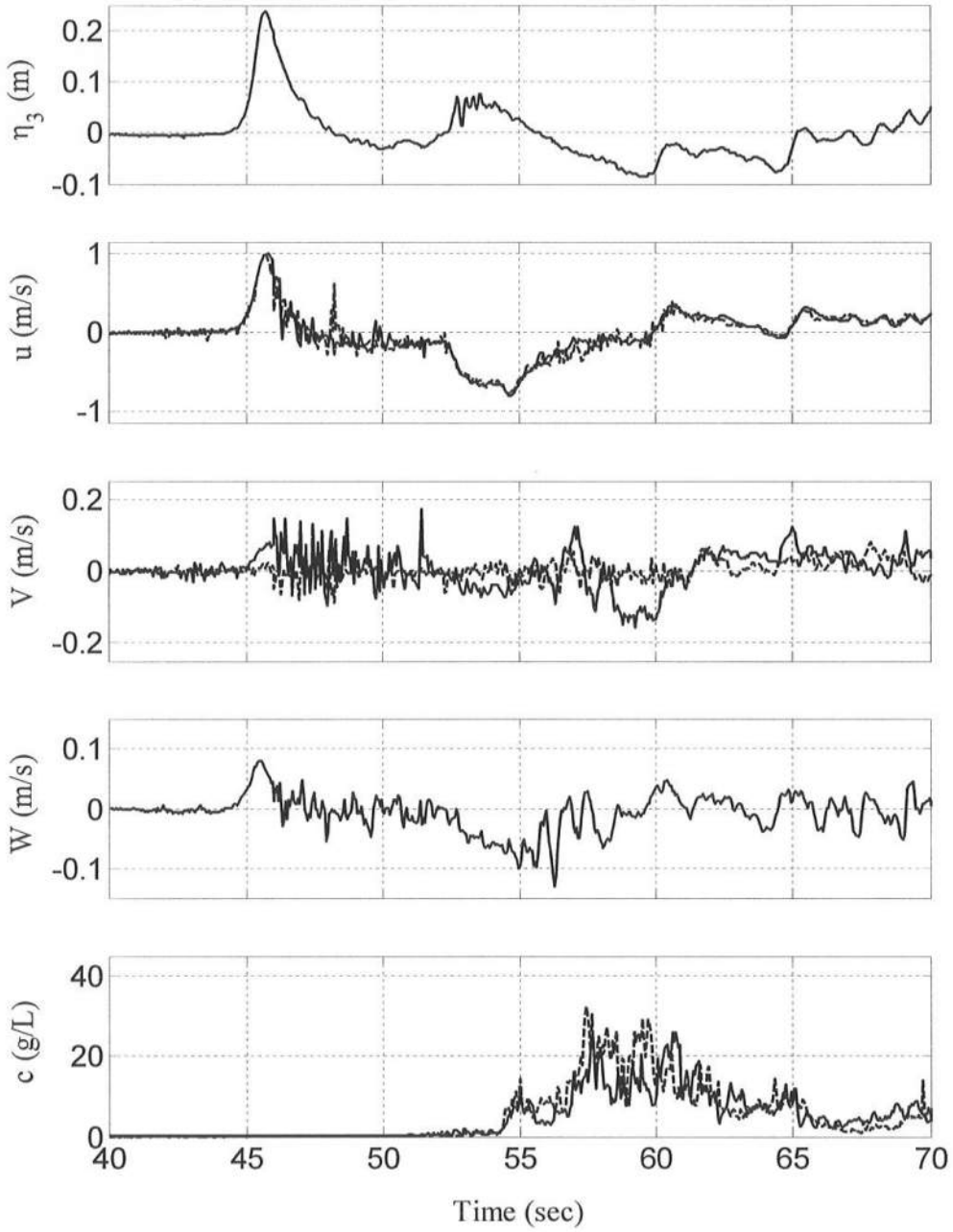

Figure 3.16: Measured Free Surface, Velocities and Sediment Concentrations for Test P7

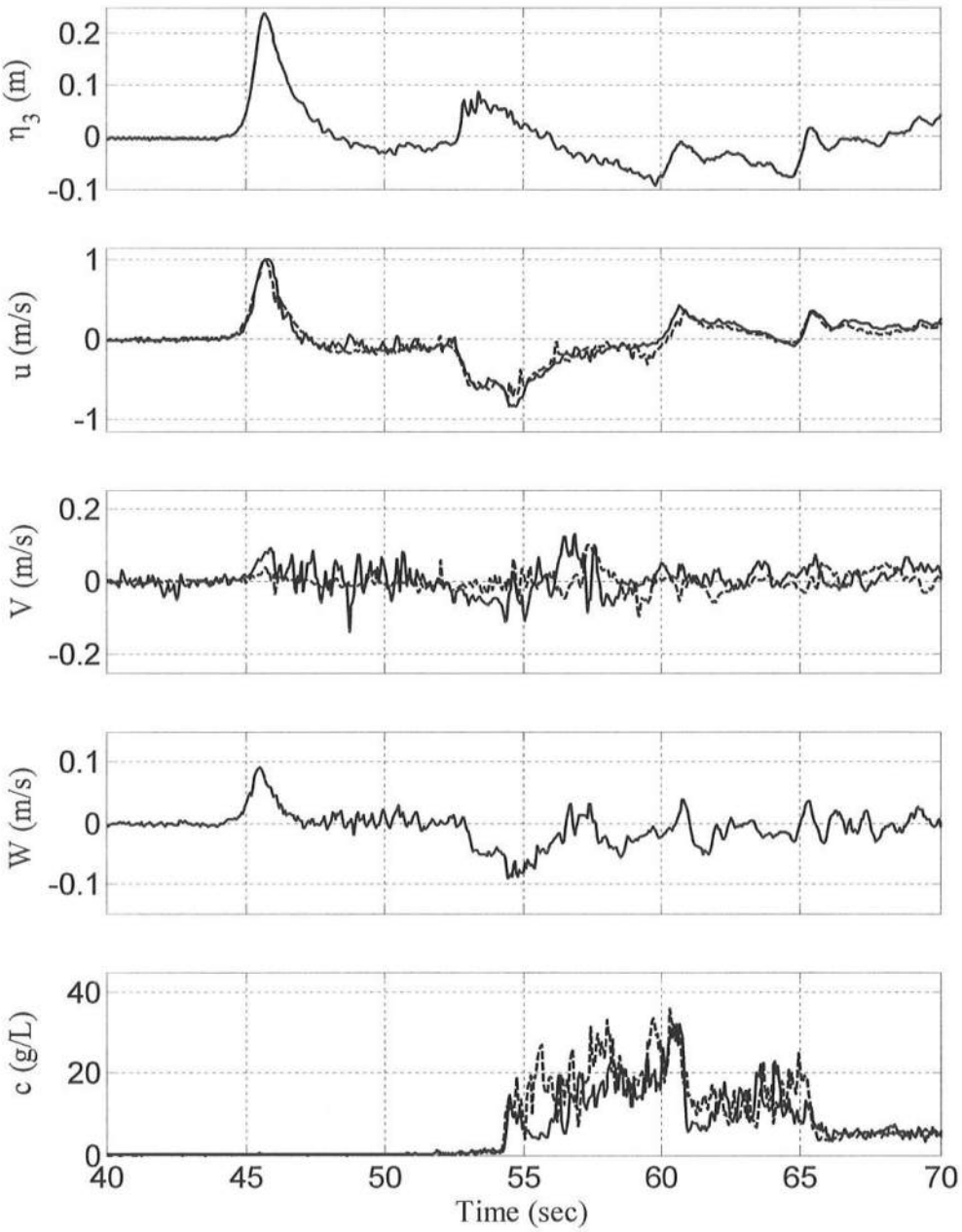

Figure 3.17: Measured Free Surface, Velocities and Sediment Concentrations for Test P8

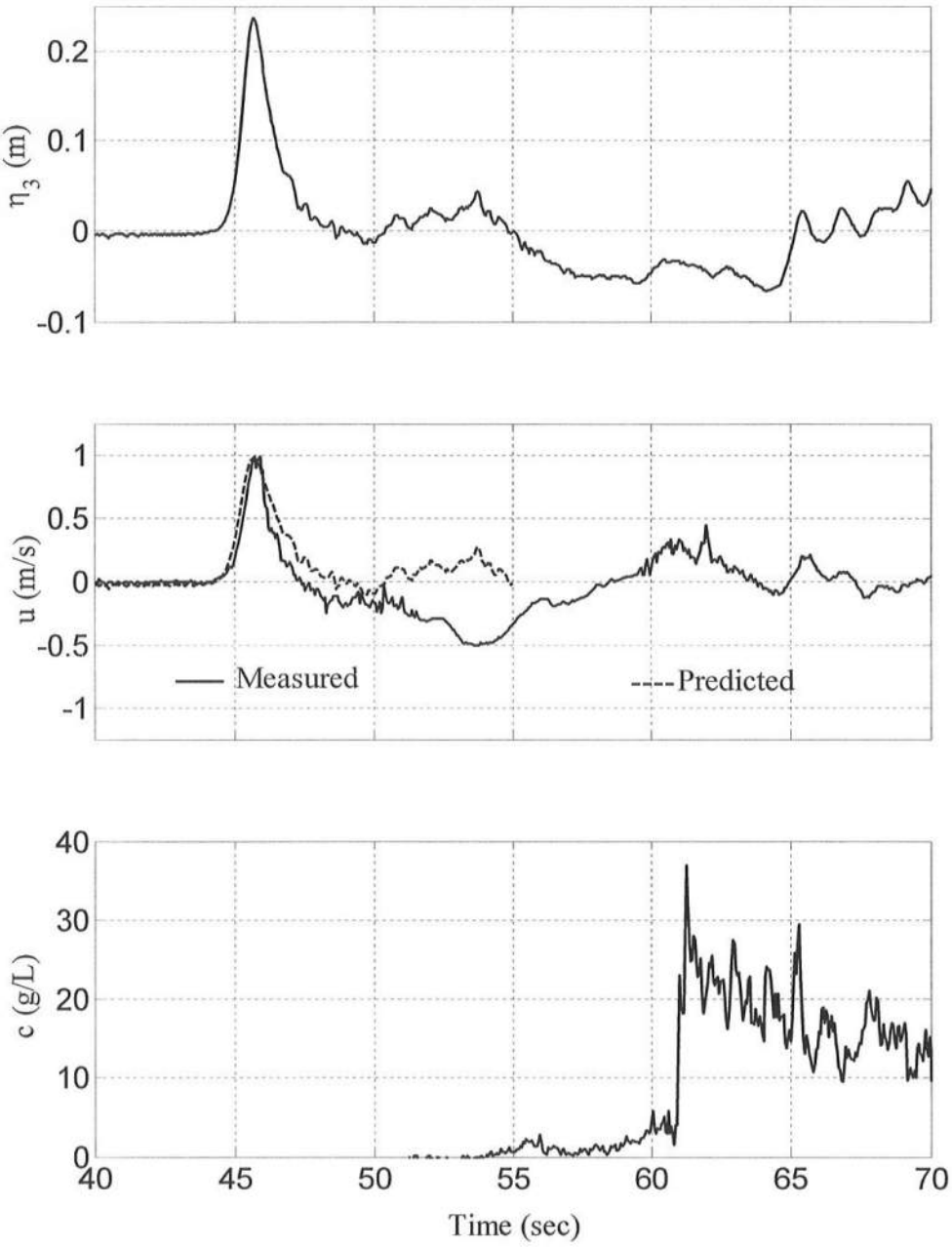

Figure 3.18: Measured Time Series of η_3, Average u and c for Test P1

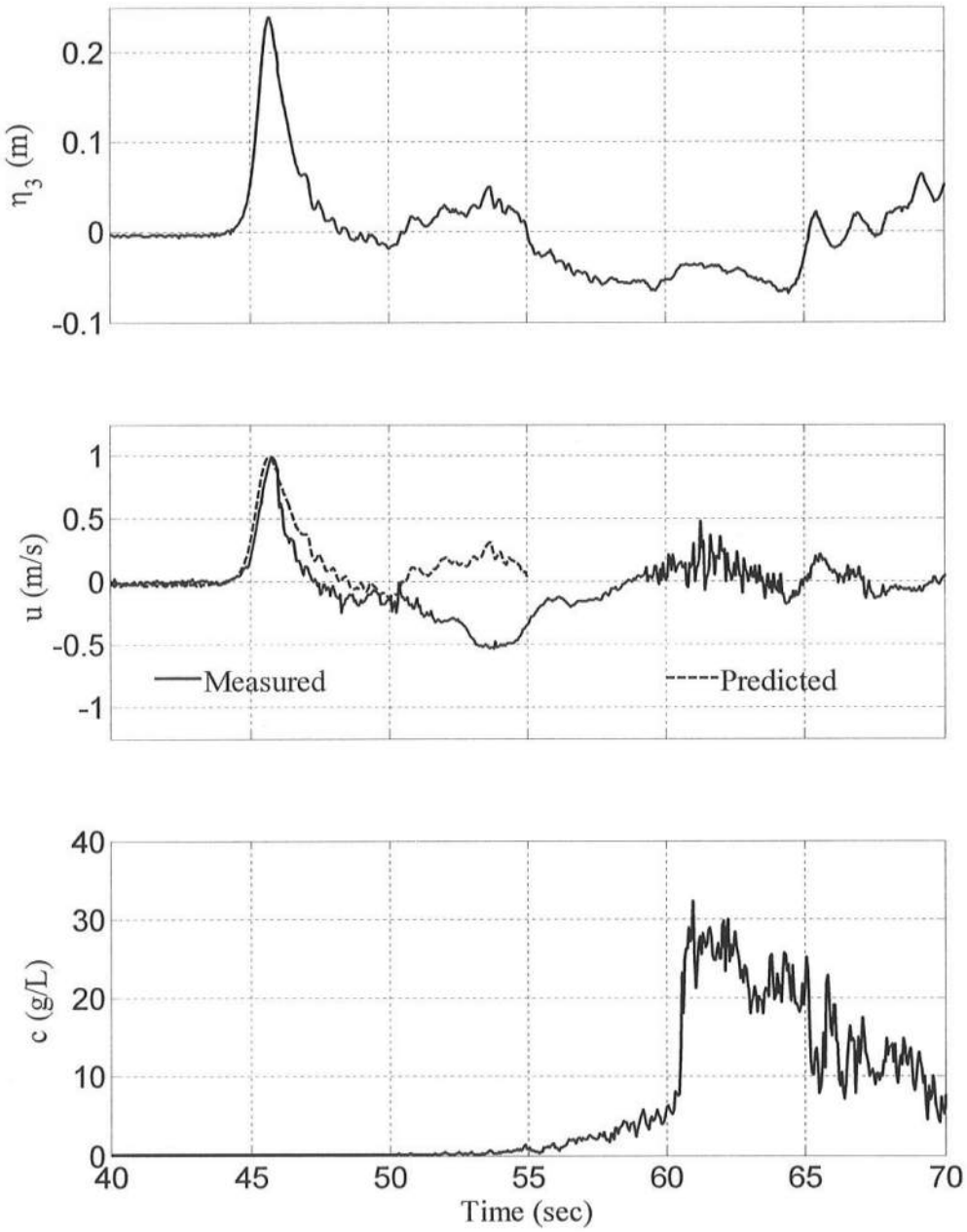

Figure 3.19: Measured Time Series of η_3, Average u and c for Test P2

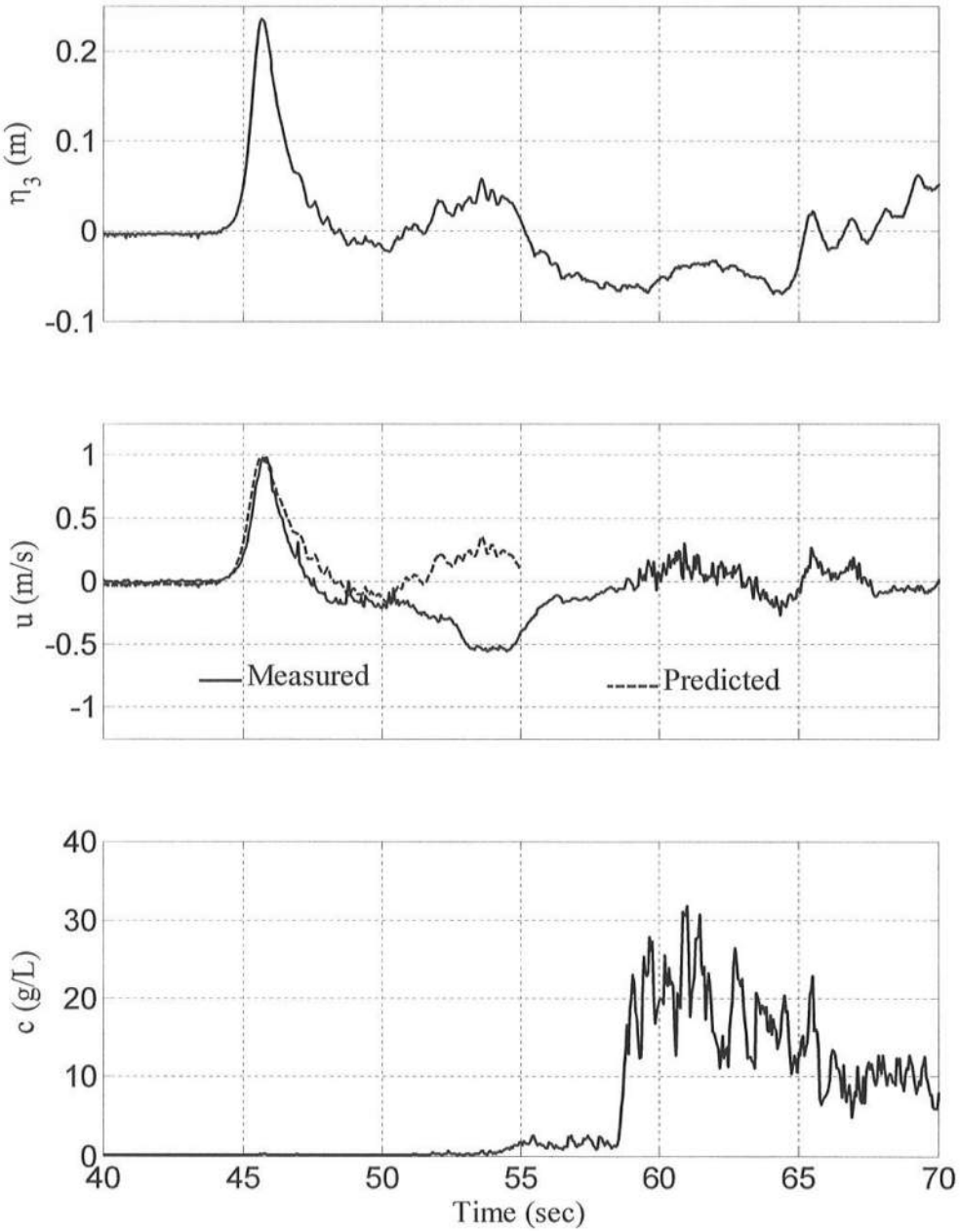

Figure 3.20: Measured Time Series of η_3, Average u and c for Test P3

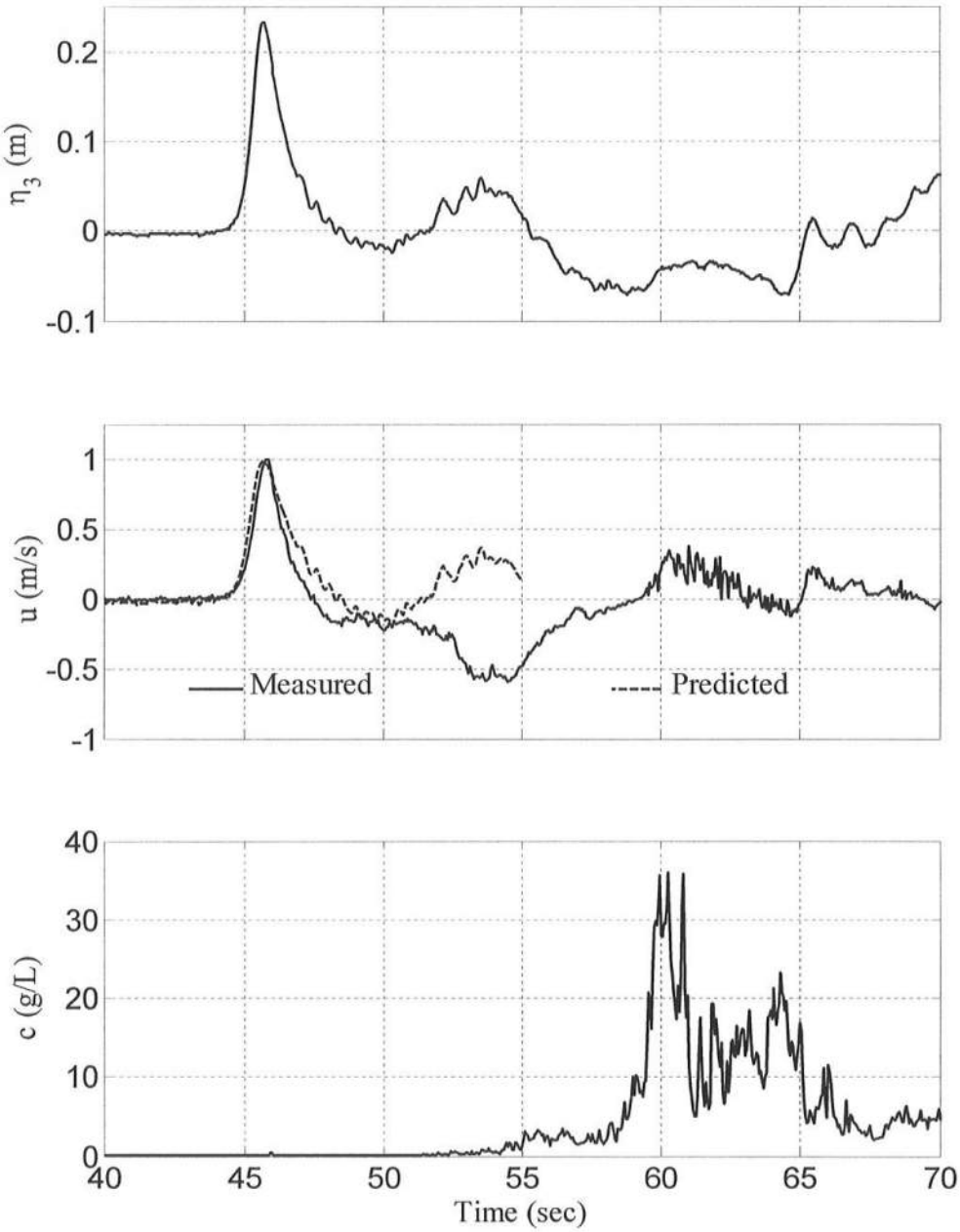

Figure 3.21: Measured Time Series of η_3, Average u and c for Test P4

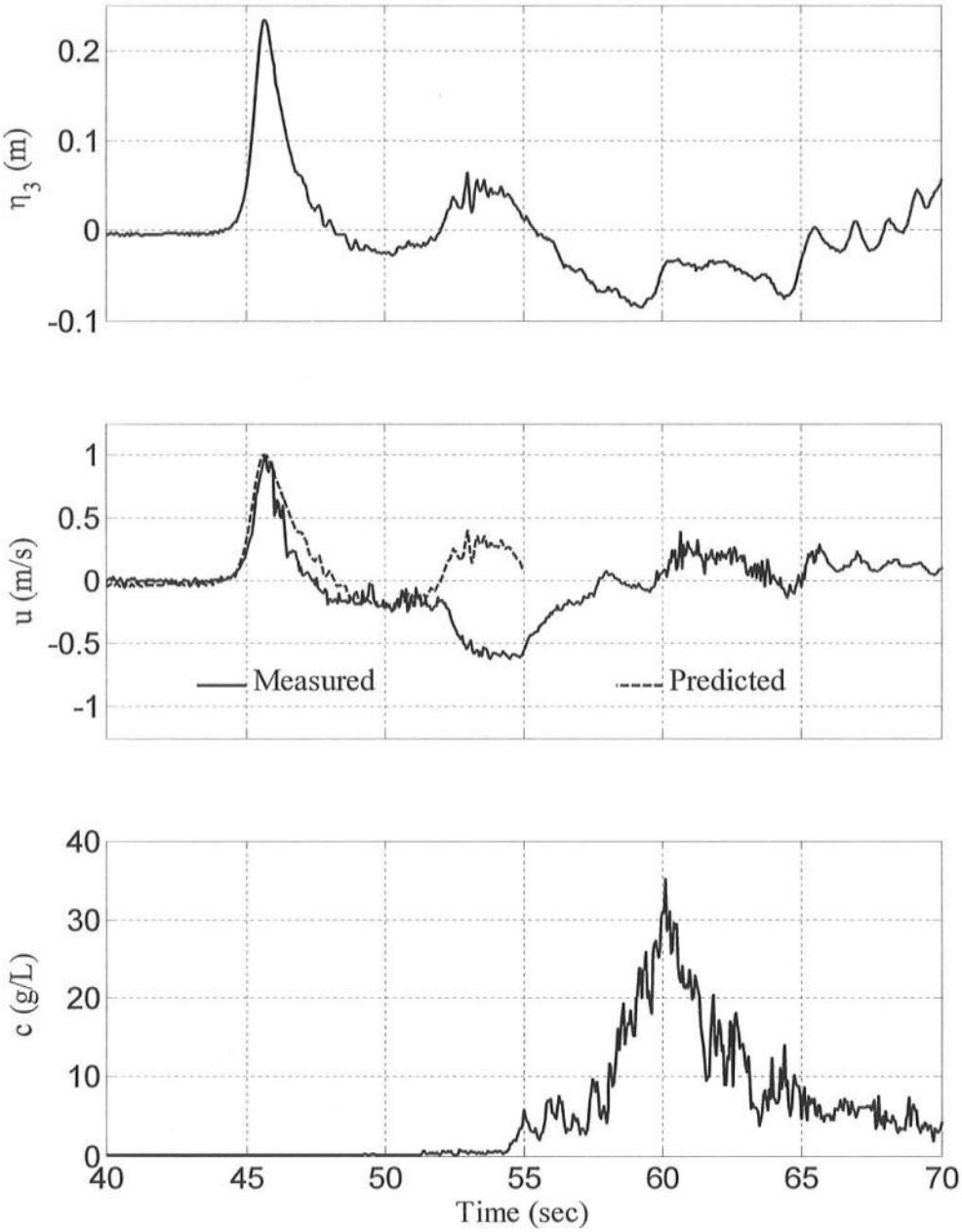

Figure 3.22: Measured Time Series of η_3, Average u and c for Test P5

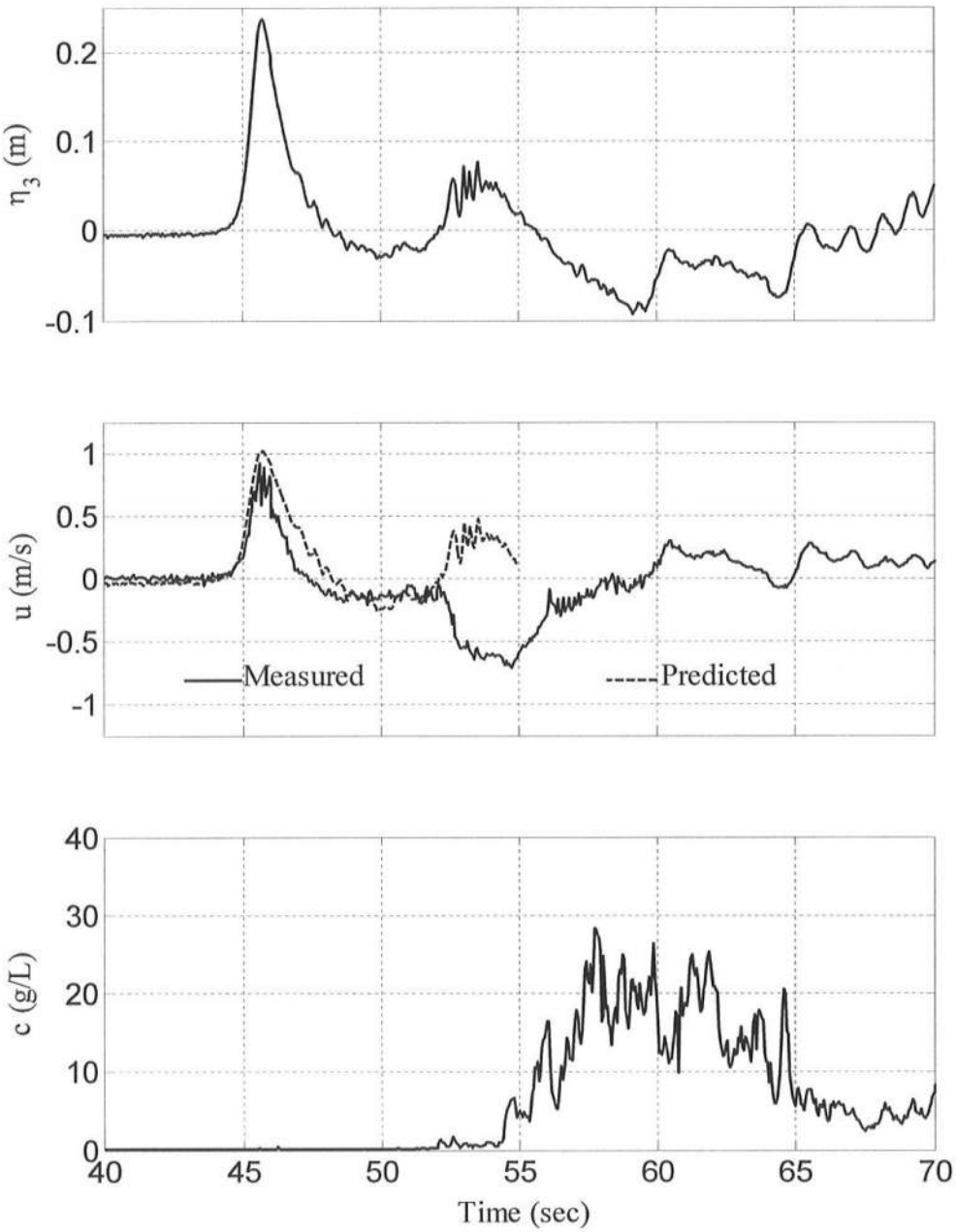

Figure 3.23: Measured Time Series of η_3, Average u and c for Test P6

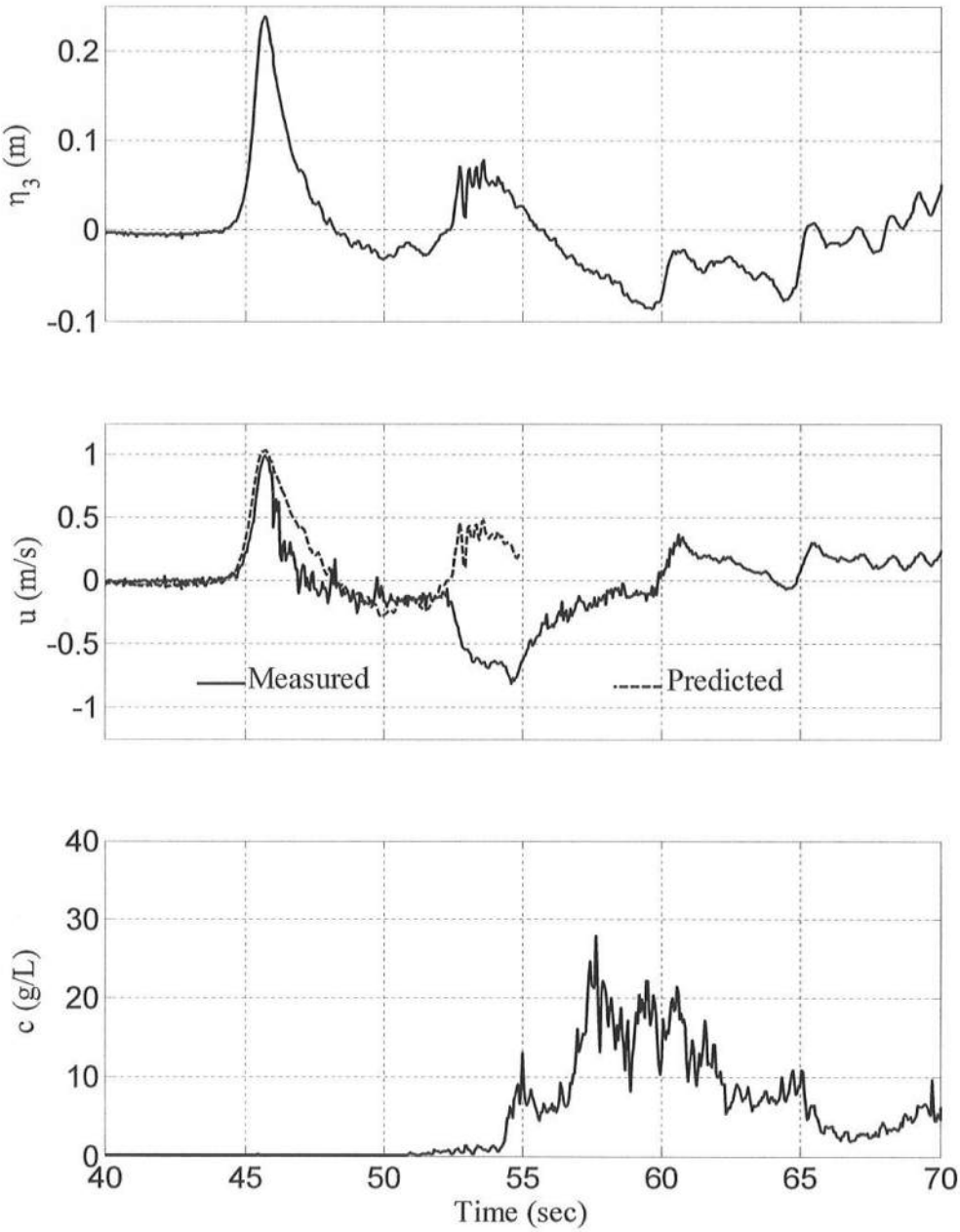

Figure 3.24: Measured Time Series of η_3, Average u and c for Test P7

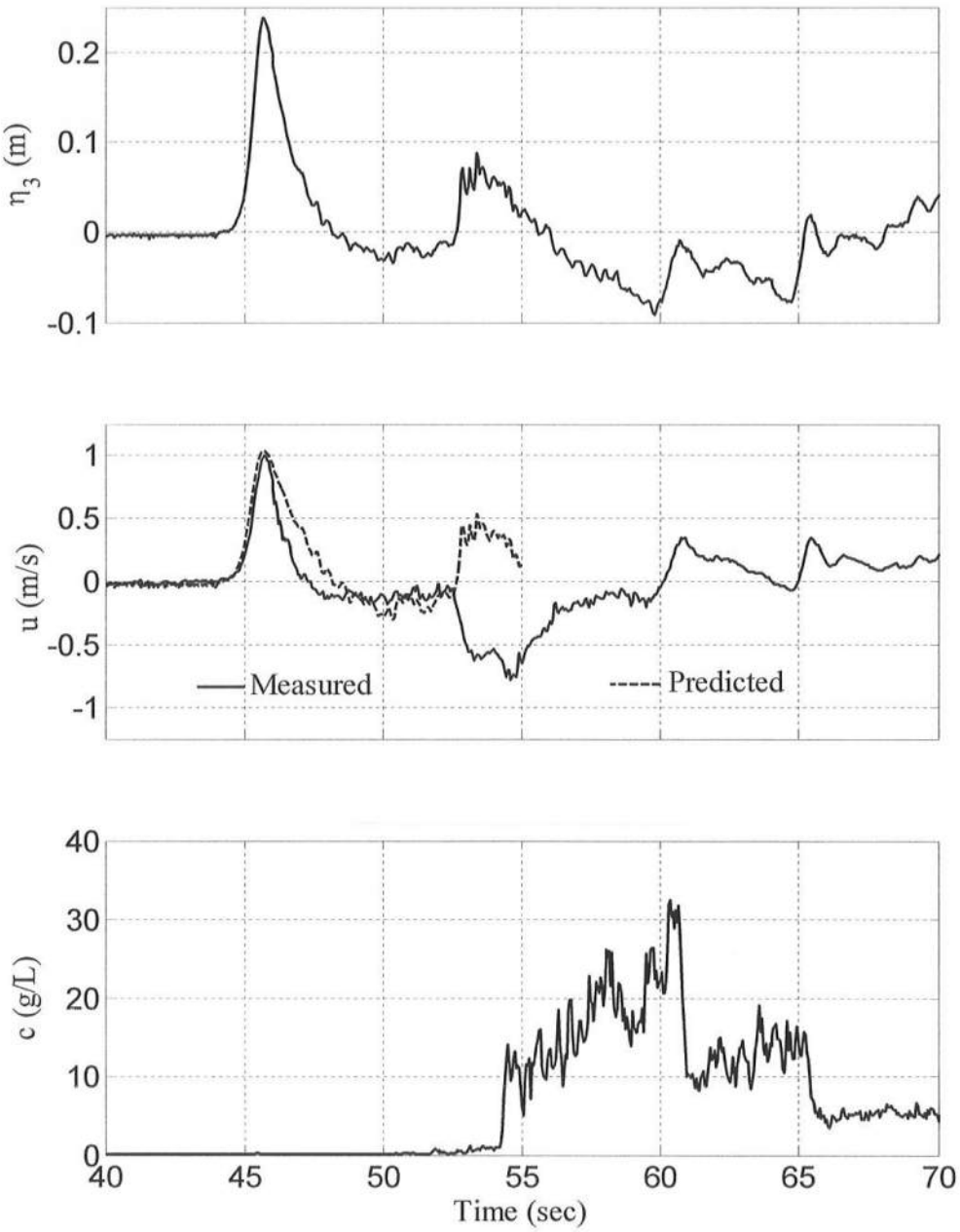

Figure 3.25: Measured Time Series of η_3, Average u and c for Test P8

However, the sand concentration under the solitary wave appeared much smaller than the high sand concentration in the downrushing water. In other words, the prediction of the measured concentration shown in Figures 3.18-3.25 will require a time-dependent model that includes sand suspension, advection and settling [Kobayashi and Johnson, 2001].

Table 3.7: Incident Solitary Wave Characteristics at Wave Gauge 3 for Tests P1-P8

Test	h (cm)	η_{max} (cm)	η_{down} (cm)	H (cm)	C (m/s)
P1	34.58	23.60	-0.79	23.59	2.39
P2	34.22	23.91	-0.84	23.90	2.39
P3	33.59	23.47	-0.75	23.46	2.37
P4	32.28	23.28	-0.72	23.27	2.33
P5	30.80	23.34	-0.68	23.33	2.30
P6	29.97	23.62	-0.88	23.61	2.29
P7	29.26	23.79	-0.87	23.78	2.28
P8	28.93	23.86	-0.72	23.85	2.28

3.5 PARAMETERIZATION OF ERODED BEACH PROFILE

In the following, the measured beach profile change relative to the initial profile is parameterized as illustrated in Figure 3.26. First, the cross-shore location x_0 and the still water depth d_0 at the intersection between the initial profile and the measured profile after each test are obtained by comparing the initial profile and the profile after each test as listed in Table 3.28. For tests P1-P8, $x_0 = 8.40 - 8.85$ m and $d_0 = 6.2 - 10.1$ cm. The average incident wave height $H = 21.6$ cm is used for the following normalization. Figure 3.27 for d_0/H as a function of the test number illustrates that the intersection point did not change much among the eight tests. The

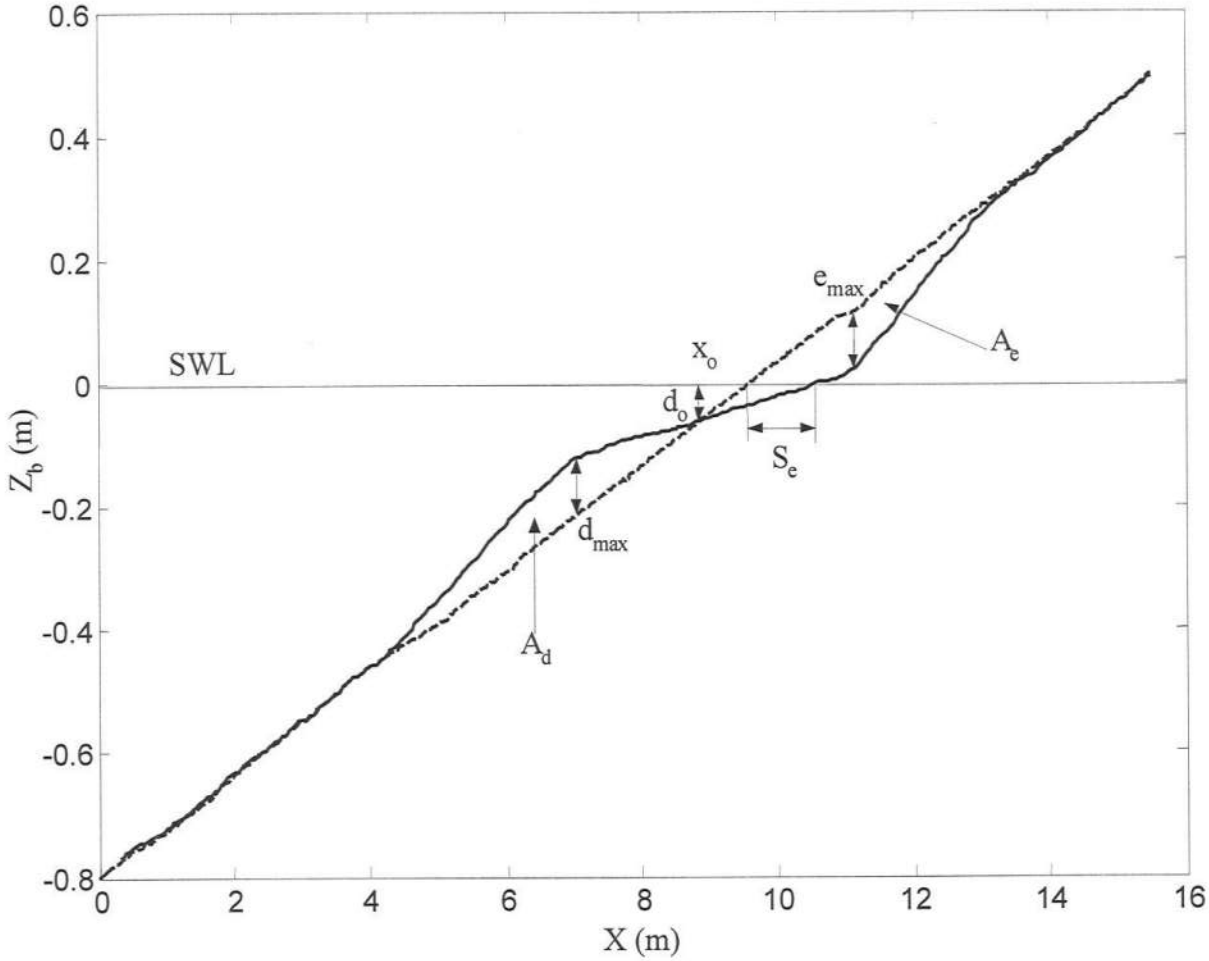

Figure 3.26: Illustration of Variables Used for Parameterization of Positive Solitary Wave Beach Profile Change

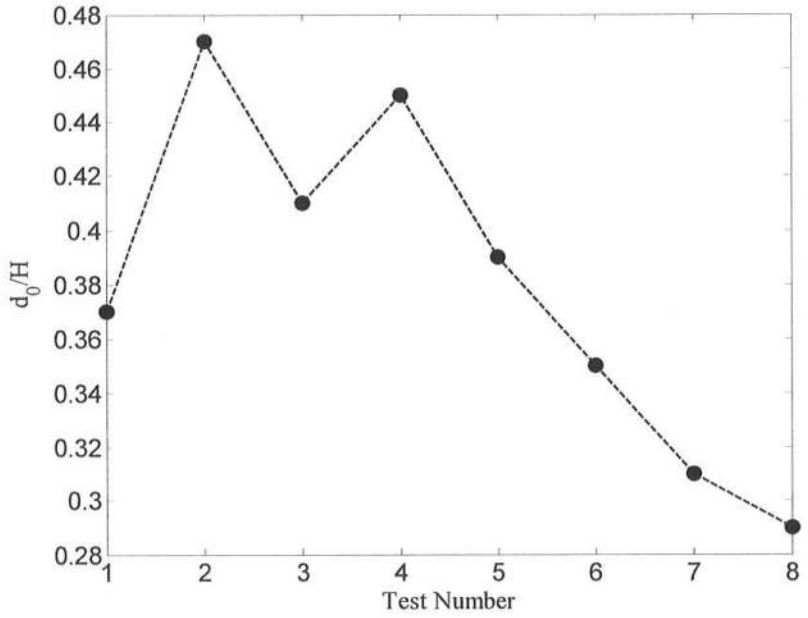

Figure 3.27: Normalized Still Water Depth d_0 at Intersection Between Initial Profile and Measured Profile After Tests P1-P8

erosion zone of $x > x_0$ in Figure 3.26 is characterized by the maximum vertical erosion depth e_{max}, the erosion area A_e, and the horizontal recession S_e of the still water shoreline. The deposition zone of $x < x_0$ in Figure 3.26 is characterized by the maximum vertical deposition depth d_{max}, and the deposition area A_d. Theses dimensional parameters are listed in Table 3.8. The normalized parameters are given in Table 3.9.

Table 3.8: Measured Profile Parameters for Tests P1-P8

Test	x_0 (m)	d_0 (cm)	d_{max} (cm)	A_d (cm^2)	e_{max} (cm)	A_e (cm^2)	S_e (cm)
P1	8.65	7.94	2.55	292.9	1.28	321.2	8.4
P2	8.40	10.10	3.22	445.6	2.92	489.5	35.0
P3	8.55	8.79	4.13	925.6	3.97	908.1	47.6
P4	8.45	9.67	4.54	1242.9	5.72	1363.9	67.2
P5	8.60	8.37	5.80	1629.7	7.16	1619.5	77.1
P6	8.70	7.50	6.94	2004.6	9.19	1970.1	90.4
P7	8.80	6.69	8.49	2347.8	9.13	2114	95.2
P8	8.85	6.20	9.44	2560.9	9.87	2304.4	95.0

Figure 3.28 shows the increase of d_{max}/H and e_{max}/H with the increase of the test number indicating the number of solitary waves which caused the beach erosion and accretion. The approximately linear increase of d_{max}/H and e_{max}/H implies that the maximum erosion depth e_{max} and the maximum deposition depth d_{max} caused by the single solitary wave were of the order of 0.06 H. The normalized horizontal shoreline recession S_e/H, shown in Figure 3.29 did not increase linearly with the test number and was 4.4 for test P8. Figure 3.30 shows the approximately linear increase of A_d/H^2 and A_e/H^2 with the test number. The conservation of the sediment volume requires $A_d = A_e$ and the difference between A_d and A_e was caused by the profile measurement error of approximately 1 mm. The deposition area A_d and the erosion area A_e caused by the single solitary wave were of the order of 0.7 H^2. These simple empirical relationships for d_{max}, e_{max}, A_d and A_e are intended as a first attempt for lack of any other data and will need to be improved in the future.

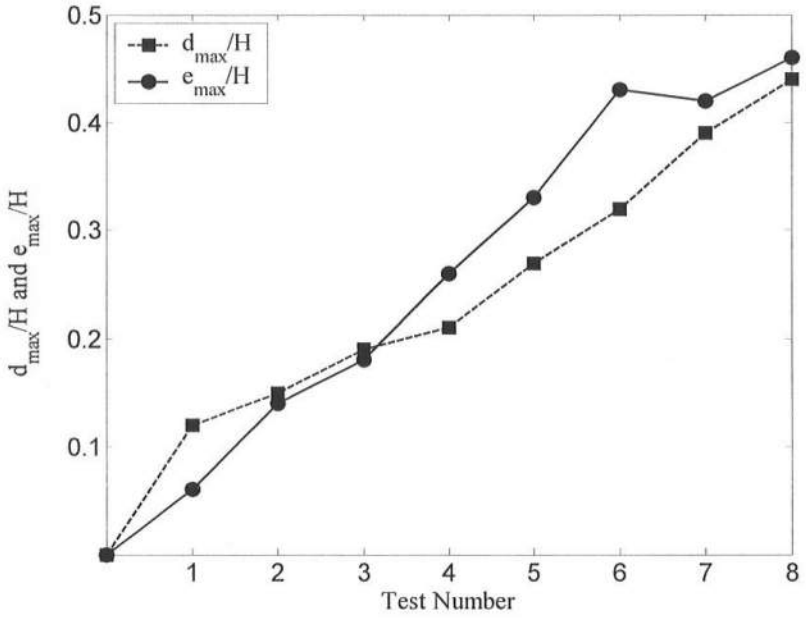

Figure 3.28: Normalized Maximum Vertical Deposition Depth d_{max} and Erosion Depth e_{max} for Tests P1-P8

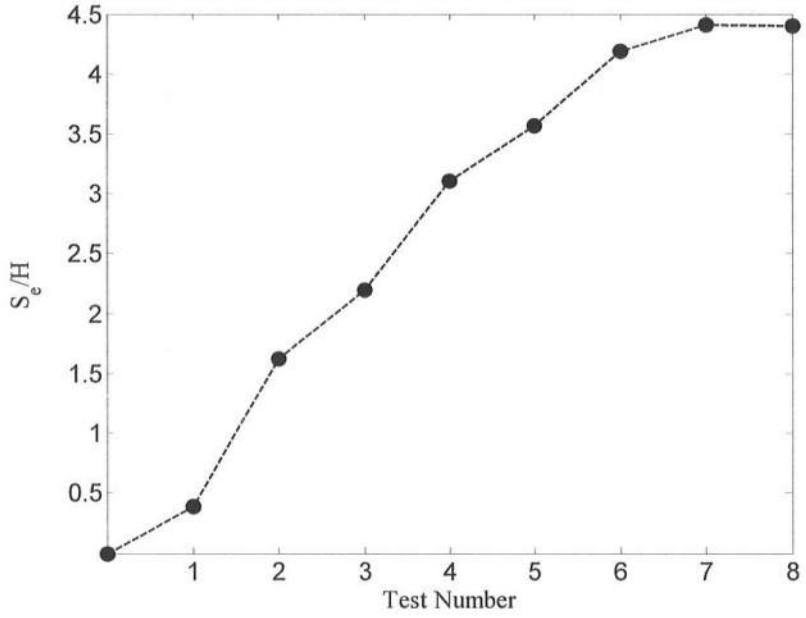

Figure 3.29: Normalized Horizontal Shoreline Recession S_e for Tests P1-P8

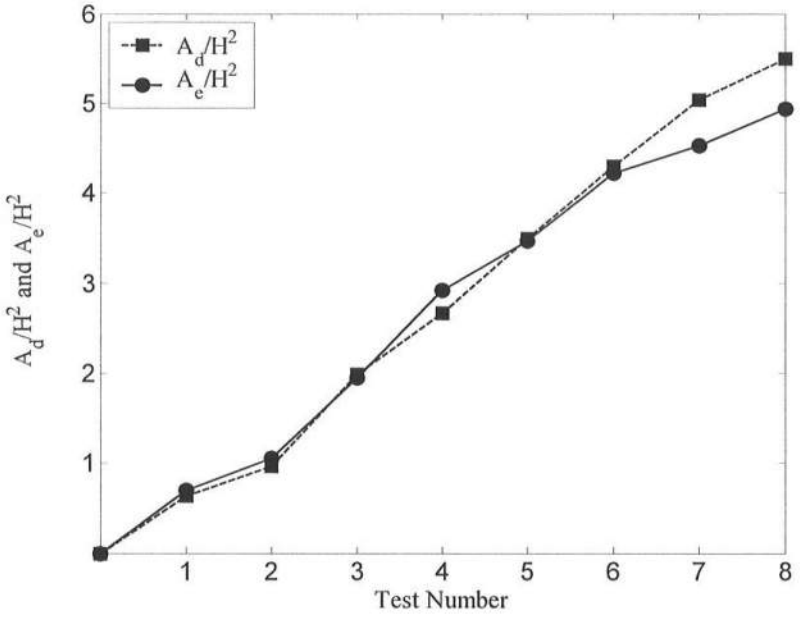

Figure 3.30: Normalized Deposition Area A_d and Erosion Area A_e for Tests P1-P8

Table 3.9: Normalized Profile Parameters for Tests P1-P8

Test	d_0/H	d_{max}/H	A_d/H^2	e_{max}/H	A_e/H^2	S_e/H
P1	0.37	0.12	0.63	0.06	0.69	0.39
P2	0.47	0.15	0.96	0.14	1.05	1.62
P3	0.41	0.19	1.98	0.18	1.95	2.20
P4	0.45	0.21	2.66	0.26	2.92	3.11
P5	0.39	0.27	3.49	0.33	3.47	3.57
P6	0.35	0.32	4.30	0.43	4.22	4.19
P7	0.31	0.39	5.03	0.42	4.53	4.41
P8	0.29	0.44	5.49	0.46	4.94	4.40

Chapter 4

NEGATIVE SOLITARY WAVE TESTS

4.1 INCIDENT SOLITARY WAVE

Figure 4.1 shows the temporal variations of the free surface elevation η_1 measured by wave gauge 1 for tests N1-N8. The forward paddle movement shown in Figure 2.3 caused the increase η_{up} = 0.3 cm of the water level for the eight tests as tabulated in Table 4.1. The wave height measured from the wave trough elevation to the increased water level was in the range of 17.8 – 18.4 cm. Use is made of the average wave height H = 18.2 cm in the following. The arrival time t_{min} of the wave trough with $\eta_1 = \eta_{min}$ at $t = t_{min}$ and $H = (\eta_{up} - \eta_{min})$ was in the range 44.5 – 44.6 s. Since no theory is available for negative solitary waves, the average of the temporal variations of η_1 for tests P1-P8 shown in Figure 3.1 is calculated and the temporal variation of the average $(-\eta_1)$ is plotted in Figure 4.1. The trough of the negative solitary wave was wider and less symmetric than the crest of the positive solitary wave. The negative wave, with celerity C = 280 cm/s, propagated slower than the positive wave with C = 316 cm/s. The negative solitary wave celerity was calculated using linear long wave theory with $C = (gh)^{1/2}$. The incident negative solitary

Table 4.1: Incident Negative Solitary Wave at Wave Gauge 1 for Tests N1-N8

Test	h (cm)	η_{up} (cm)	H (cm)	t_{min} (sec)	C (m/s)
N1	80.0	0.30	-17.8	44.5	2.80
N2	80.0	0.30	-18.3	44.6	2.80
N3	80.0	0.30	-18.4	44.6	2.80
N4	80.0	0.30	-18.1	44.5	2.80
N5	80.0	0.30	-18.2	44.5	2.80
N6	80.0	0.30	-18.3	44.5	2.80
N7	80.0	0.30	-18.4	44.5	2.80
N8	80.0	0.30	-18.3	44.5	2.80
Mean	80.0	0.30	-18.2	44.5	2.80

wave characteristics for tests N1-N8 are summarized in Table 4.1.

4.2 MEASURED BEACH PROFILES

Figure 4.2 shows the measured beach profiles and the locations of the eight wave gauges for tests N1-N8. The profile change from the initial profile was approximately proportional to the number of negative solitary waves indicted by the numeral next to the letter N, as shown in Figure 4.3. The location of wave gauge 1 was the same for tests N1-N8 and P1-P8. The locations of wave gauges 2 – 8 were changed to measure the negative solitary wave transformation, breaking and runup for tests N1-N8. The negative solitary wave collapsed near wave gauge 4 in Figure 4.2 due to the seaward flow toward the wave trough. The collapsing wave caused noticeably less sediment suspension and smaller runup than the plunging wave for tests P1-P8. The wave runup height was approximately 0.2 m above SWL. The weak downrush following the small runup resulted in accretion on the foreshore and

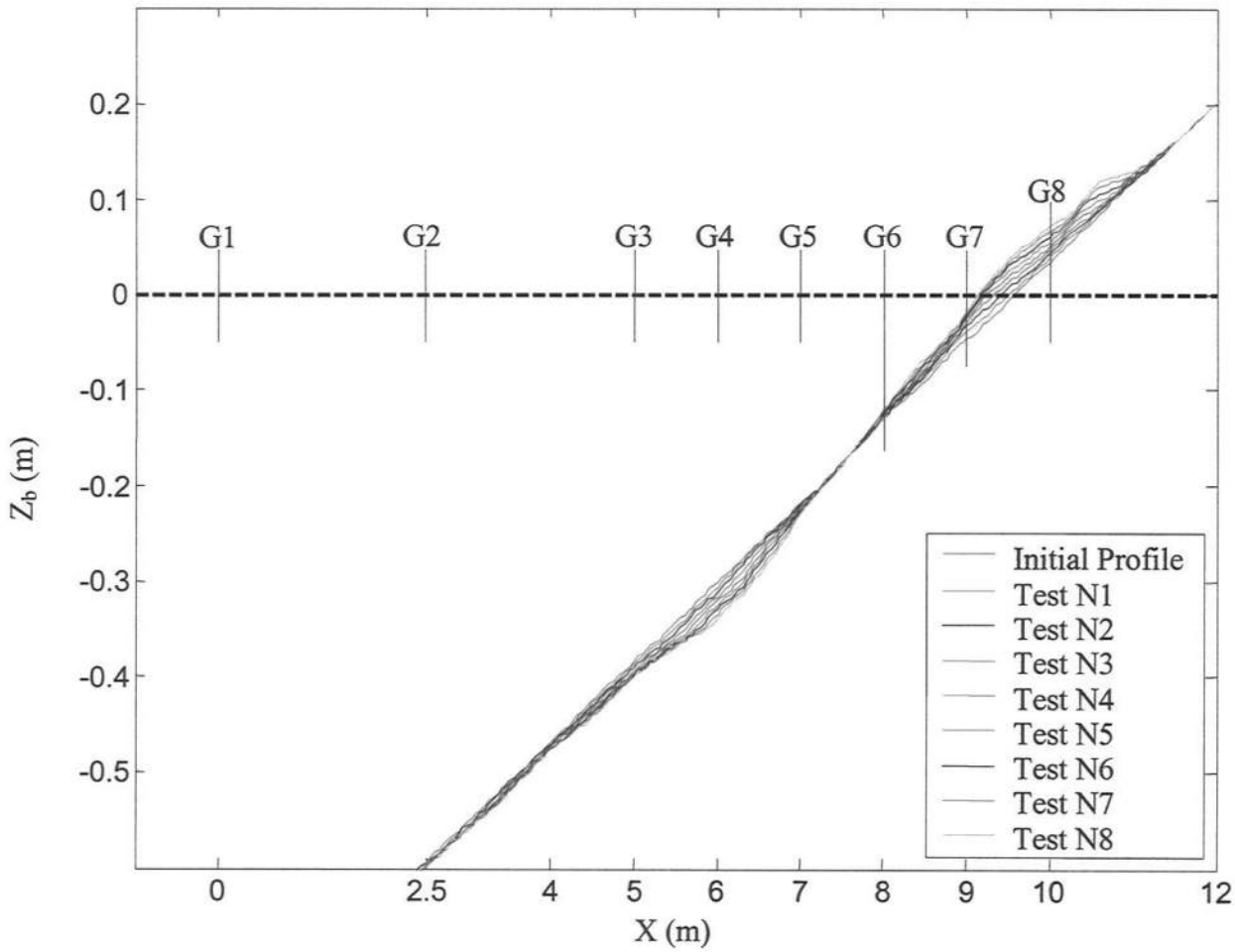

Figure 4.2: Measured Beach Profiles and Wave Gauge Locations for Tests N1-N8

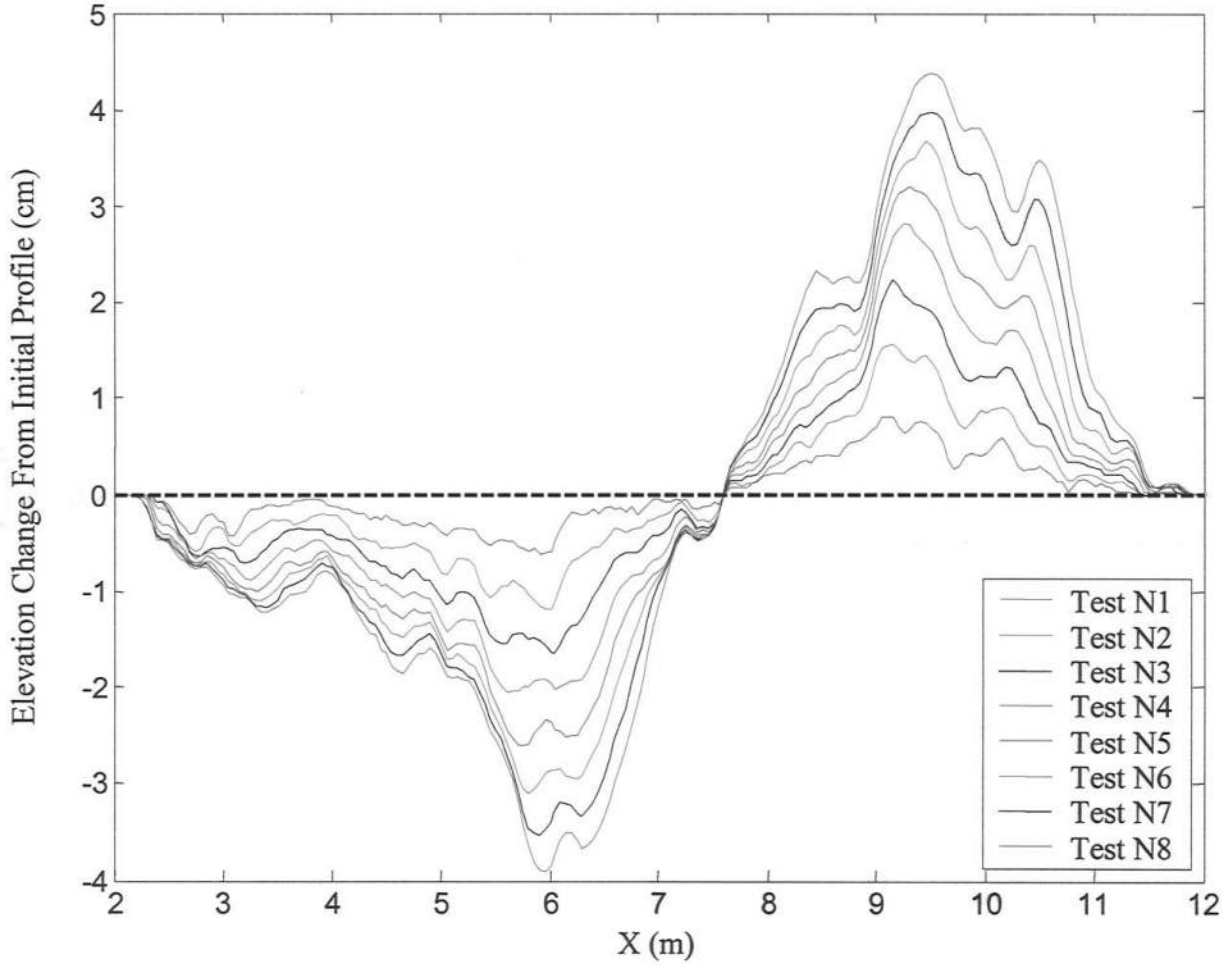

Figure 4.3: Elevation Change from Initial Profile for Tests N1-N8

erosion near the wave collapsing point. The comparison of the profile changes in Figures 3.2 and 4.2 indicates the importance of the incident wave profile for the direction and magnitude of net sediment transport affected by the breaker type, sediment suspension, wave uprush and downrush.

4.3 CROSS-SHORE WAVE TRANSFORMATION

Figures 4.4-4.7 show the measured time series of the free surface elevation η_j at wave gauge $j = 1 - 7$ for tests N1-N8 where the instantaneous water depth h_8 above the local bed measured before each test is plotted because the bed level at wave gauge 8 was above SWL as shown in Figure 4.2. The positive value of h_8 at the end of each test corresponded approximately to the deposition depth at wave gauge 8. As the negative solitary wave propagated landward, the landward side of the wave trough, which arrived earlier, became gentler and its seaward side became steeper and collapsed near wave gauge 4. The wave trough depth was limited by the bed level at wave gauges 6 and 7 and no trough existed at wave gauge 8 located above SWL. The reflection of the negative solitary wave from the foreshore is not apparent in Figures 4.4-4.7. Table 4.2 lists the minimum free surface elevation η_{min} at wave gauges 1-7 and the minimum water depth h_{min} at wave gauge 8.

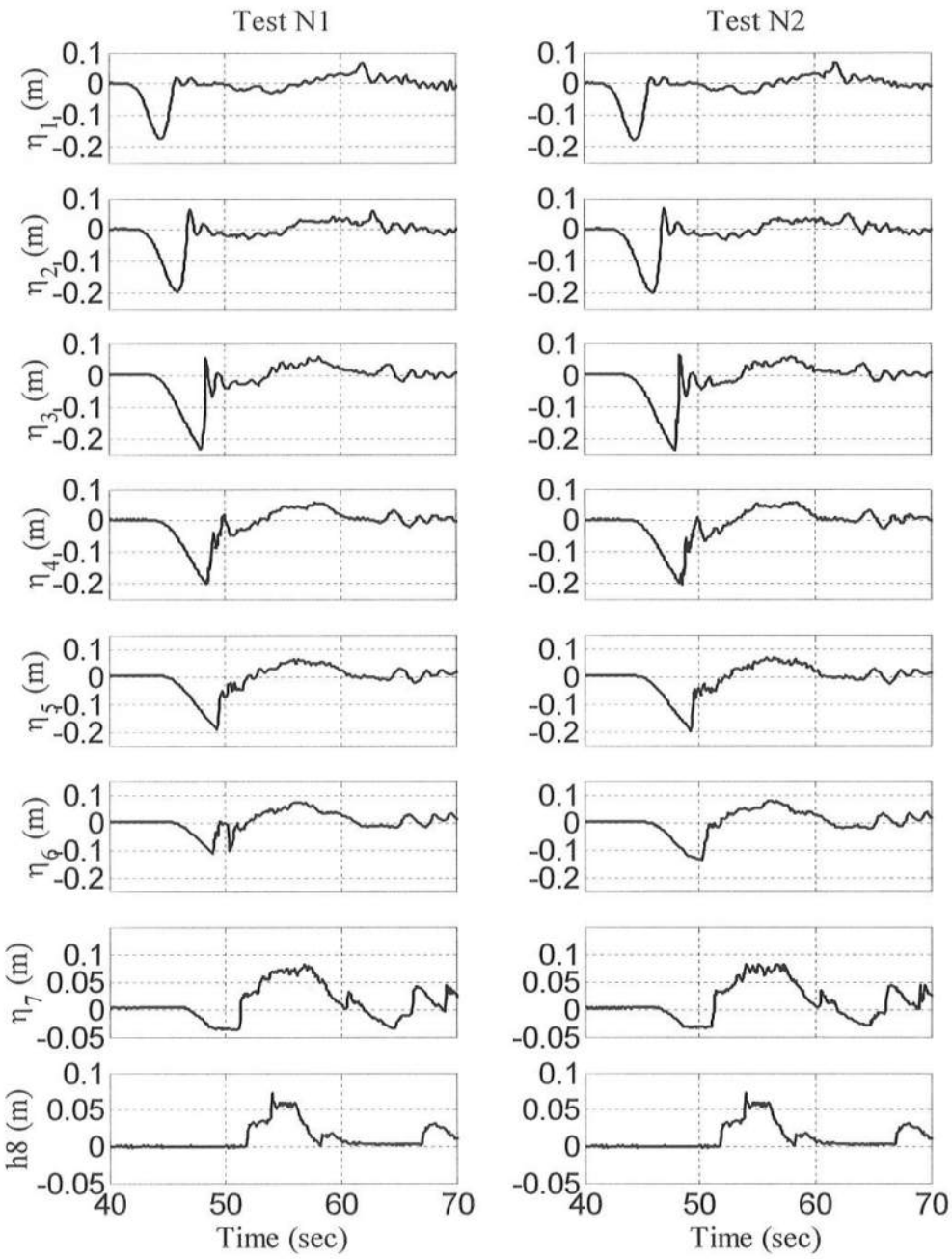

Figure 4.4: Measured Free Surface Elevations at Wave Gauges 1-7 and Water Depth at Wave Gauge 8 for Tests N1 and N2

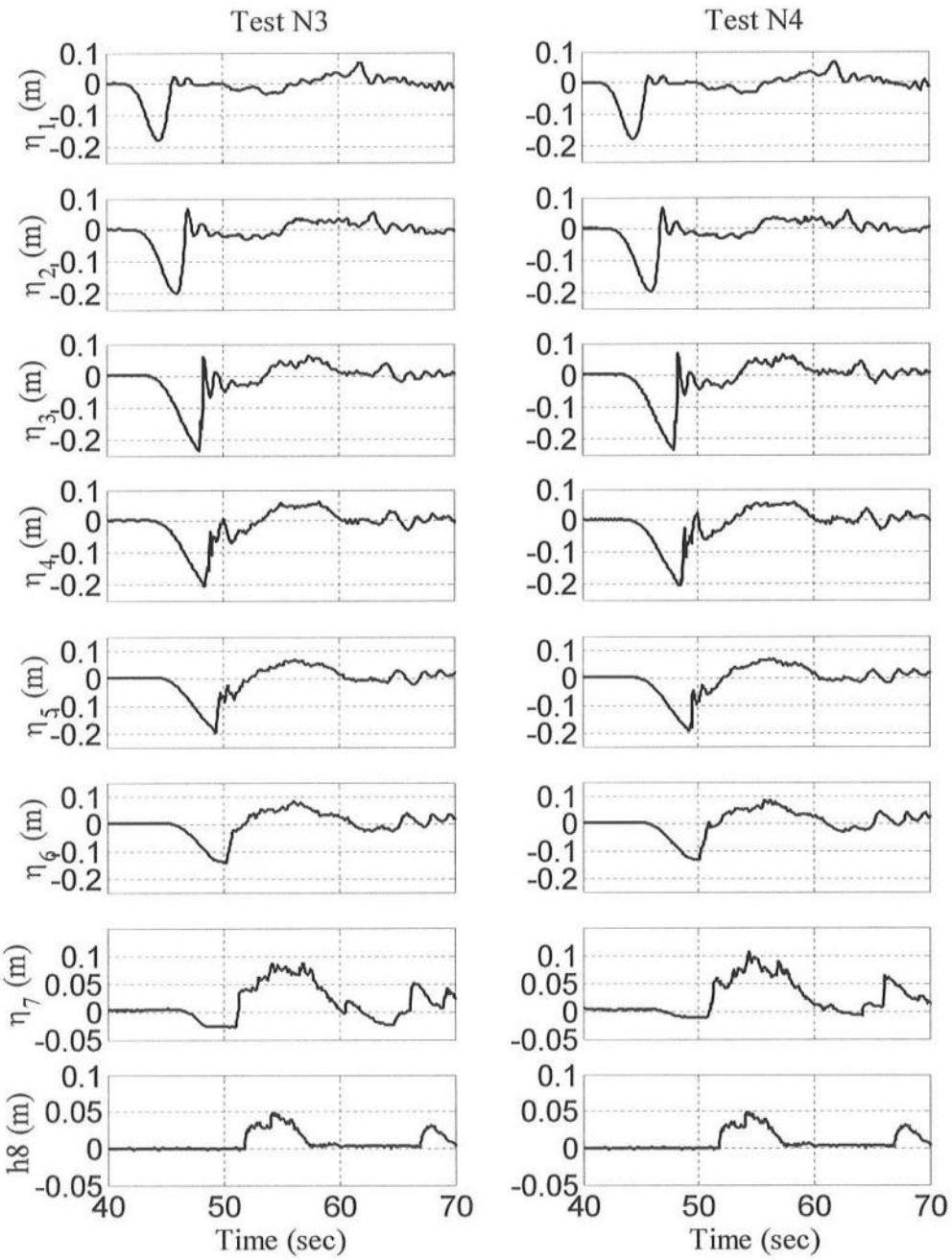

Figure 4.5: Measured Free Surface Elevations at Wave Gauges 1-7 and Water Depth at Wave Gauge 8 for Tests N3 and N4

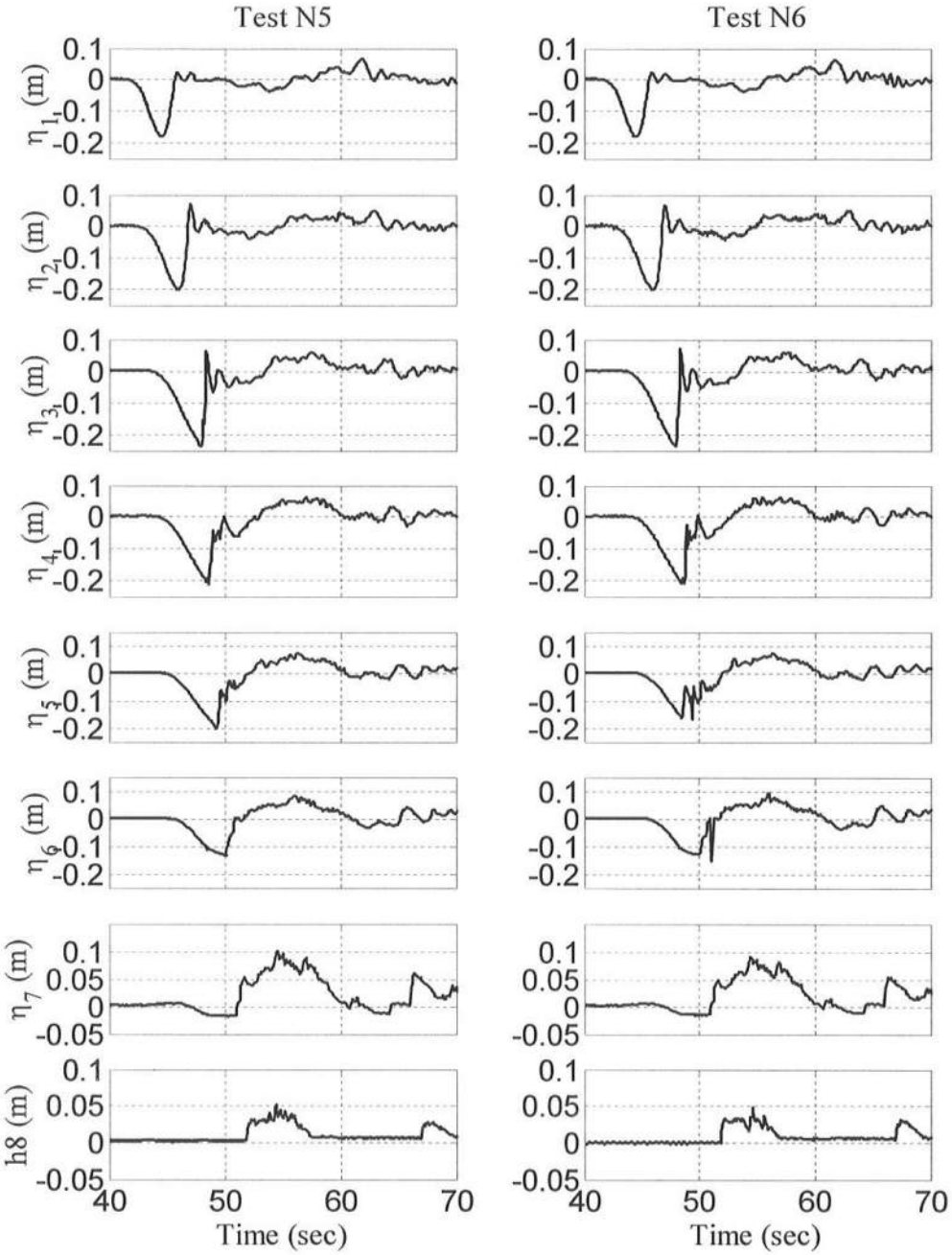

Figure 4.6: Measured Free Surface Elevations at Wave Gauges 1-7 and Water Depth at Wave Gauge 8 for Tests N5 and N6

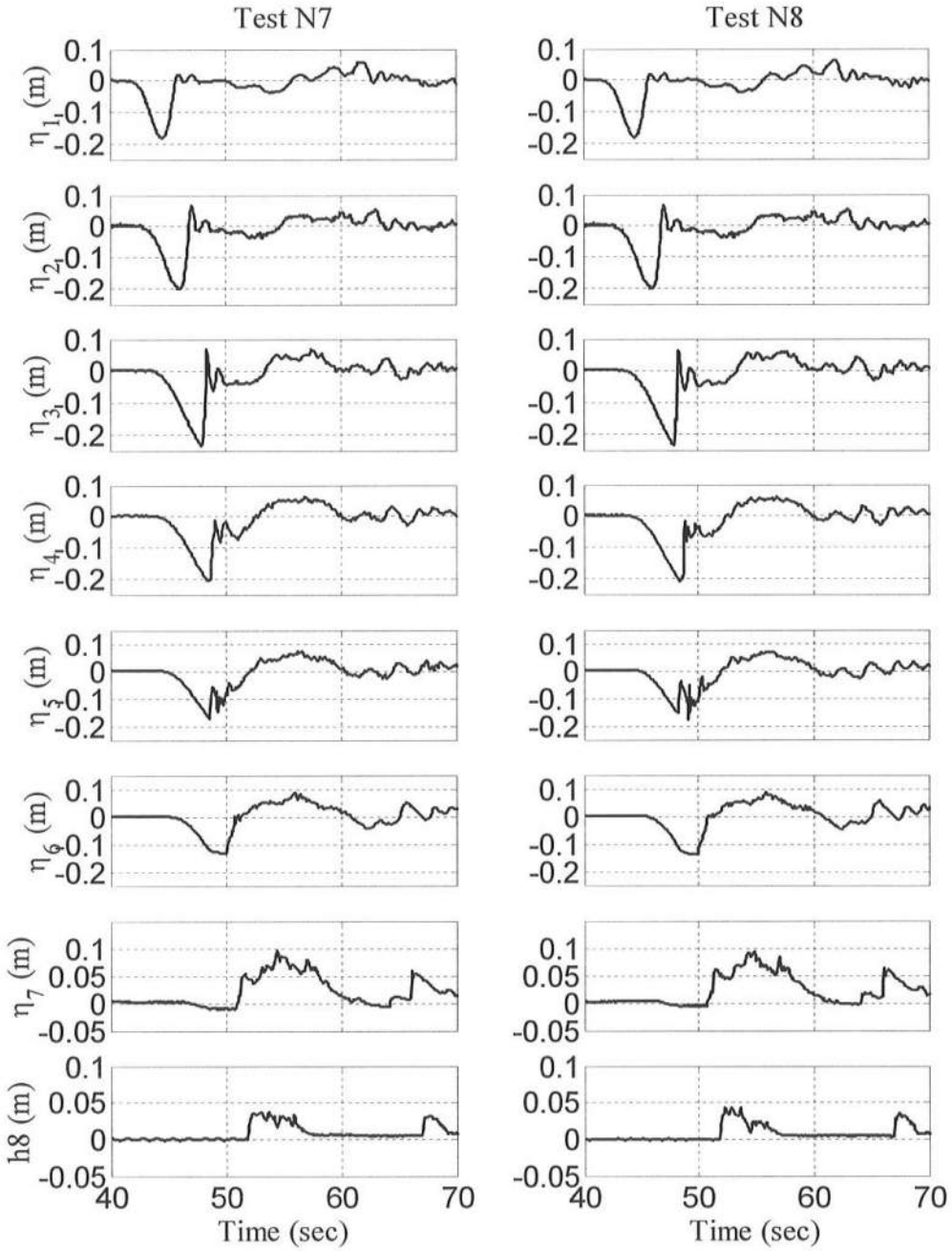

Figure 4.7: Measured Free Surface Elevations at Wave Gauges 1-7 and Water Depth at Wave Gauge 8 for Tests N7 and N8

Table 4.2: Minimum Free Surface Elevation η_{min} (cm) for Wave Gauges 1-7 and Water Depth h_{min} (cm) for Wave Gauge 8 for Tests N1-N8

Gauge	x (m)	Test N1	Test N2	Test N3	Test N4	Test N5	Test N6	Test N7	Test N8
1	0	-17.5	-18.0	-18.1	-17.8	-17.9	-18.0	-18.1	-18.0
2	2.5	-19.5	-20.0	-19.9	-19.6	-19.9	-19.8	-20.3	-20.3
3	5	-23.1	-23.4	-23.4	-23.3	-23.5	-23.5	-23.4	-23.5
4	6	-19.9	-20.6	-20.4	-20.6	-21.2	-20.7	-20.6	-20.6
5	7	-19.0	-19.7	-20.0	-19.3	-20.3	-16.6	-17.2	-17.6
6	8	-10.3	-13.5	-14.1	-13.5	-13.1	-12.9	-13.2	-13.7
7	9	-3.7	-3.3	-2.9	-1.2	-1.8	-1.6	-1.1	-0.7
8	10	-0.08	-0.08	0.06	0.06	0.22	0.00	0.04	0.06

Figure 4.8 and Table 4.3 show the arrival time $t_{\min}$ of the wave trough at wave gauges 1-8 for tests N1-N8 where the arrival time at wave gauge 8 is taken at the time when h_8, as shown in Figures 4.4-4.7, increased suddenly from zero. The trough arrival time $t_{\min}$ is larger than the crest arrival time $t_{\max}$ shown in Figure 3.8. The straight line fitted to the data points in Figure 4.8 indicates that the celerity C of the negative solitary wave is approximately 1.39 m/s and much smaller than 3.16 m/s in Figure 3.8.

Figure 4.9 shows the cross-shore variation of the wave trough elevation $\eta_{\min}$ relative to SWL for tests N1-N8 where the solid line in this figure is the average profile of the measured profiles before and after each test. Figure 4.9 was plotted using Table 4.4 together with 4.5, which was used to find the average bottom elevation $(Z_b)_{average}$. The minimum free surface elevation at wave gauge 8 is given by $\eta_{min} = h_{min} + (Z_b)_{average}$. The wave trough elevation decreased slightly landward and became limited by the bed level near the wave collapsing point.

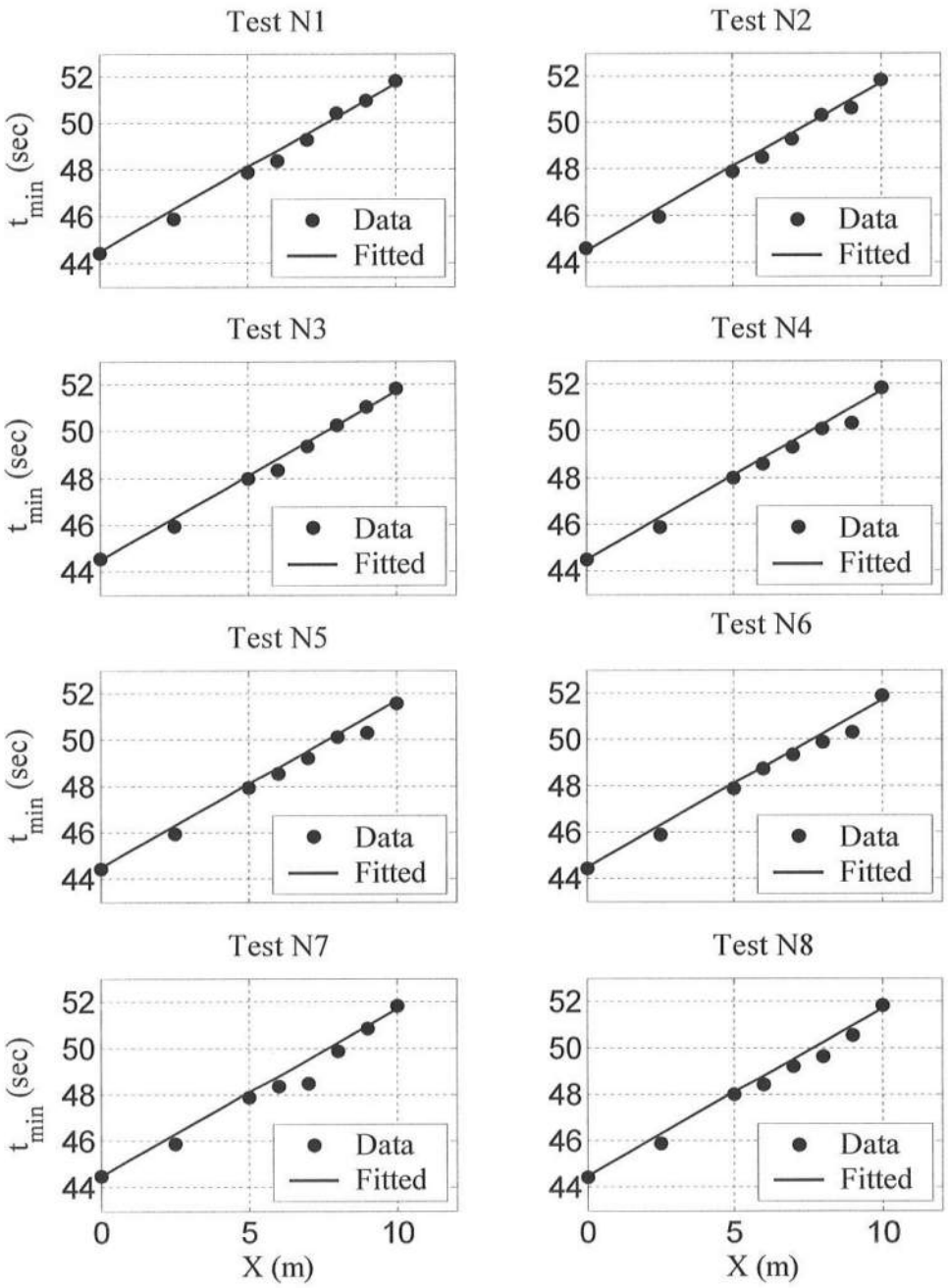

Figure 4.8: Arrival Time t_{min} of Negative Solitary Wave Trough at Wave Gauges 1-8 for Tests N1-N8

Table 4.3: Time t_{min} (sec) when $\eta = \eta_{min}$ at Wave Gauges 1-7 and $h = h_{min}$ at Wave Gauge 8 for Tests N1-N8

Gauge	x (m)	Test N1	Test N2	Test N3	Test N4	Test N5	Test N6	Test N7	Test N8
1	0	44.5	44.6	44.6	44.5	44.5	44.5	44.5	44.5
2	2.5	45.9	46.0	45.9	45.9	46.0	45.9	45.9	45.9
3	5	47.9	47.9	48.0	48.0	48.0	47.9	47.9	48.0
4	6	48.4	48.5	48.4	48.6	48.6	48.7	48.4	48.4
5	7	49.3	49.3	49.4	49.3	49.2	49.4	48.5	49.2
6	8	50.4	50.3	50.3	50.1	50.1	49.9	49.9	49.7
7	9	51.0	50.6	51.1	50.3	50.3	50.3	50.9	50.6
8	10	51.8	51.8	51.8	51.8	51.6	51.9	51.8	51.8

Table 4.4: Minimum Free Surface Elevation η_{min} (cm) at Wave Gauges 1-8 for Tests N1-N8

Gauge	x (m)	Test N1	Test N2	Test N3	Test N4	Test N5	Test N6	Test N7	Test N8
1	0	-17.5	-18.0	-18.1	-17.8	-17.9	-18.0	-18.1	-18.0
2	2.5	-19.5	-20.0	-19.9	-19.6	-19.9	-19.8	-20.3	-20.3
3	5	-23.1	-23.4	-23.4	-23.3	-23.5	-23.5	-23.4	-23.5
4	6	-19.9	-20.6	-20.4	-20.6	-21.2	-20.7	-20.6	-20.6
5	7	-19.0	-19.7	-20.0	-19.3	-20.3	-16.6	-17.2	-17.6
6	8	-10.1	-12.9	-13.5	-13.5	-12.8	-12.7	-12.8	-12.8
7	9	-3.7	-3.3	-2.9	-1.2	-1.8	-1.6	-1.1	-0.7
8	10	3.7	4.1	4.6	5.0	5.6	5.9	6.5	7.1

Table 4.5: Measured Bottom Elevation Z_b (cm) Before and After Tests N1-N8

Gauge	x (m)	Test N0	Test N1	Test N2	Test N3	Test N4	Test N5	Test N6	Test N7	Test N8
1	0	-80.00	-80.00	-80.00	-80.00	-80.00	-80.00	-80.00	-80.00	-80.00
2	2.5	-59.32	-59.42	-59.50	-59.54	-59.63	-59.73	-59.77	-59.78	-59.83
3	5	-38.27	-38.66	-39.09	-39.33	-39.59	-39.76	-39.85	-39.93	-40.03
4	6	-30.07	-30.65	-31.27	-31.71	-32.03	-32.43	-32.93	-33.46	-33.92
5	7	-21.80	-21.85	-22.04	-22.23	-22.46	-22.60	-22.65	-22.73	-22.94
6	8	-13.04	-12.83	-12.76	-12.68	-12.54	-12.45	-12.32	-12.19	-12.04
7	9	-4.60	-3.89	-3.20	-2.85	-2.53	-2.32	-2.12	-1.93	-1.67
8	10	3.53	3.96	4.38	4.74	5.11	5.62	6.21	6.76	7.23

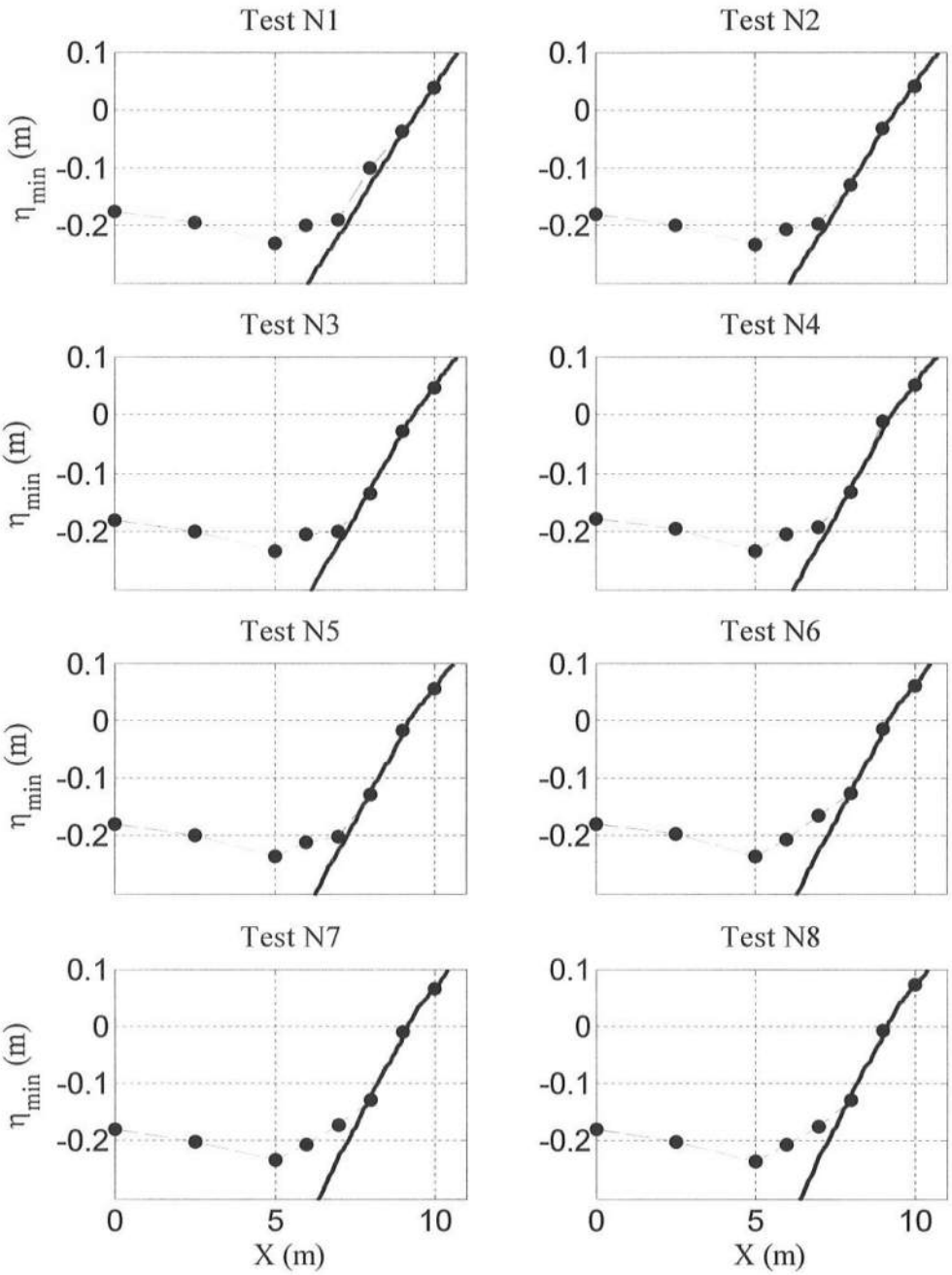

Figure 4.9: Cross-Shore Variation of Wave Trough Elevation above Measured Beach Profile for Tests N1-N8

4.4 VELOCITY AND CONCENTRATION DATA

The velocities and sand concentrations were measured at the elevation of 6 cm above the local bottom at the cross-shore location of wave gauge 4 near the wave collapsing point as shown in Figure 4.2. Figures 4.10-4.17 show the measured free surface elevation η_4, horizontal velocities u, alongshore velocities V, vertical velocity W, and suspended sediment concentration c at wave gauge 4 for tests N1-N8. Reliable measurements of these quantities were possible at this location because the collapsing breaker was not violent. The measured alongshore and vertical velocities fluctuated rapidly due to eddies generated by the collapsing wave. The cross-shore velocities and sand concentrations measured at the two alongshore locations were essentially in phase apart from high frequency oscillations caused by the collapsing wave. The cross-shore velocity u and the sand concentration c presented in the following is the average of the measured two time series.

Figures 4.18-4.25 show the temporal variations of u and c together with the free surface elevation η_4 at wave gauge 4 for tests N1-N8. To explain the simultaneous decrease of η_4 and u on the landward side of the wave trough, use was made of (3) where the subscript 3 was replaced by 4 and the local wave height H_4 was regarded to be negative. This modified equation predicted u to be nearly –2 m/s. The dotted line in the middle panel in Figures 4.18-4.25 is the cross-shore velocity u predicted by linear long wave theory

$$u(t) = C_4 \eta_4(t) / h_4 \quad ; \quad C_4 = (g h_4)^{1/2} \tag{4}$$

where the still water depth h_4 at wave gauge 4 increased from 30.4 cm for test N1 to 33.7 cm for test N8 as listed in Table 4.6. Correspondingly, the celerity C_4 increased from 1.73 m/s to 1.82 m/s. Equation (4) for the wave propagating landward explains the relationship between $\eta_4(t)$ and $u(t)$ until u became positive (onshore) under the negative η_4. The measured offshore velocity under the wave trough was less than 1 m/s in comparison to the predicted offshore velocity exceeding 1 m/s. The high frequency oscillations associated with the collapsing wave appeared earlier in the measured time series of u relative to η_4 for tests N3, N4, N7 and N8, indicating the variability of the wave breaking. It may be noted that the measured time series of u for test N6 was noisier. The measured concentration c increased suddenly under the steep seaward side of the wave trough where the wave collapsing occurred. The lower concentration event approximately during $59 < t < 67$ s lasting longer was associated with the wave downrush with $u < 0$. The measured time series of u and c for the tests N1-N8 are similar apart from the variability of u associated with the wave breaking.

Table 4.6: Incident Solitary Wave Characteristics at Wave Gauge 4 for Tests N1-N8

Test	h (cm)	η_{up} (cm)	η_{min} (cm)	H (cm)	C (m/s)
N1	30.36	0.43	-19.87	-20.30	1.73
N2	30.96	0.43	-20.56	-20.99	1.74
N3	31.49	0.47	-20.42	-20.89	1.76
N4	31.87	0.41	-20.58	-20.99	1.77
N5	32.23	0.43	-21.19	-21.62	1.78
N6	32.68	0.47	-20.71	-21.18	1.79
N7	33.20	0.43	-20.59	-21.02	1.80
N8	33.69	0.41	-20.59	-21.00	1.82

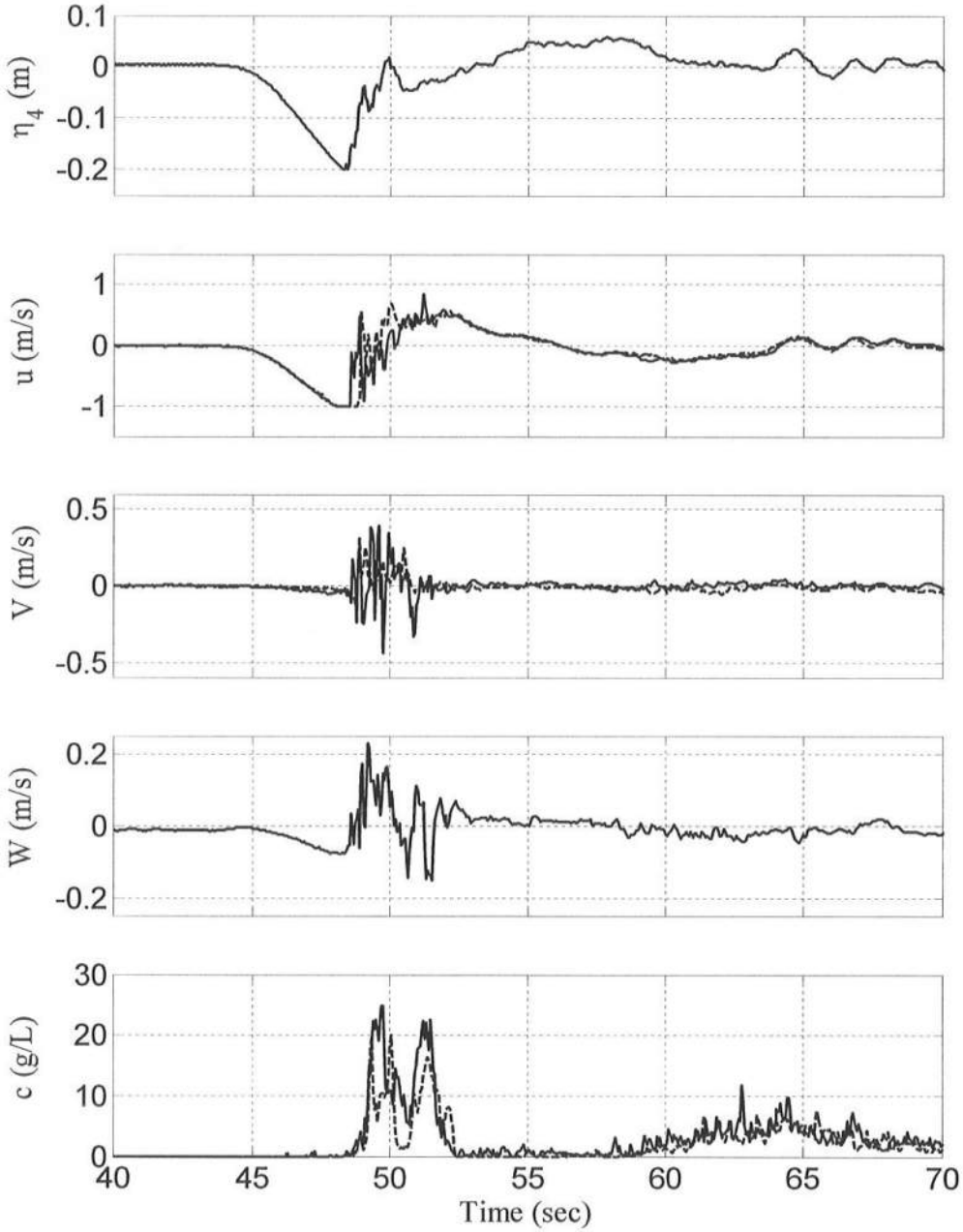

Figure 4.10: Measured Free Surface, Velocities and Sediment Concentrations for Test N1

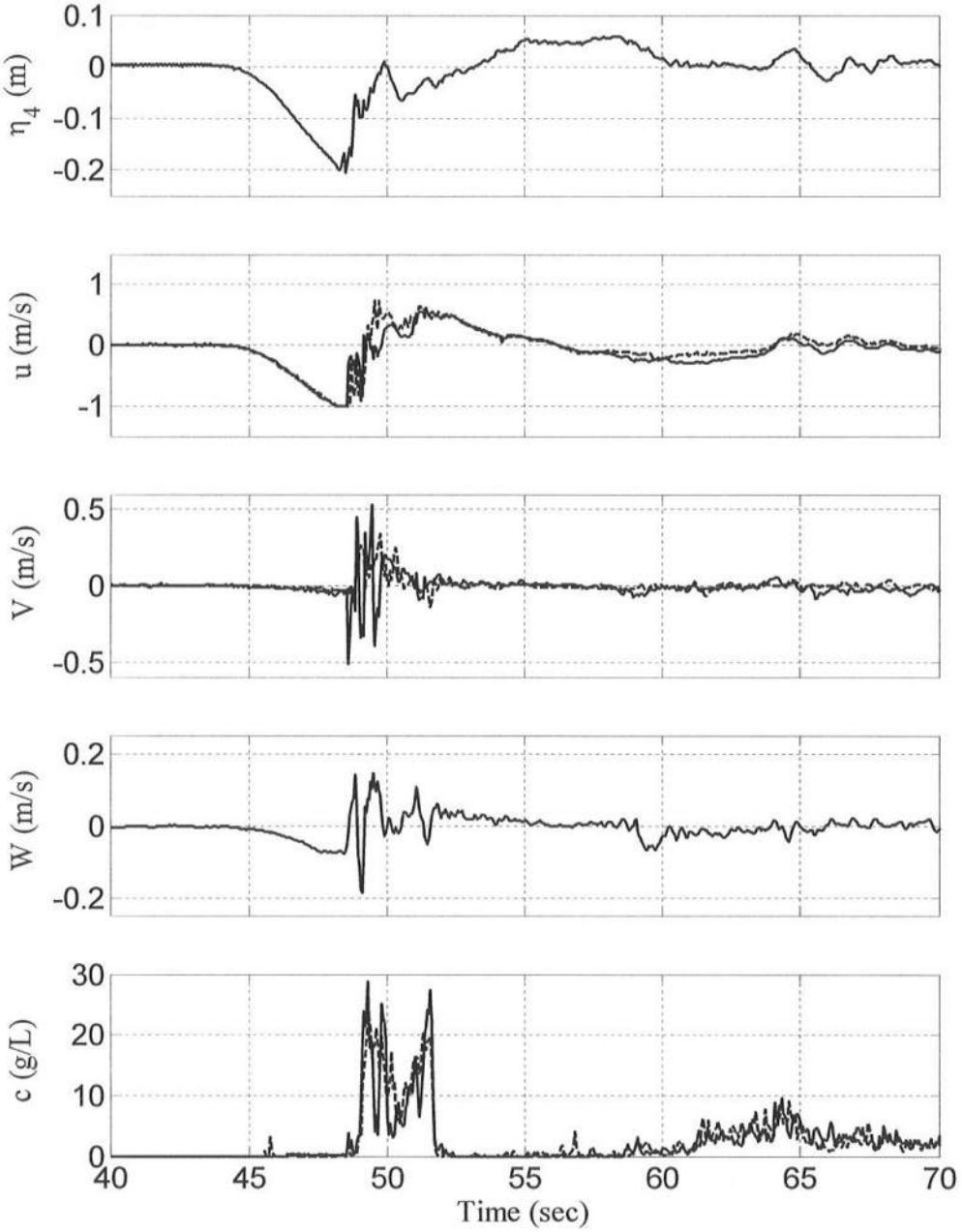

Figure 4.11: Measured Free Surface, Velocities and Sediment Concentrations for Test N2

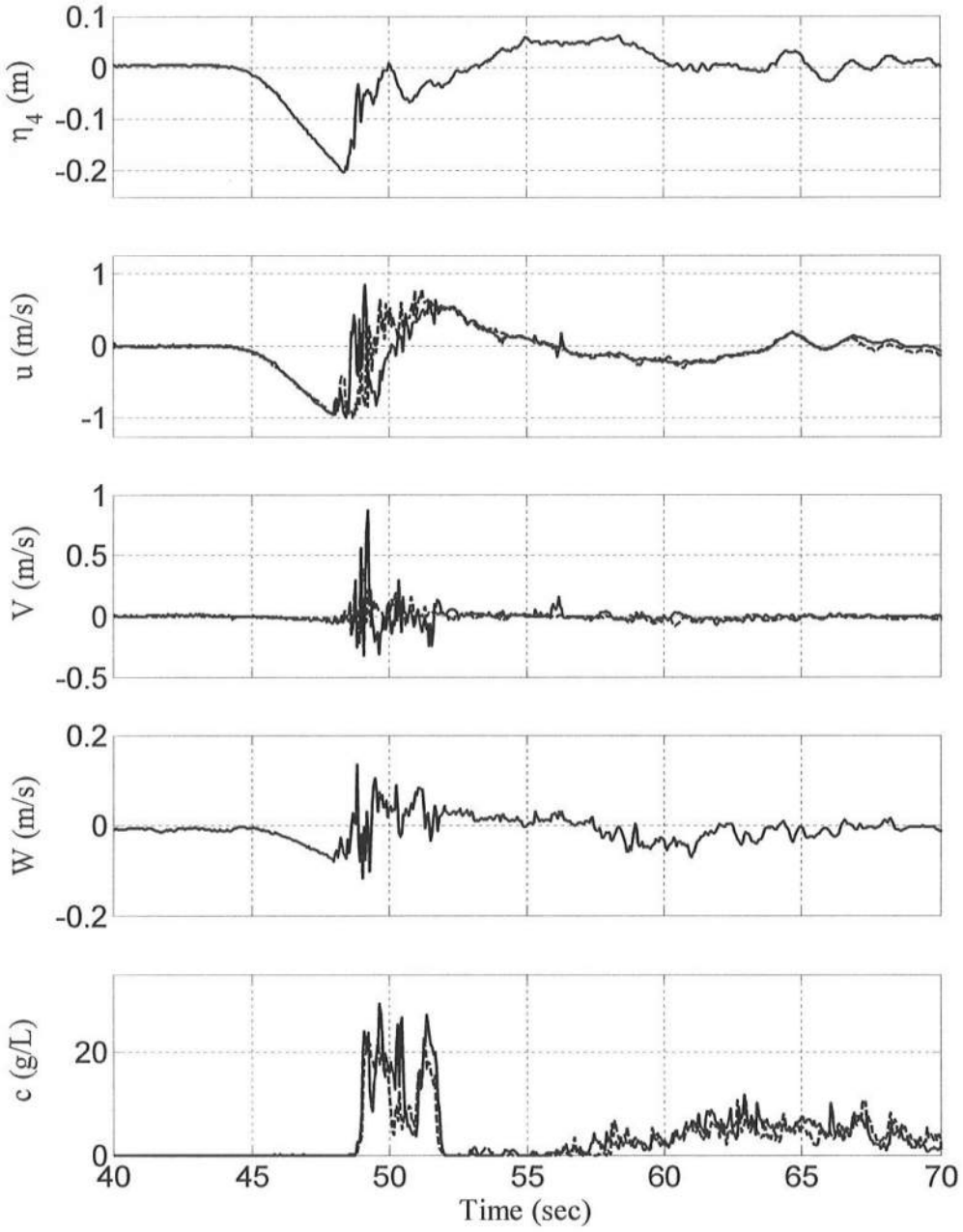

Figure 4.12: Measured Free Surface, Velocities and Sediment Concentrations for Test N3

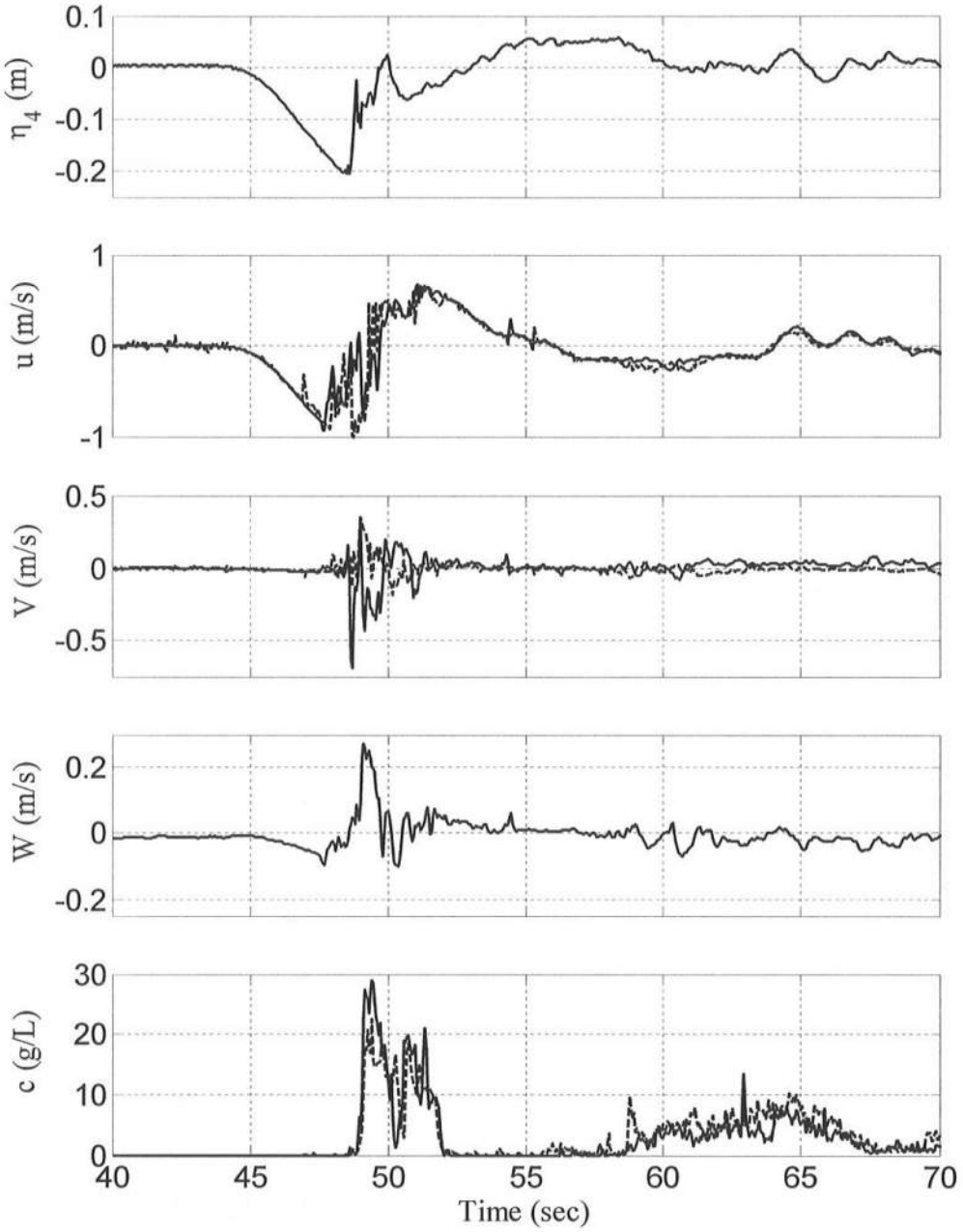

Figure 4.13: Measured Free Surface, Velocities and Sediment Concentrations for Test N4

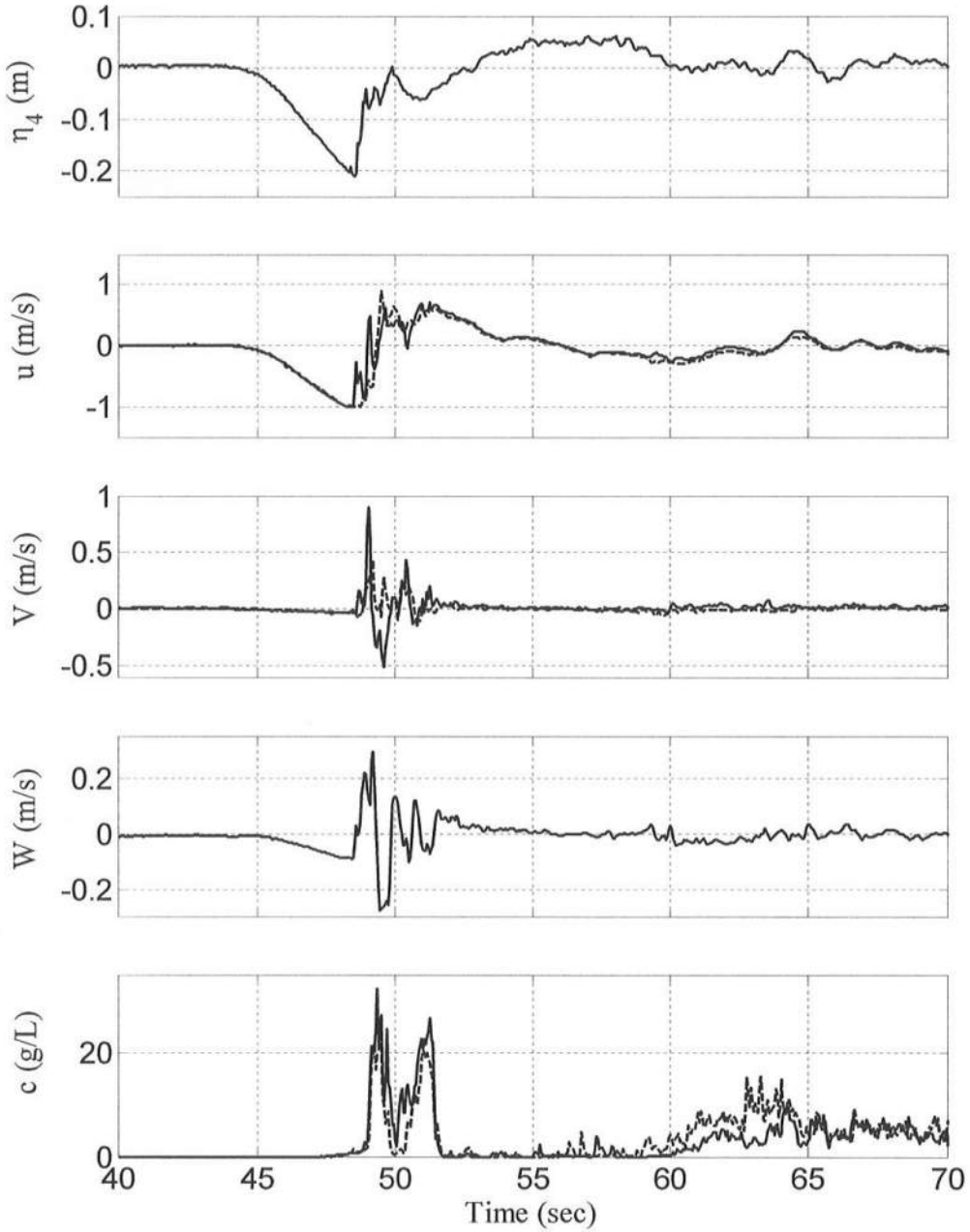

Figure 4.14: Measured Free Surface, Velocities and Sediment Concentrations for Test N5

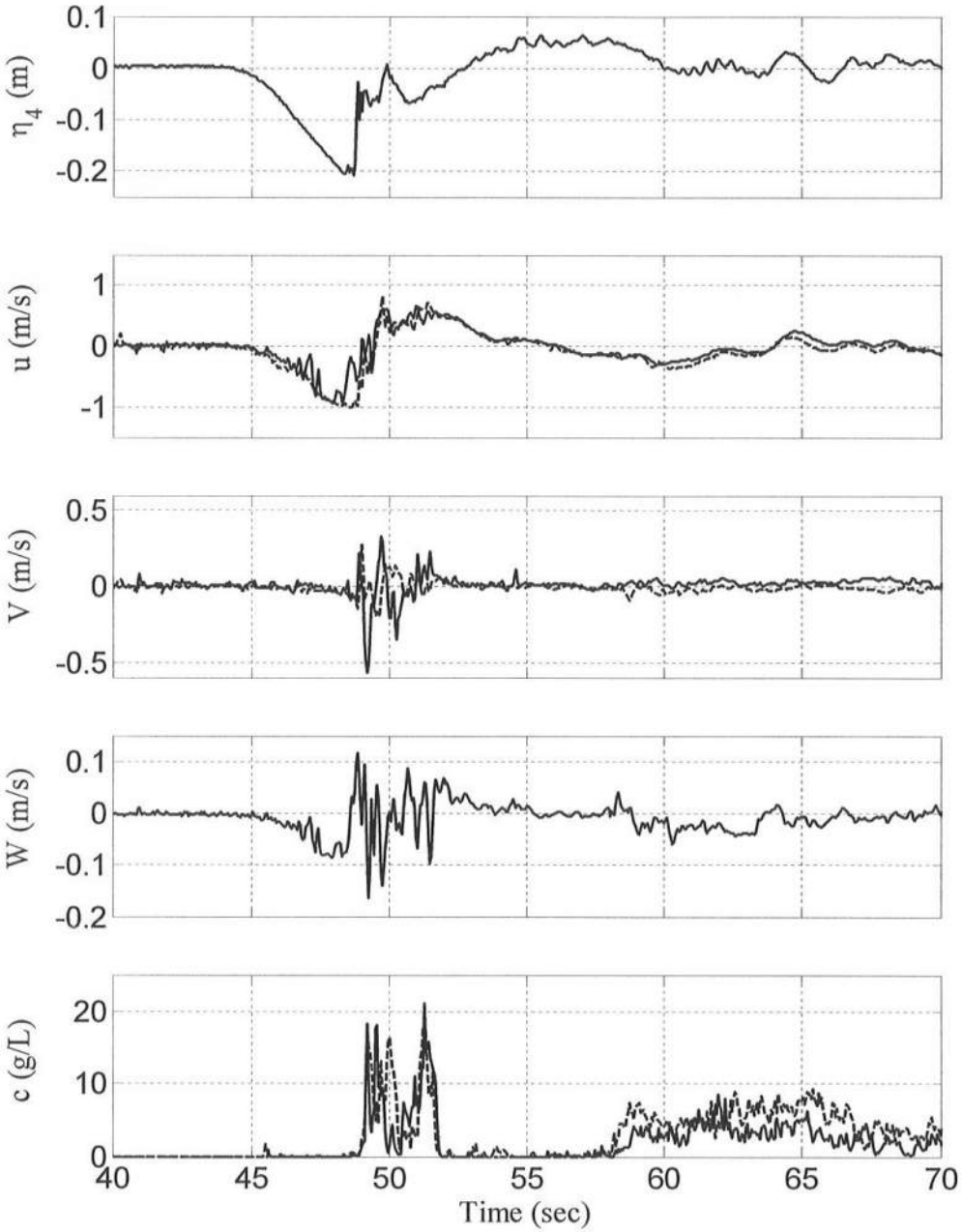

Figure 4.15: Measured Free Surface, Velocities and Sediment Concentrations for Test N6

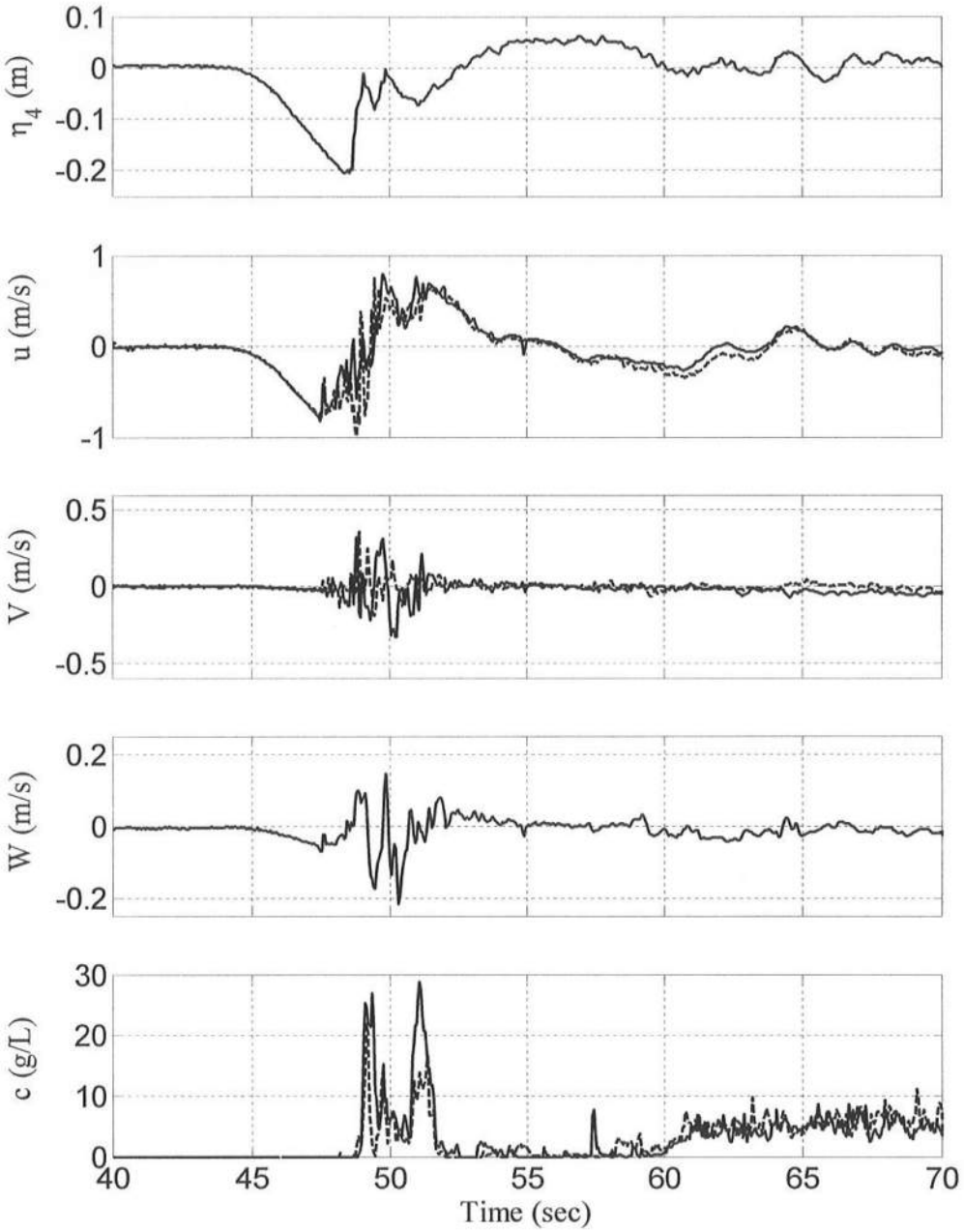

Figure 4.16: Measured Free Surface, Velocities and Sediment Concentrations for Test N7

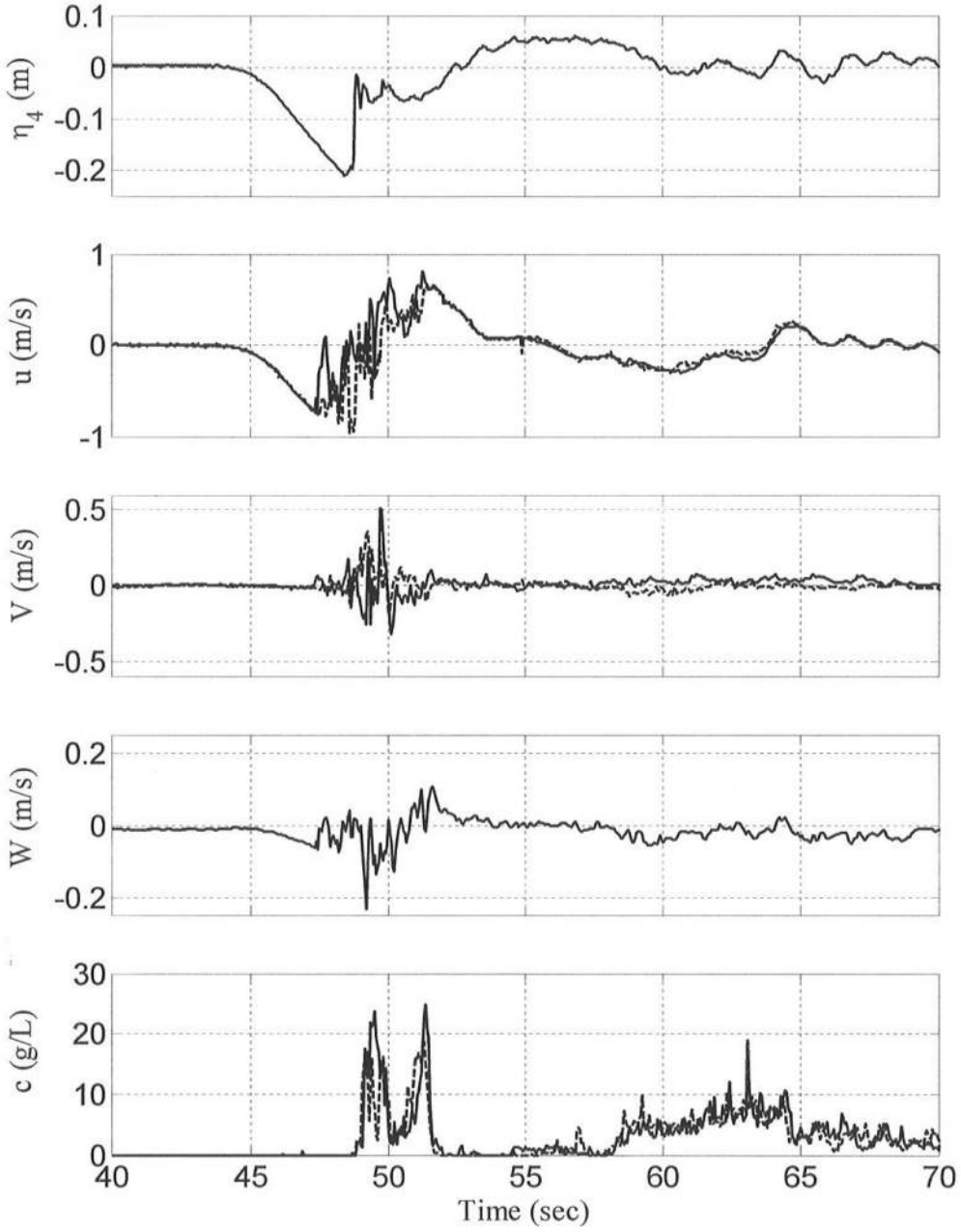

Figure 4.17: Measured Free Surface, Velocities and Sediment Concentrations for Test N8

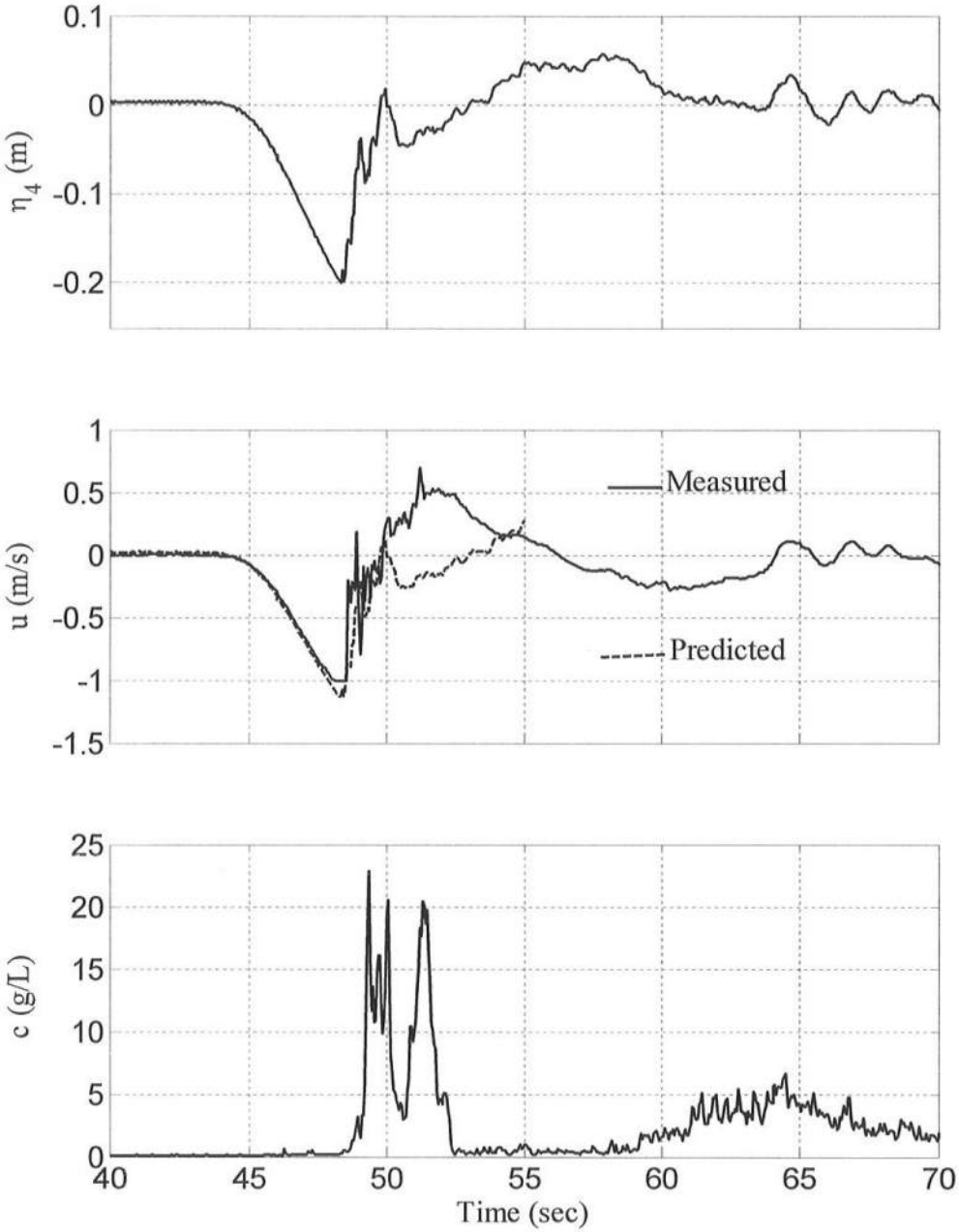

Figure 4.18: Measured Time Series of η_4, Average u and c for Test N1

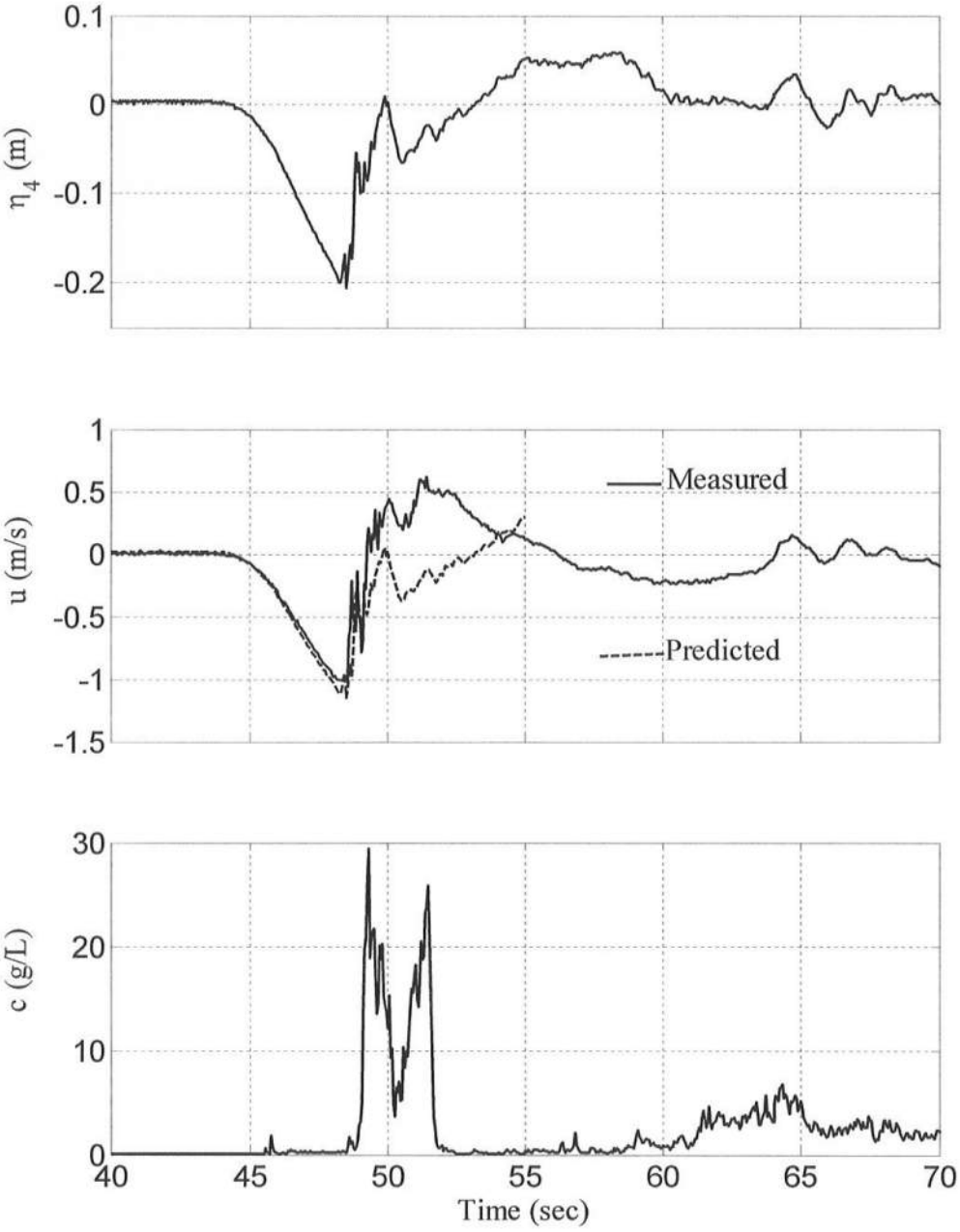

Figure 4.19: Measured Time Series of η_4, Average u and c for Test N2

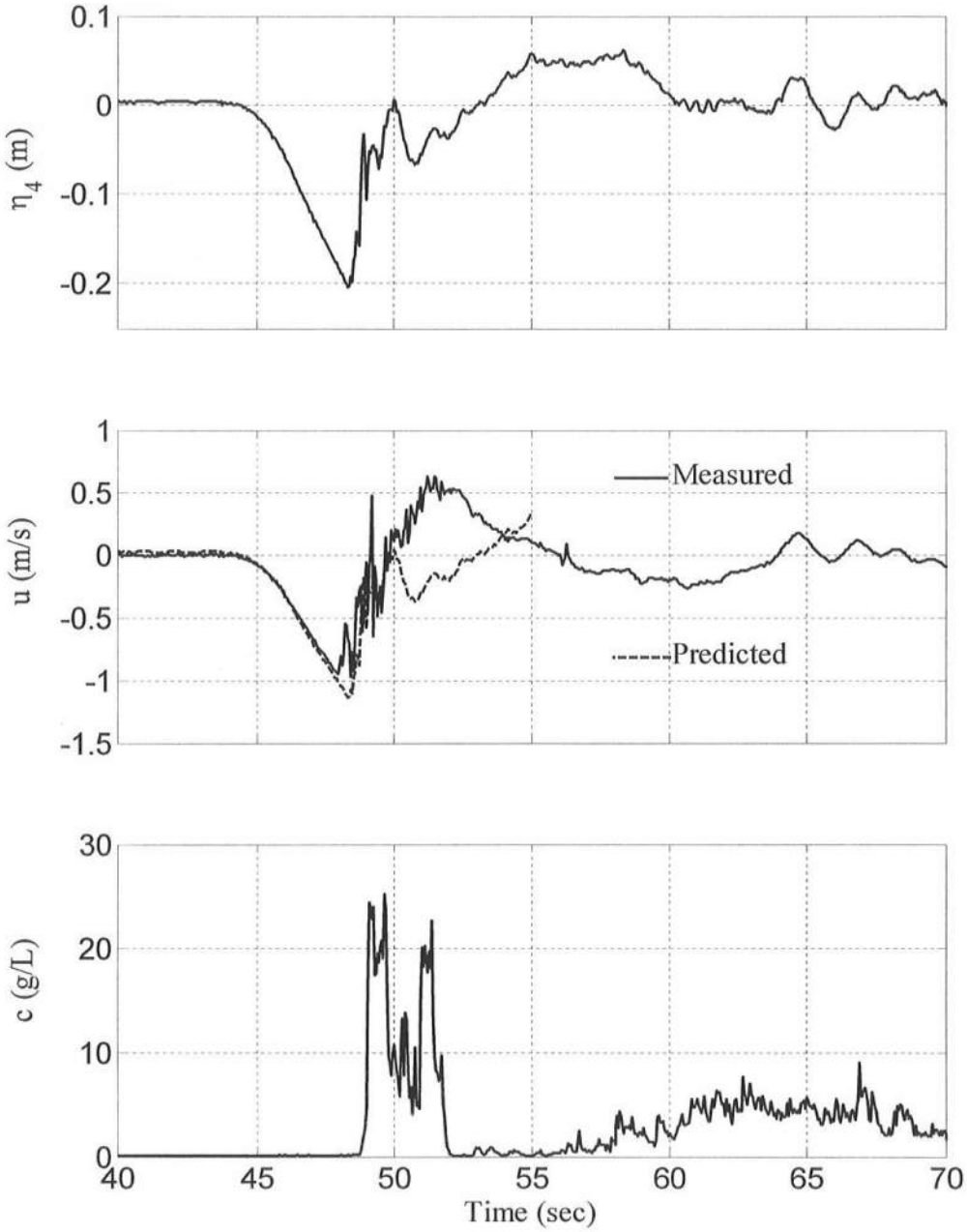

Figure 4.20: Measured Time Series of η_4, Average u and c for Test N3

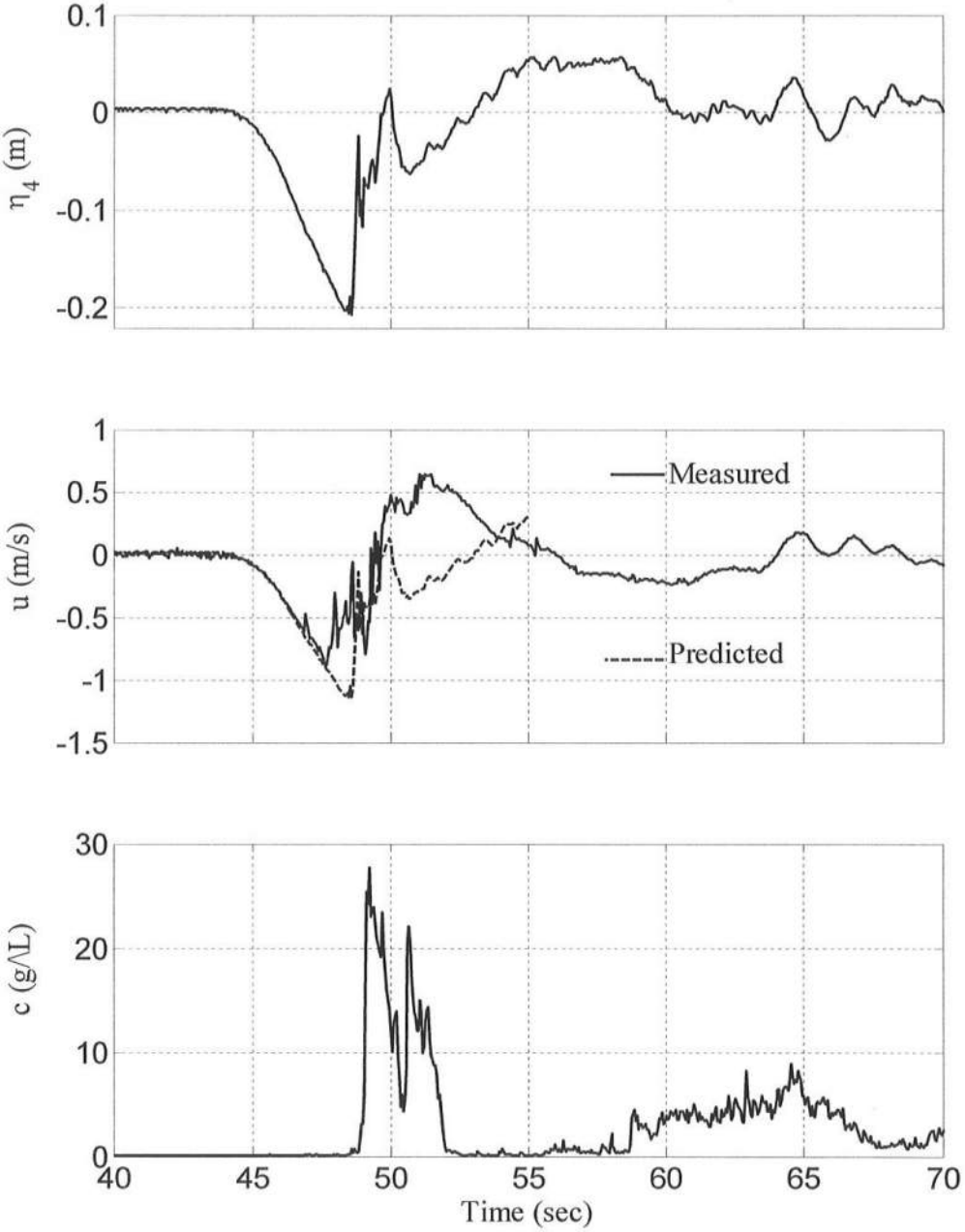

Figure 4.21: Measured Time Series of η_4, Average u and c for Test N4

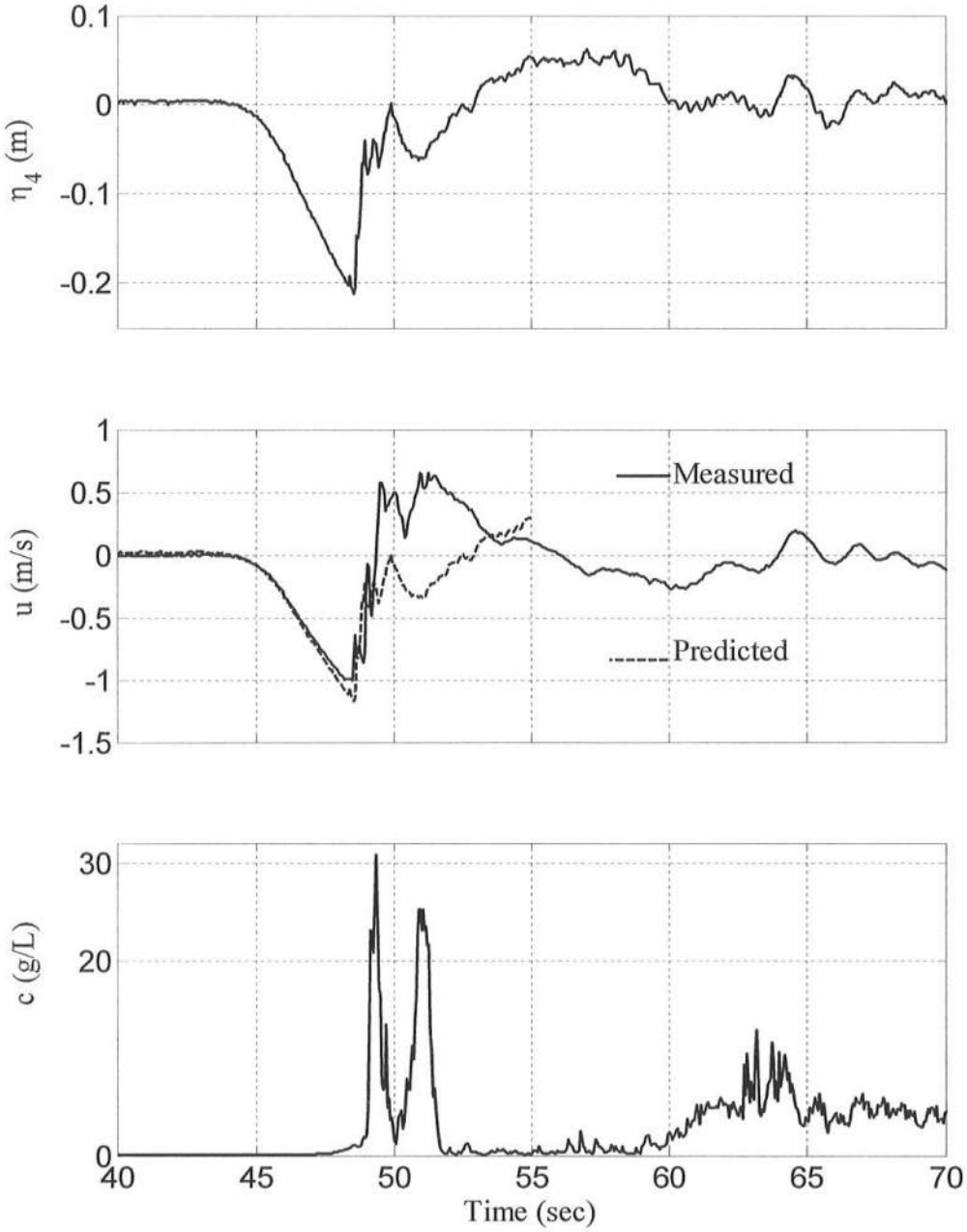

Figure 4.22: Measured Time Series of η_4, Average u and c for Test N5

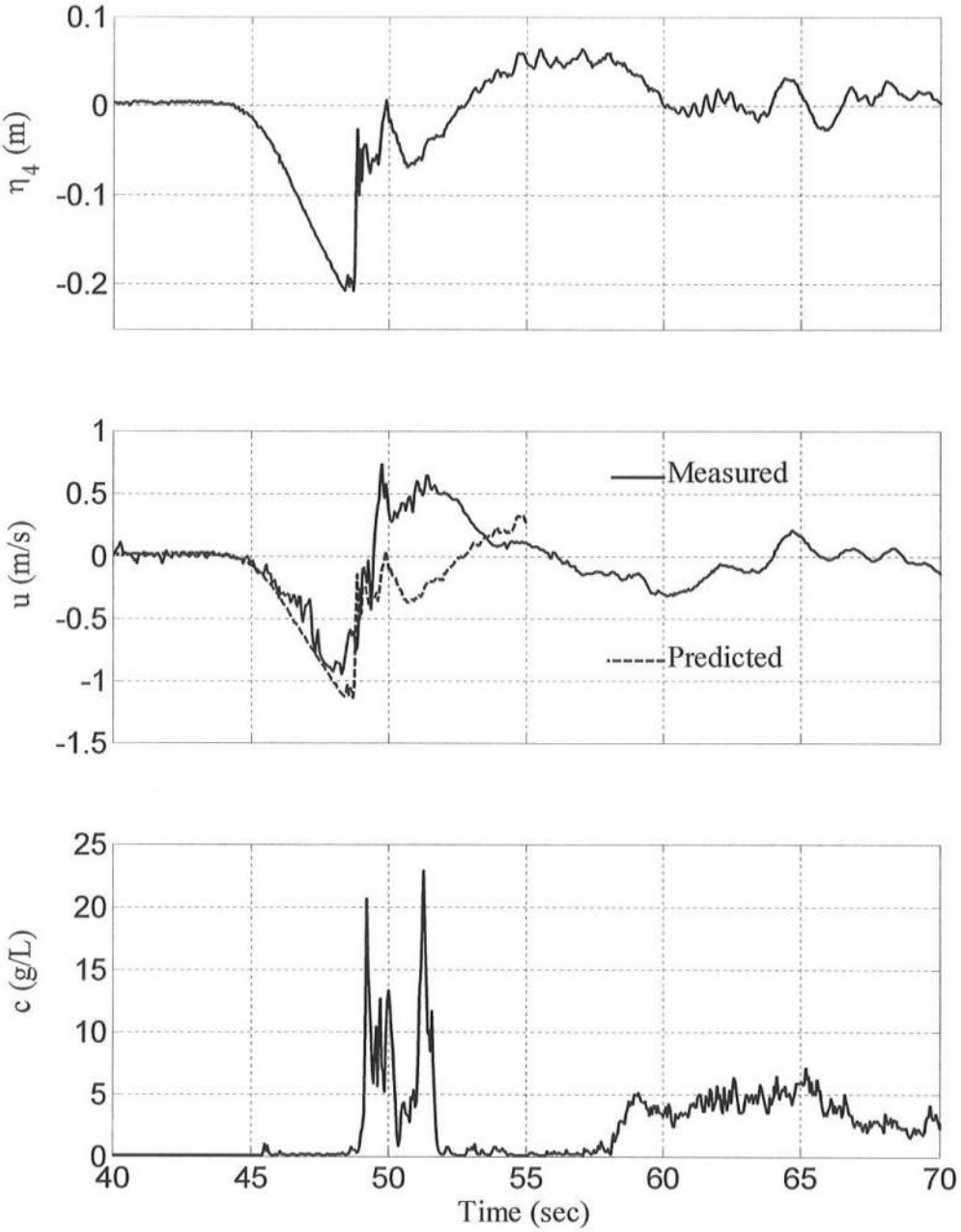

Figure 4.23: Measured Time Series of η_4, Average u and c for Test N6

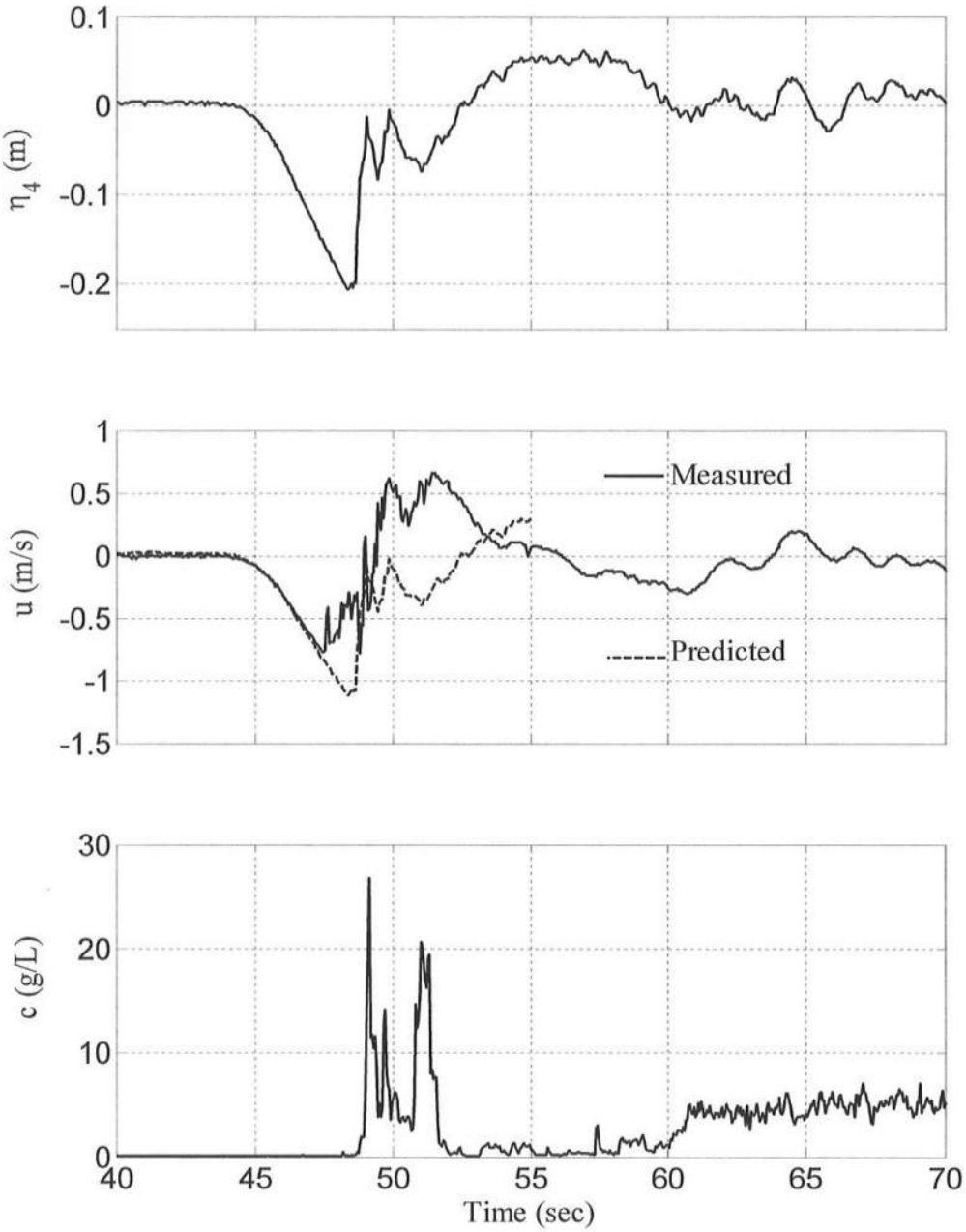

Figure 4.24: Measured Time Series of η_4, Average u and c for Test N7

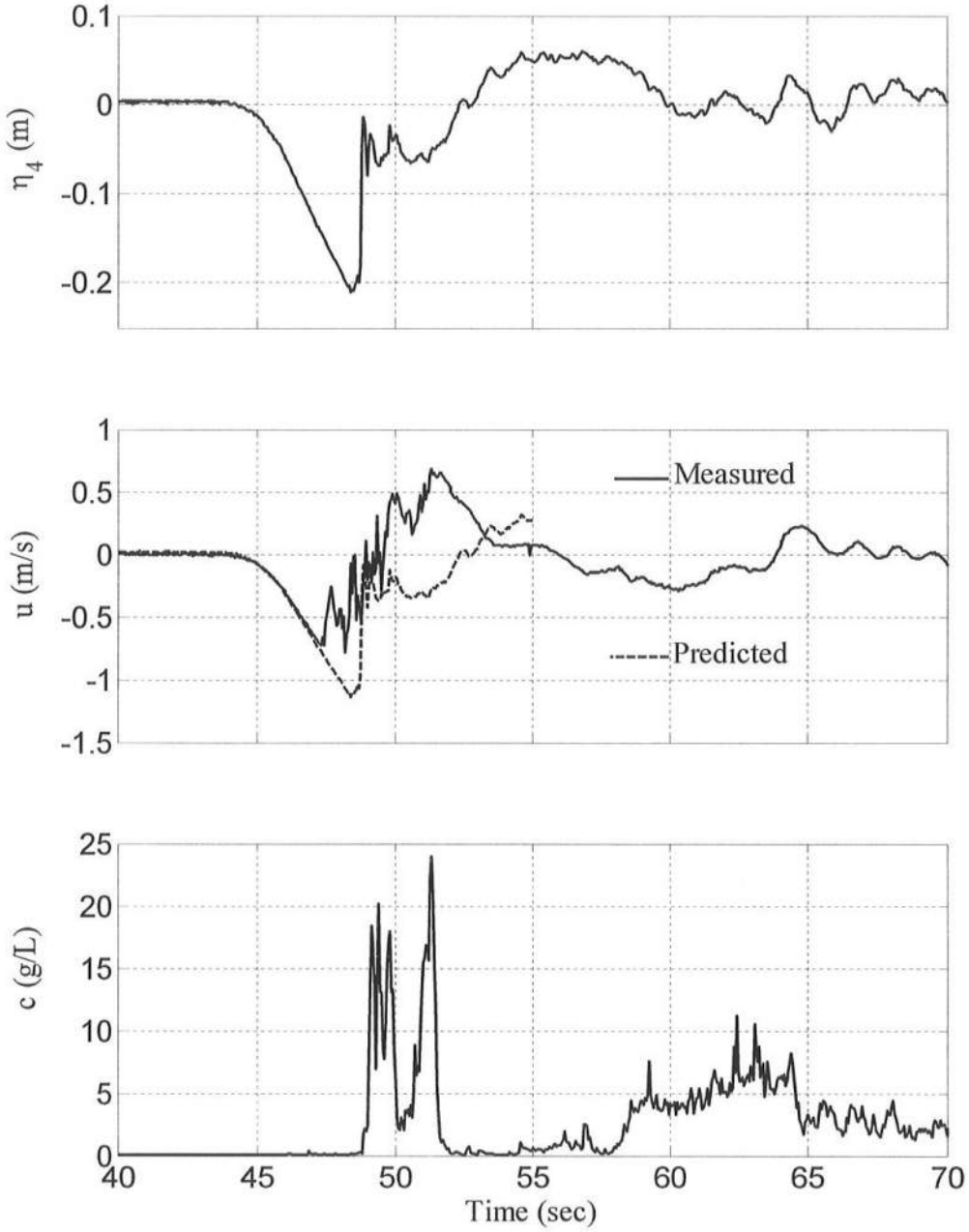

Figure 4.25: Measured Time Series of η_4, Average u and c for Test N8

4.5 PARAMETERIZATION OF ACCRETED BEACH PROFILE

The measured beach profile change relative to the initial profile is parameterized as shown in Figure 4.26 in the same way as in Section 3.5 except that the erosion and accretion zones were reversed for tests N1-N8. The cross-shore location x_0 of the intersection of the two profiles listed in Table 4.7 was in the range 7.58 – 7.60 m and remained practically constant. The still water depth d_0 at this intersection was in the range 16.7 – 16.9 cm.

The maximum vertical erosion depth $e_{\max}$ and the erosion area A_e for the erosion zone of $x < x_0$ in Figure 4.26 are obtained for the measured profile after each test. For the deposition zone of $x > x_0$, the maximum vertical deposition depth $d_{\max}$ and the deposition area A_d are calculated for each measured profile. In addition, the shoreline advancement S_d for the still water shoreline is obtained as depicted in Figure 4.26. These parameters summarized in Table 4.7 are normalized by the averaged wave height H = 18.2 cm at wave gauge 1. The results of the normalized profile parameters are give in Table 4.8. The ratio d_0/H is 0.92 for the eight tests as shown in Figure 4.27, whereas S_d/H increased approximately linearly to 1.82 for test N4 and slowly to 2.35 for test N8, as shown in Figure 4.28.

Figure 4.29 shows the approximately linear increase of $d_{\max}/H$ and $e_{\max}/H$ with the test number. The maximum deposition depth $d_{\max}$ and the maximum erosion depth e_{max} caused by the single negative solitary wave were of the order of 0.03 H. Figure 4.30 shows the almost linear increase of A_d/H^2 and A_e/H^2 with the test number where the requirement of $A_d = A_e$ was nearly satisfied. The deposition area A_d and the

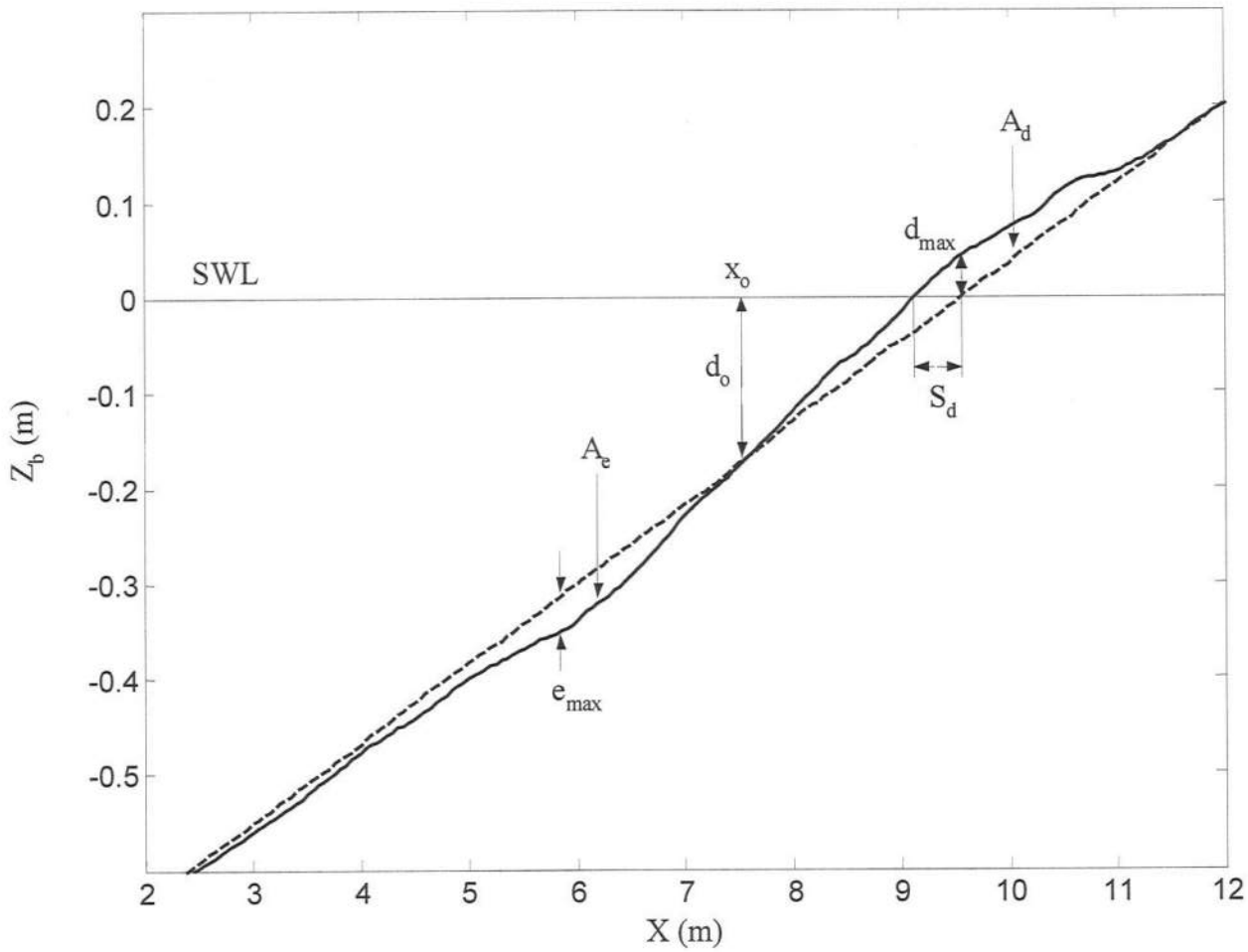

Figure 4.26: Illustration of Variables Used for Parameterization of Negative Solitary Wave Beach Profile Change

erosion area A_e caused by the single negative solitary wave were of the order of 0.35 H^2. Comparison of Figures 4.29 and 4.30 with Figures 3.28 and 3.30 indicates that the profile change caused by the negative solitary wave was approximately a half of that by the positive solitary wave, although the reversal of the deposition and erosion zones is more important in terms of sediment transport dynamics.

Table 4.7: Measured Profile Parameters for Tests N1-N8

Test	x_0 (m)	d_0 (cm)	e_{max} (cm)	A_e (cm^2)	d_{max} (cm)	A_d (cm^2)	S_d (cm)
N1	7.60	16.69	0.62	129.7	0.80	131.4	7.94
N2	7.59	16.78	1.20	263.6	1.57	247.1	16.56
N3	7.59	16.77	1.65	394.2	2.23	356.1	23.57
N4	7.59	16.76	2.06	519.8	2.82	468.0	33.18
N5	7.59	16.75	2.62	637.8	3.20	575.5	36.92
N6	7.59	16.75	3.10	730.6	3.67	696.7	38.83
N7	7.59	16.75	3.52	816.9	3.96	819.3	40.70
N8	7.58	16.85	3.91	894.3	4.36	939.1	42.85

Table 4.8: Normalized Profile Parameters for Tests N1-N8

Test	d_0/H	e_{max}/H	A_e/H^2	d_{max}/H	A_d/H^2	S_d/H
N1	0.916	0.03	0.39	0.04	0.40	0.44
N2	0.920	0.07	0.79	0.09	0.74	0.91
N3	0.920	0.09	1.19	0.12	1.07	1.29
N4	0.919	0.11	1.56	0.15	1.41	1.82
N5	0.919	0.14	1.92	0.18	1.73	2.03
N6	0.919	0.17	2.20	0.20	2.10	2.13
N7	0.919	0.19	2.46	0.22	2.47	2.23
N8	0.924	0.21	2.69	0.24	2.83	2.35

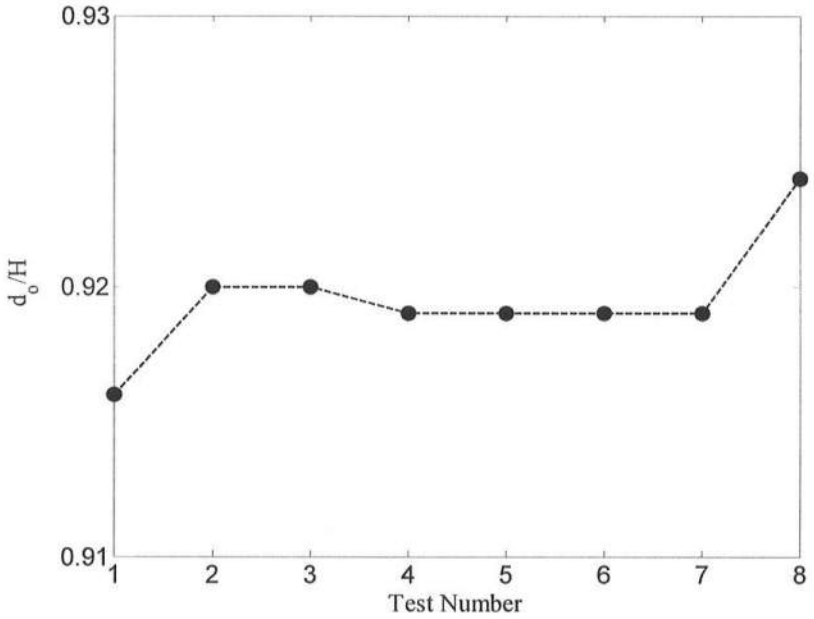

Figure 4.27: Normalized Still Water Depth d_0 at Intersection Between Initial Profile and Measured Profile After Tests N1-N8

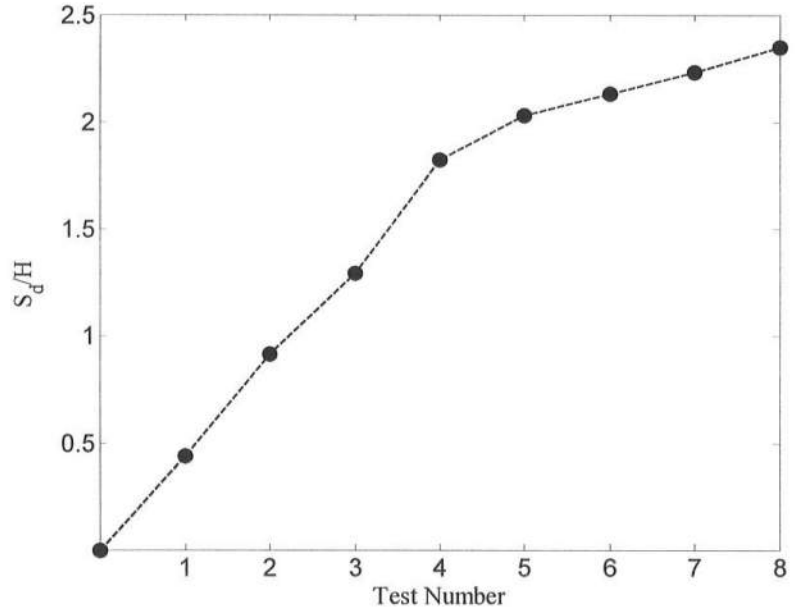

Figure 4.28: Normalized Horizontal Shoreline Advancement S_d for Tests N1-N8

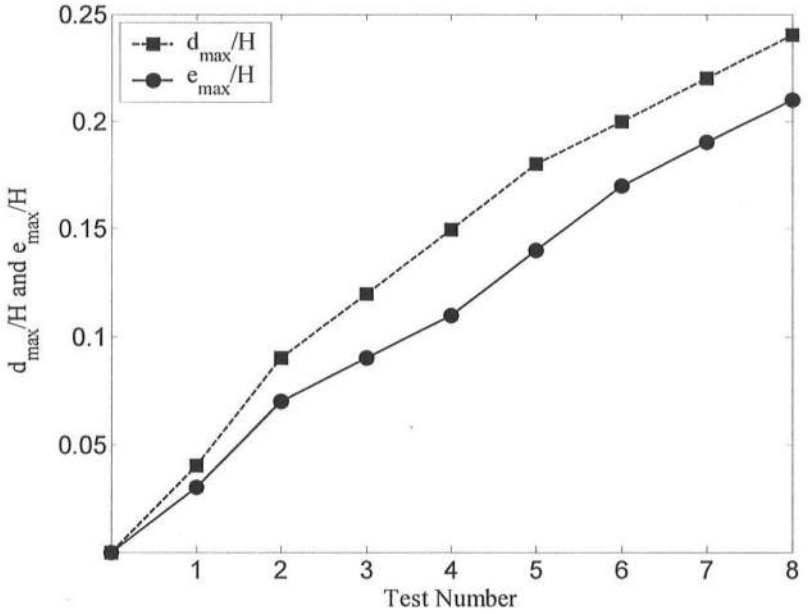

Figure 4.29: Normalized Maximum Vertical Deposition Depth d_{max} and Erosion e_{max} Depth for Tests N1-N8

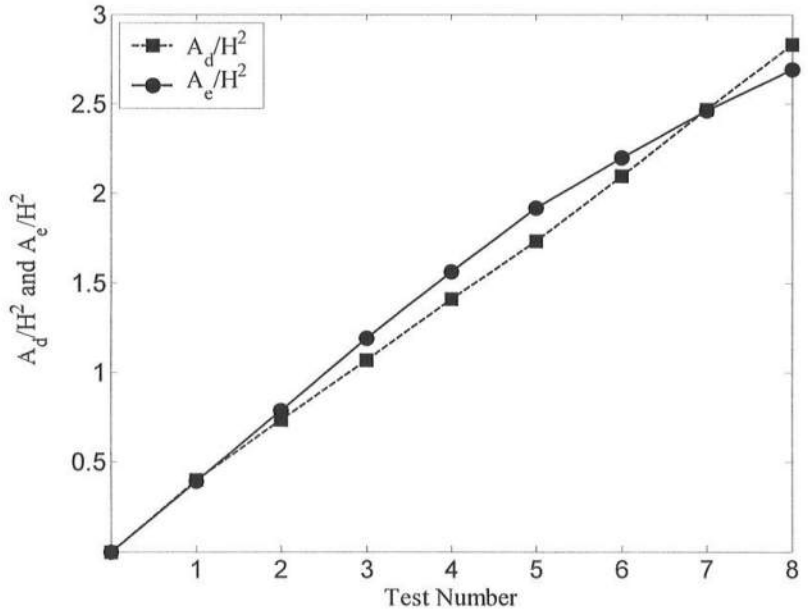

Figure 4.30: Normalized Deposition Area A_d and Erosion Area A_e for Tests N1-N8

Chapter 5

CONCLUSIONS

Laboratory experiments were performed to examine the cross-shore sediment transport processes under breaking solitary waves on a fine sand beach. Positive and negative solitary waves were generated in water depth of 0.8 m. The wave height H was approximately 21.6 and 18.2 cm for the positive and negative waves, respectively. The initial beach slope of 1:12 was exposed to the eight positive solitary waves (tests P1-P8) and the eight negative solitary waves (tests N1-N8). For each test, measurements were made of the beach profile, free surface elevations, fluid velocities and sand concentrations. The limited velocity and concentration measurements were augmented by visual observations. The wave motion and sediment transport were not affected much by the profile change from the initial profile.

For tests P1-P8, the positive solitary wave plunged violently near the shoreline and suspended a considerable volume of sand. The plunging wave with no seaward flow impeding its runup caused large runup on the foreshore. The strong downrush following the large runup resulted in erosion on the foreshore and deposition seaward of wave run-down. The single positive solitary wave caused the deposition and

erosion depths of the order of 0.06 H and the deposition and erosion areas of the order of 0.7 H^2.

For tests N1-N8, the negative solitary wave collapsed against the seaward flow induced by the free surface inclined downward toward the wave trough. The collapsing wave suspended less sediment than the plunging wave. The wave runup was much smaller in the presence of the seaward flow. The weak downrush following the small runup induced deposition on the foreshore and erosion near the wave collapsing point. The reversal of the incident solitary wave profile resulted in the reversal of the erosion and deposition zones on the beach. The single negative solitary wave caused the deposition and erosion depths of the order of 0.03 H and the deposition and erosion areas of approximately 0.35 H^2.

The present experiments were limited to the particular solitary waves on a relatively steep beach but indicate the importance of the incident wave profile in influencing the breaker type, sediment suspension, wave runup and downrush, net sediment transport and resulting profile change. Furthermore, the sediment transport capacity of a single solitary wave may be appreciated if comparison is made with the dune erosion area of 50 m^2 under the 100-year event along the U.S. Atlantic and Gulf coasts adopted for the U.S. National Flood Insurance Program [Hallermeier and Rhodes, 1988]. Assuming the erosion area A_e = 0.7 H^2, the erosion area of 50 m^2 could be caused by a single solitary wave whose height is 8.5 m. However, the empirical formulas developed using the limited small-scale experiments will need to be verified using field data.

erosion depths of the order of 0.06 H and the deposition and erosion areas of the order of 0.7 H^2.

For tests N1-N8, the negative solitary wave collapsed against the seaward flow induced by the free surface inclined downward toward the wave trough. The collapsing wave suspended less sediment than the plunging wave. The wave runup was much smaller in the presence of the seaward flow. The weak downrush following the small runup induced deposition on the foreshore and erosion near the wave collapsing point. The reversal of the incident solitary wave profile resulted in the reversal of the erosion and deposition zones on the beach. The single negative solitary wave caused the deposition and erosion depths of the order of 0.03 H and the deposition and erosion areas of approximately 0.35 H^2.

The present experiments were limited to the particular solitary waves on a relatively steep beach but indicate the importance of the incident wave profile in influencing the breaker type, sediment suspension, wave runup and downrush, net sediment transport and resulting profile change. Furthermore, the sediment transport capacity of a single solitary wave may be appreciated if comparison is made with the dune erosion area of 50 m^2 under the 100-year event along the U.S. Atlantic and Gulf coasts adopted for the U.S. National Flood Insurance Program [Hallermeier and Rhodes, 1988]. Assuming the erosion area $A_e = 0.7\ H^2$, the erosion area of 50 m^2 could be caused by a single solitary wave whose height is 8.5 m. However, the empirical formulas developed using the limited small-scale experiments will need to be verified using field data.

BIBLIOGRAPHY

Clague, J.J., I. Hutchinson, R.W. Mathewes, and R.T. Patterson, Evidence for late Holocene tsunamis at Catala Lake, British Columbia, *J. Coastal Res.,* 15, 45-60, 1999.

Carrier, G.F., T.T. Wu, and H. Yeh, Tsunami run-up and draw-down on a plane beach, *J. Fluid Mech.,* 475, 79-99, 2003.

Dalrymple, R.A., Prediction of storm/normal beach profiles, *J. Waterw. Port Coastal Ocean Eng.,* 118, 193-200, 1992.

Downing, J.P., R.W. Sternberg, and C.R.B. Lister, New instrumentation for the investigation of sediment suspension processes in the shallow marine environment, *Mar. Geol.,* 42, 19-34, 1981.

Giovannozzi, M.A., and N. Kobayashi, Intermittent high sand concentrations measured under irregular breaking waves, paper presented at *28th Coastal Engineering Conference,* World Scientific, Singapore, 2002.

Goring, D.G., Tsunamis – the propagation of long waves on to a shelf, *Rep. No. KH-R-38*, W.M. Keck Lab., Cal. Inst. of Tech., Pasadena, Cal., 1978.

Hallermeier, R.J., and P.E. Rhodes, Generic treatment of dune erosion for 100-year event, paper presented at *21st Coastal Engineering Conference*, Am. Soc. of Civ. Eng., Malaga, Spain, 1988.

Kobayashi, N., and B.D. Johnson, Sand suspension, storage, advection, and settling in surf and swash zones, *J. Geophys. Res.*, 106, 9363-9376, 2001.

Kobayashi, N., and E.A. Karjadi, Surf-similarity parameter for breaking solitary-wave runup, *J. Waterw. Port Coastal Ocean Eng.*, 120, 645-650, 1994.

Kobayashi, N., and A. R. Lawrence, Cross-shore sediment transport under breaking solitary waves, J. Geophys. Res., submitted in August, 2003.

Kobayashi, N., and Y. Tega, Sand suspension and transport on equilibrium beach, *J. Waterw. Port Coastal Ocean Eng.*, 128, 238-248, 2002.

Li, Y., and F. Raichlen, Energy balance model for breaking solitary wave runup, *J. Waterw. Port Coastal Ocean Eng.*, 129, 47-59, 2003.

Puleo, J.A., R.A. Beach, R.A. Holman, and J.S. Allen, Swash zone sediment suspension and transport and the importance of bore-generated turbulence, *J. Geophys. Res.*, 105, 17,021-17,044. 2000.

Synolakis, C., F. Imamura, Y. Tsuji, H. Matsutomi, S. Tinti, B. Cook, Y.P. Chandra, and M. Usman, Damage, conditions of East Java tsunami of 1994 analysed, *EOS, Transactions,* AGU, 76, 257, 261-262, 1995.